School of Molecular Science

The University of Western Australia

Biomass Pyrolysis: Identification and Characterisation of Products and the Mechanisms of Their Interactions and Transformations

Wenchao Wan

Bachelor of Engineering

This thesis is presented for the Degree of

Doctor of Philosophy

The University of Western Australia

July 2017

THESIS DECLARATION

I, Wenchao Wan, certify that:

This thesis has been substantially accomplished during enrolment in the degree.

This thesis does not contain material which has been accepted for the award of any other degree or diploma in my name, in any university or other tertiary institution.

No part of this work will, in the future, be used in a submission in my name, for any other degree or diploma in any university or other tertiary institution without the prior approval of The University of Western Australia and where applicable, any partner institution responsible for the joint-award of this degree.

This thesis does not contain any material previously published or written by another person, except where due reference has been made in the text.

The work(s) are not in any way a violation or infringement of any copyright, trademark, patent, or other rights whatsoever of any person.

This thesis contains published work and/or work prepared for publication, some of which has been co-authored.

Signature: 

Date: 22-07-2017

To My Beloved Family

ABSTRACT

Biomass pyrolysis is a promising technology for biomass utilisation as it could convert all kinds of biomass into liquid, gas and solid fuels. However, the fact that the poor quality of the pyrolysis products hinders its further application demands a better understanding of the reaction mechanisms involved in pyrolysis. The present research combines extensive experimental and theoretical approaches to systematically study the reaction mechanism underlying biomass pyrolysis, focusing on (i) the interactions among cellulose, hemicellulose and lignin, (ii) characterisation of cellulose pyrolysis products, (iii) the formation of cellulose pyrolysis products and (iv) the reaction mechanisms underlying their transformations.

First of all, this study investigated the interactions among cellulose, hemicellulose and lignin during pyrolysis. It was found that the pyrolysis of mixture of cellulose, hemicellulose and lignin showed a different kinetic characteristics compared to cellulose, hemicellulose and lignin. This reveals that the interactions between cellulose, hemicellulose and lignin play an important role during pyrolysis. As a result of their interactions, the formation of lignin derived compounds was promoted while the formation of cellulose derived and hemicellulose derived compounds was inhibited.

Secondly, a comprehensive identification and characterisation of cellulose pyrolysis products was carried out. In pyrolysis experiments at 1023 K the primary products of cellulose were anhydrosugar, furans and ketones, whereas at 823 K and 923 K only anhydrosugars and furans were formed. Disaccharides were identified in cellulose pyrolysis products. Compared to all other primary products, levoglucosenone showed different formation characteristics. All pyrolysis liquid products were classified into eight groups, including anhydro-sugars, furans, ketones, acids, aldehydes, esters, phenols and benzenes.

Thirdly, the effect of temperature and residence time on the formation of cellulose pyrolysis products was studied and the transformation mechanism among main anhydrosugar compounds was investigated. Thirteen major pyrolysis products were identified and quantified and revealed four different formation dependences on temperature and residence time. These results indicates that 1,4:3,6-dianhydro-α-D-glucopyranose (DGP) and levoglucosenone were mainly produced in the early stage of cellulose pyrolysis, while temperature elevation promoted the production of levoglucosan and levoglucosan-furanose. The formation of levoglucosenone was found to be more favored in secondary reactions. Further thermal analysis showed that levoglucosan was found to be thermally stable whereas DGP might be an intermediate for the formation of levoglucosenone.

Fourthly, high-level computational modelling was carried out in order to elucidate the reaction pathway from DGP to levoglucosenone. It was found that this multistep conversion involves seven elementary steps, including ring-opening, enol-to-keto tautomerisation, dehydration, and hydration reactions. The reaction energy profile was studied using high-level thermochemical protocols. In the uncatalysed mechanism, enol-to-keto tautomerisation was the rate-determining step, whereas in the water-catalysed mechanism the rate-determining step shifted to the ring-opening reaction. It was also found that the Gibbs free energy of the final product (levoglucosenone) lies 11.6 kcal•mol^{-1} below the starting material (DGP), which provides a thermodynamic driving force for process.

Fifthly, this study reported an application of high-level thermochemical protocols for obtaining a highly accurate heat of formation for Buckminsterfullerene (C_{60}). Buckminsterfullerene is a

key molecule in nanochemistry and its discovery was awarded the 1996 Nobel Prize in Chemistry. Nevertheless, its experimental heat of formation is not accurately known and is associated with a very large error bar of ±100 kJ•mol^{-1}. This study used high-level thermochemical protocols along with sophisticated thermochemical cycles for obtaining the most accurate theoretical heat of formation for C_{60} to date. The best theoretical value falls within the limits of the error bars of the experimental value adopted by the NIST thermochemical database. However, it is associated with a much smaller error bar.

Overall, the present research has valuable implications into the mechanism of biomass pyrolysis. The understanding on the interactions among cellulose, hemicellulose and lignin, the characterisation and formation characteristics of cellulose pyrolysis products and their transformation mechanisms provide fundamental base for optimising the quality of pyrolysis products.

ACKNOWLEDGEMENT

Firstly, I would like to express my gratitude to my supervisor, Dr. Amir Karton for his constructive guidance, invaluable suggestions and patience throughout my study. His perpetual commitment and passion for science has greatly inspired and spurred my career. I would like to thank Professor Dongke Zhang *FTSE*, who provided me the opportunity to complete the experimental work of this research in Centre for Energy. I would also like to acknowledge the support received from the Australian Research Council (ARC) under the ARC Linkage Projects scheme (ARC LP100200135) with BHP Billiton Iron Ore, Ansac and ENN as the industry partners.

I could also like to extend my thanks to many colleagues and friends in UWA as they were a great source of advice and encouragement. Firstly I could like to thank Mrs. Li-Juan Yu, who was always willing to give up her time to help or provide advice when needed for which I am deeply grateful. Appreciations also go to Dr. Mingming Zhu, Dr. Jiguang Zhang, Mr. Zhezi Zhang, Mr. Pengfei Liu, and Mr. Yuan Peng, who provided valuable advice and support about research, career and life. In addition, I would like to thank the staff of the Graduate Research School, Dr. Joanne Edmondston, Dr. Louise Wedlock and Dr. Sudarsan Krishnaswamy for their assistance with writing and general support they provided.

My utmost gratitude to Associate Professor Judith Berman and Professor Ian McArthur, who have supported me from the first day I came to Australia with ongoing family-like care and love. Without their support, none of this could be possible.

A special thankyou to my parents and my wife Huiying Hu for their love and support throughout. Thank you for putting up with me and making the most difficult times bearable. I would not be where I am without you.

AUTHORSHIP DECLARATION: CO-AUTHORED PUBLICATIONS

This thesis contains work that has been published.

Details of the work: Wenchao Wan, Li-Juan Yu and Amir Karton, Mechanistic Insights into Water-catalyzed Formation of levoglucosenone from Anhydrosugar Intermediates by Means of High-Level Theoretical Procedures. Australian Journal of Chemistry, 2016. **69**(9): p. 943-949.
Location in thesis: Chapter 6
Student contribution to work: Wenchao and Amir designed the research. Wenchao completed the calculation with the help of Yu. Wenchao and Amir finalized the manuscript (overall contribution: 80%).

Details of the work: Wenchao Wan and Amir Karton, Heat of formation of C60 by means of the G4(MP2) thermochemical protocol through reactions in which C60 is broken down into corannulene and sumanene. Chemical Physics Letters, 2016. 643: p. 34-38.
Location in thesis: Chapter 7
Student contribution to work: Wenchao and Amir designed the research. Wenchao and Amir completed the calculation and finalized the manuscript (overall contribution: 80%).

Student signature: [redacted] Date: 22-07-2017
I, Amir Karton certify that the student statements regarding their contribution to each of the works listed above are correct Coordinating supervisor signature: [redacted] Date: 22-07-2016

TABLE OF CONTENTS

ABSTRACT ..... **V**

ACKNOWLEDGEMENT ..... **VIII**

TABLE OF CONTENTS ..... **XI**

LIST OF TABLES ..... **XVII**

LIST OF FIGURES ..... **XIX**

Chapter 1. Introduction **1**

1.1 Background 1

1.2 Research aims 2

1.3 Thesis outline 3

Chapter 2. Literature Review **5**

2.1 Introduction 5

2.2 Structures and main characteristics of biomass 5

2.2.1 Lignocellulose 5

2.2.2 Cellulose 6

2.2.3 Hemicellulose 7

2.2.4 Lignin 8

2.3 Biomass pyrolysis 10

2.3.1 Pyrolysis 10

2.3.2 Pyrolysis reactors 11

2.4 Identification and characterisation of pyrolysis products 15

2.4.1 Established methodology and approaches 15

2.4.2 Effect of operating parameters on pyrolysis process 17

2.5 Chemistry and reactions in biomass pyrolysis 23

2.5.1 Depolymerisation 23

2.5.2 Dehydration reactions 25

2.5.3 Formation of levoglucosan 26

2.5.4 Fragmentation– the formation of low molecular weight compounds 28

2.5.5 Charring process (polymerisation) 31

2.5.6 Lignin pyrolysis 32

2.5.6.1 Mechanisms of phenolic monomer and oligomer formations 33

2.5.6.2 Pyrolysis of phenolic monomeric compounds 35

2.5.6.3 Pyrolysis of phenolic dimeric and trimetric compounds 37

2.6 The interactions among cellulose, hemicellulose and lignin during pyrolysis 39

2.7 *Ab initio* thermochemical protocols 42

2.7.1 The Schrödinger equation 42

2.7.2 The Born-Oppenheimer approximation 43

2.7.3 Slater determinants 44

2.7.4 Hartree-Fock theory 44

2.7.5 The electron correlation problem 46

2.7.6 Møller-Plesset perturbation theory 46

2.7.7 Coupled Cluster methods 47

2.7.8 Basis sets 49
2.7.8.1 Gaussian type orbitals 49
2.7.8.2 Pople style and correlation consistent basis sets 50
2.7.8.3 Basis set extrapolation 52
2.7.9 Other energetic contributions 53
2.7.9.1 Relativistic effects 53
2.7.9.2 Spin-orbit coupling 53
2.7.9.3 ZPVE (zero-point vibrational energy) 53
2.7.10 Composite methods 54
2.7.10.1 Gn methods 55
2.7.10.2 W1 theory and W1-F12 theory 59
2.7 Conclusions and gaps 60
2.8 Specific research objectives 61
Chapter 3. Investigation into the Interactions between Cellulose, Hemicellulose, Lignin during Pyrolysis 64
3.1 Introduction 64
3.2 Methodology and experimental details 64
3.2.1 Non-isothermal pyrolysis in TGA 64
3.2.2 Kinetic analysis using the Friedman method 65
3.2.3 Pyrolysis in a fixed-bed reactor 66
3.3 Results and discussion 68
3.3.1 Kinetic analysis 68

3.3.2 Pyrolysis in a fixed-bed reactor 70
3.3.2.1 Yields of pyrolysis gas, liquid and char 71
3.3.2.2 Yields and composition of pyrolysis liquid compounds 73
3.4 Conclusions 76
Chapter 4. Identification and Characterisation of Cellulose Pyrolysis Products 77
4.1 Introduction 77
4.2 Methodology and experimental details 78
4.3 Results and discussion 81
4.3.1 Non-isothermal cellulose pyrolysis in TGA 81
4.3.2 Cellulose pyrolysis in the micropolyser (CDS Pyroprobe) 82
4.3.2.1 Characterisation of cellulose pyrolysis products 82
4.3.2.2 Formation of furfural, levoglucosan and levoglucosenone 85
4.3.3 Cellulose pyrolysis in a fixed-bed reactor 87
4.3.3.1 Yields of pyrolysis gas, liquid and char 87
4.3.3.2 Yields of pyrolysis liquid compounds 88
4.3.3.3 Yields of pyrolysis gas compounds 89
4.4 Conclusions 90
Chapter 5. Unravelling the Formation Characteristics of Cellulose Pyrolysis Products and the Mechanisms of their Transformations 93
5.1 Introduction 93
5.2 Methodology and experimental details 94
5.2.1 Cellulose pyrolysis in a micro fixed-bed reactor 94

5.2.2 Product identification and calibration 96

5.3 Results and discussion 97

5.3.1 Yields of pyrolysis liquid, gas and char 97

5.3.2 Effect of temperature and residence time on the formation of pyrolysis liquid 99

5.3.3 Thermal analysis of cellobiose, levoglucosan, levoglucosenone and DGP 104

5.4 Conclusions 105

Chapter 6. Mechanistic Modelling of Levoglucosenone Formation from Anhydrosugar Intermediates 107

6.1 Introduction 107

6.2 Methodology and computational details 107

6.3 Results and discussion 108

6.3.1 Uncatalysed mechanism for the formation of levoglucosenone 108

6.3.2 Water-catalysed mechanism for the formation of levoglucosenone 115

6.4 Conclusions 117

Chapter 7. Heat of Formation for C_{60} by means of the G4(MP2) Thermochemical Protocol 119

7.1 Introduction 119

7.2 Methodology and computational details 123

7.3 Results and discussion 125

7.3.1 W1h heat of formation for sumanene 125

7.3.2 Heat of Formation of C_{60} 128

7.4 Conclusions 131

Chapter 8. Evaluation and Implications 133

8.1 Introduction 133

8.2 Interactions among cellulose, hemicellulose and lignin during pyrolysis 133

8.3 Identification and characterisation of cellulose pyrolysis products 135

8.4 Formation of cellulose pyrolysis products and their transformations 136

8.5 Formation of levoglucosenone from anhydrosugar intermediates 137

8.6 Application of high-level thermochemical protocols: heat formation of C_{60} 139

8.7 Overall evaluation and implications 140

Chapter 9. Conclusions and Recommendations 141

9.1 Introduction 141

9.2 Conclusions 141

9.2.1 Interactions between cellulose, hemicellulose and lignin during pyrolysis 141

9.2.2 Identification and characterisation of cellulose pyrolysis products 141

9.2.3 Formation of cellulose pyrolysis products and their transformations 142

9.2.4 Formation mechanisms of levoglucosenone 143

9.2.5 Heat formation of C_{60} by means of high-level thermochemical protocols 143

9.3 Recommendations 144

References 146

Appendix A Supporting Information 163

Appendix B Publications 183

LIST OF TABLES

Table 2-1 Variation range of composition of different feedstocks [12] (data on dry basis).....6

Table 2-2 Different types of linkages in lignin.....9

Table 2-3 Bond distribution in softwood and hardwood lignin.....10

Table 2-4 Overview the characteristics of pyrolysis reactors.....11

Table 2-5 Main characteristics of established approaches.....16

Table 2-6 Typical lignocellulose content of plant materials (data on dry basis).....17

Table 2-7 Four temperature zones for cellulose pyrolysis.....18

Table 2-8 Effect of main inorganic minerals on the pyrolysis process..... 错误!未定义书签。

Table 2-9 Temperature regions for lignin pyrolysis reactions.....33

Table 2-10 List of dimers investigated along with a schematic representation of the structures. 37

Table 4-1 Identification of cellulose pyrolysis products at 823 K, 923 K and 1023 K in a micropolyser 84

Table 4-2 Yields and compositions of cellulose pyrolysis products in a fixed-bed reactor at different pyrolysis temperatures 92

Table 5-1 Calibration of pure chemicals using GC-FID/MS.....96

Table 5-2 Yields and composition of cellulose pyrolysis products in a micro fixed-bed reactor 98

Table 5-3 Products yields from pyrolysis of cellobiose, levoglucosenone and DGP.....104

Table 6-1 G4(MP2) Gibbs free energies (ΔG_{298}, kcal•mol^{-1}) for the first step in the competing reaction mechanism proposed by Shafizadeh *et al*. (shown in Figure 6-2).....110

Table 7-1 Experimental ATcT heats of formation at 298 K ($\Delta_f H^\circ 298$) for species involved in reactions 7.2–7.4 and 7.6–7.9 (kJ•mol^{-1}) [309-311].....125

Table 7-2 Component breakdown of the W1h reaction enthalpies and predicted theoretical enthalpies of formation for sumanene (kJ•mol^{-1}). 126

Table 7-3 G4(MP2) reaction enthalpies for reactions 7.4–7.9 and predicted theoretical enthalpies of formation for C_{60} (kJ•mol^{-1})..... 129

Table 8-1 Comparison of the results of the present study and previous studies regarding the interactions between cellulose, hemicellulose and lignin during pyrolysis 134

Table 8-2 Comparison of the results of the present study and previous studies regarding the characterisation of biomass pyrolysis products 135

Table 8-3 Comparison of the results of the present study and previous studies regarding the formation of levoglucosenone..... 138

LIST OF FIGURES

Figure 1-1 Thesis map and how they are related to each other 4

Figure 2-1 Cellulose atomic structure model 6

Figure 2-2 Main hemicellulose components 7

Figure 2-3 Main lignin components: monolignols: paracoumaryl alcohol (1), coniferyl alcohol (2) and sinapyl alcohol (3) 8

Figure 2-4 Scheme of cellulose chain cleave (adapted from [43]) 24

Figure 2-5 Scheme of intra-ring dehydration reaction (adapted from [76]) 25

Figure 2-6 Scheme of inter-ring dehydration reaction (adapted from [77]) 26

Figure 2-7 Scheme of radical-chain decomposition of cellulose (adapted from [83]) 27

Figure 2-8 A schematic illustration of the two possible pathways for the conversion of cellulose to 29

Figure 2-9 Scheme for the conversion of levoglucosenone to DGP proposed by Shafizadeh *et al.* [108]. 30

Figure 2-10 Scheme of levoglucosan fragmentation (adapted from [86]) 31

Figure 2-11 Scheme of cellulose pyrolysis pathway via anhydromonosaccharide (adapted from [87]) 32

Figure 2-12 Scheme of lumped lignin pyrolysis mechanisms (adapted from [101]) 35

Figure 2-13 Scheme of reaction pathways of pyrolysis of lignin oligomeric compound (adapted from [115]) 39

Figure 2-14 Network of research methodology 63

Figure 3-1 A schematic diagram of a fixed-bed reactor setup 66

Figure 3-2 Pyrolysis mass loss and mass loss rate of cellulose, hemicellulose, lignin and sample mixture in a TGA at a heating rate of 30 $K \cdot min^{-1}$ 68

Figure 3-3 The Arrhenius plots for pyrolysis of cellulose, hemicellulose, lignin and sample mixture using the Friedman method 70
Figure 3-4 Plots of activation energy as a function of conversion for cellulose, hemicellulose, lignin and sample mixture 71
Figure 3-5 Yields of gas (a), liquid (b) and char (c) in pyrolysis of cellulose, hemicellulose, lignin, sample mixture and calculated average as a function of temperature in a fixed-bed reactor 72
Figure 3-6 Variations of composition and relative peak areas of pyrolysis liquid compounds as a function of temperature in a fixed-bed reactor 75
Figure 4-1 A schematic diagram of a micropolyser setup 80
Figure 4-2 Cellulose pyrolysis in TGA at heating rate of 3, 15, 60, and 90 K•min^{-1} with a final temperature of 1123 K; (a) TG curves and (b) DTG curves 81
Figure 4-3 The ion chromatograph of cellulose pyrolysis products obtained at 823 K (a), 923 K (b) and 1023 K (c) in a micropolyser 83
Figure 4-4 The ion chromatograms of silyl derivatives of levoglucosan (a), silyl derivatives of cellobiose (b and c), and silyl derivatives of cellulose pyrolysis products obtained at 823 K, 923 K and 1023 K (d) in a micropolyser 86
Figure 4-5 Yields of furfural, levoglucosenone and levoglucosan as a function of pyrolysis temperature in the micropolyser 86
Figure 4-6 Yields of gas, liquid and char from cellulose pyrolysis as a function of temperature in a fixed-bed reactor 87
Figure 4-7 Peak area of anhydro-sugar (a), furans (b), ketones (c), acids (d), aldehydes (e), esters (f), phenols (g) and benzenes (h) as a function of pyrolysis temperature in a fixed-bed reactor 91
Figure 5-1 A schematic diagram of a micro fixed-bed reactor setup 96

Figure 5-2 Yields of pyrolysis liquid (a), char (b) and gas (c) as a function of temperature and residence time in a micro fixed-bed reactor at 823K, 923K and 1023K 97
Figure 5-3 Yields of levoglucosan (a), levoglucosan-furanose (b), DGP (c) and levoglucosenone (d) as a function of temperature and residence time in a micro fixed-bed reactor at 823K, 923K and 1023K 101
Figure 5-4 Yields of furfural (a), 5-methyl furfural (b), 5-HMF (c), acetic acid (d), hydroxyl acetone (e), 2,3-butanedione (f), phenol (g), phenol, 2-methyl (h), phenol, 4-methyl (i) as a function of temperature and residence time in a micro fixed-bed reactor at 823K, 923K and 1023K.....102
Figure 5-5 Effect of residence time and temperature on the formation of pyrolysis liquid compounds ((+): promoted, (-): inhibited).....103
Figure 6-1 Scheme for the conversion of DGP to levoglucosenone proposed.....109
Figure 6-2 Competing reaction mechanism proposed by Shafizadeh *et al.* 110
Figure 6-3 Reaction profile (G4(MP2), ΔG_{298}, kcal•mol^{-1}) for the uncatalysed (bslack line), water- catalysed (blue line), and self-catalysed (red line) conversion of DGP to levoglucosenone.....111
Figure 6-4 B3LYP/6-31G(2df,p) optimised transition structures TS1–TS7 in the reaction profile for the uncatalysed conversion of DGP to levoglucosenone (Figure 6-3). The bonds being broken and formed in the TSs are represented by dashed lines. Atomic color scheme: H, white; C, gray; O, red. The carbon atoms involved in the TSs are labeled in the same way as in Figure 6-1.....112
Figure 6-5 B3LYP/6-31G(2df,p) optimised transition structures TS2–TS6 in the reaction profile for the catalysed conversion of DGP to levoglucosenone. The catalysed reaction profile is shown in Figure 6-3. The bonds being broken and formed in the TSs are represented by

dashed lines. Atomic color scheme: H, white; C, gray; O, red. The carbon atoms involved in the TSs are labeled in the same way as in Figure 6-1. 115
Figure 7-1 B3LYP/6-31G(2df,p) optimised structure of C_{60} and its two basic fragments (a) corannulene ($C_{20}H_{10}$) and (b) sumanene ($C_{21}H_{12}$). 122

Chapter 1. Introduction

1.1 Background

Since the industrial revolution, fossil fuels have been the predominant global energy source. However, increasing consumption of these resources worldwide has created two major problems. First, it is widely agreed that reserves of traditional fossil fuels will run out in the not too distant future. Second, the burning of fossil fuels is the largest source of CO_2 emission, leading to adverse environmental impacts such as global warming. Therefore, it is essential to develop alternative renewable sources of energy to power expanding global economies.

An important candidate for a renewable energy feedstock is biomass. Biomass is inexpensive as it is produced via photosynthesis, in which the plant converts solar energy, CO_2 and water to solid phase biomass. Plants produce over 100 billion tons of biomass carbon per year, which could potentially provide 1.4 times the current global energy consumption [1-4]. More importantly, the utilisation of biomass can be theoretically carbon-cyclical and CO_2 neutral if the biomass is processed efficiently and all the carbon is converted to CO_2. Thus, an effective technique for biomass conversion could contribute to a more secure and sustainable energy supply in the future.

One of the major types of biomass conversion is thermochemical conversion. Thermochemical conversion can utilize energy contained in the non-edible portion of plants and the biomass is converted to energy using three major thermochemical reactions: combustion, gasification and pyrolysis. Pyrolysis is a very important thermochemical process as it can convert all kinds of biomass into fuels and chemicals as well as being a sub-process of combustion and gasification [5, 6]. During pyrolysis, biomass components undergo several simultaneous reactions including dehydration, depolymerisation, fragmentation and condensation. Depending on the

reaction conditions, the products from these reactions can undergo further secondary reactions, including cracking and repolymerisation [7-9]. The products of biomass pyrolysis include liquid, gas and biochar. Liquid and gas products are considered as important fuel sources as they can be used for the production of heat, power and chemicals. However, several drawbacks hinder a further application of these products. Pyrolysis liquid is low in energy density and heating value, and high in moisture content and viscosity whereas the tar component contained in pyrolysis gas could cause block and corrosion of the downstream equipment. In order to improve the quality of pyrolysis products and optimise pyrolysis process, a better understanding of the mechanisms of biomass pyrolysis is required.

1.2 Research aims

The present research aims to develop a better understanding of the mechanisms of biomass pyrolysis by understanding the components' interactions, product formation characteristics and reaction pathways. The detailed objectives are:

- To investigate how the interactions among cellulose, hemicellulose and lignin during pyrolysis affect the pyrolysis process, including reaction kinetics and product formation.
- To identify and characterise the cellulose pyrolysis products generated from reactors at different scales and using different techniques.
- To quantitatively assess the effect of residence time and temperature on the formation of cellulose pyrolysis products and to investigate the mechanism underlying their transformations.
- To investigate the reaction mechanism for the formation of levoglucosenone in cellulose pyrolysis using high-level thermochemical protocols.
- To apply high-level thermochemical protocols to obtain the heat of formation value for Buckminsterfullerene (C_{60}).

1.3 Thesis outline

This thesis has a total of nine chapters as outlined below. The thesis structure is shown in Figure 1-1.

Chapter 1 defines the background, overall aims and the thesis structure.

Chapter 2 reviews the current state of the literature with respect to biomass pyrolysis and outlines the theoretical foundation of high-level thermochemical protocols. Current research gaps are identified and the specific objectives for the present research are stated.

Chapter 3 investigates how cellulose, hemicellulose and lignin interact during pyrolysis, including the effect of interaction on the reaction kinetics and product formation.

Chapter 4 characterises and identifies cellulose pyrolysis products generated from different stages of pyrolysis process.

Chapter 5 quantifies the effects of residence time and temperature on the formation characteristics of cellulose pyrolysis products and investigates the mechanisms underlying their formation.

Chapter 6 investigates the reaction mechanism for the formation of levoglucosenone from DGP in cellulose pyrolysis using high-level thermochemical protocols.

Chapter 7 reports an application of high-level thermochemical protocols in obtaining the heat of formation value for Buckminsterfullerene (C_{60}).

Chapter 8 evaluates the findings from the present research and discusses the implications of these findings for practical processes, along with the new knowledge gaps identified for further research.

Chapter 9 draws conclusions from the present research and provides a set of recommendations for future research.

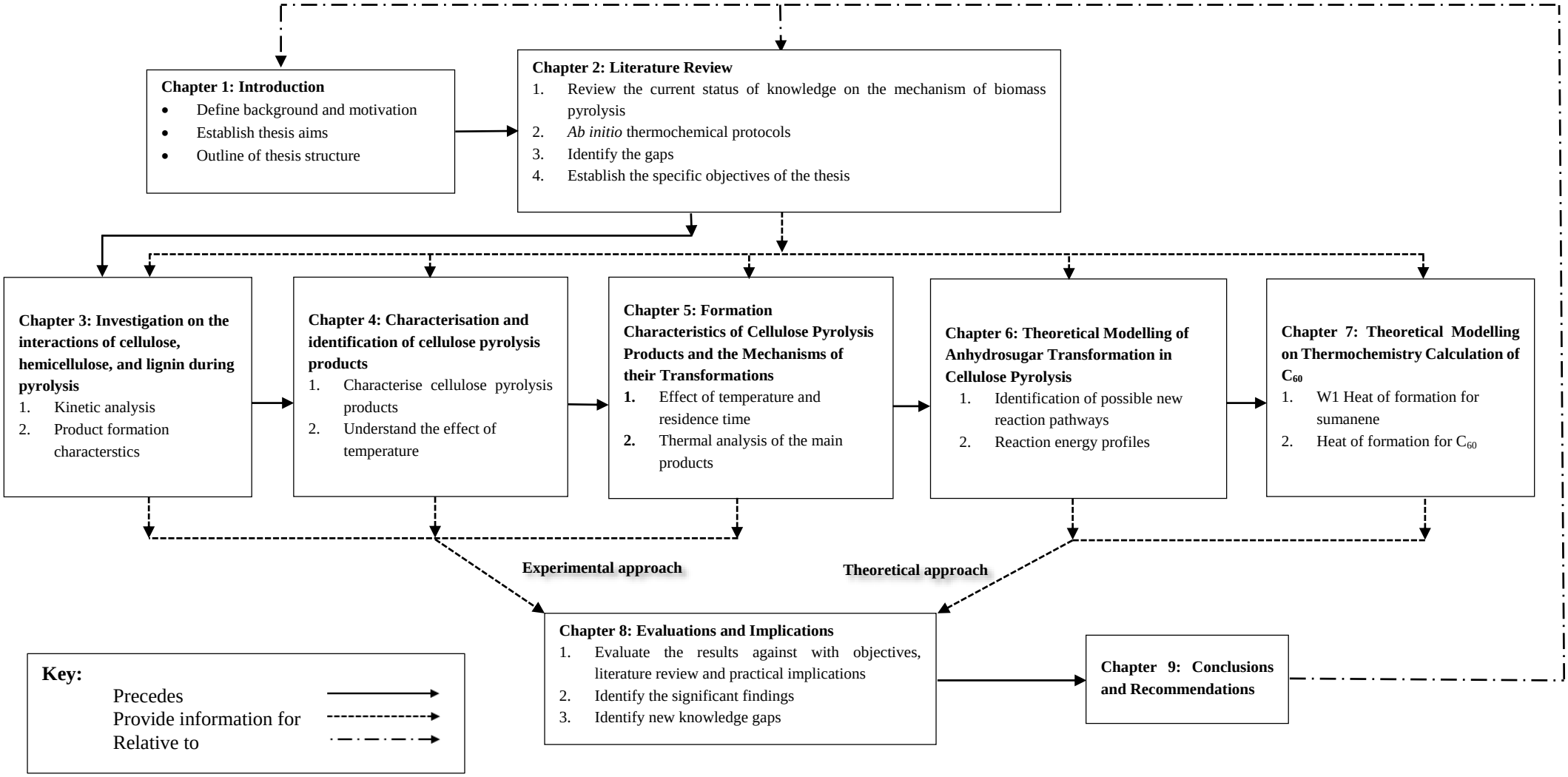

Figure 1-1 Thesis map and how they are related to each other

Chapter 2. Literature Review

2.1 Introduction

Pyrolysis dates back to at least Egyptian times when tar and certain embalming agents were produced by means of pyrolysis of wood [10]. Almost any kind of biomass can be used and upgraded to liquid fuel showing great potential in the production of an alternative renewable energy source. Extensive research efforts have been focused on biomass pyrolysis [13-17]. However, the commercialisation of pyrolysis liquids is still suffering from serial drawbacks, such as low energy values, high viscosity, high density and the problems with long-term storage stability. A key bottleneck to developing an efficient pyrolysis strategy is the lack of an in-depth understanding of the mechanisms of biomass pyrolysis at the molecular level. This thesis aims at characterising the products from biomass pyrolysis and looking into the mechanisms of their interactions and transformations. Before stepping into that level, this chapter first reviews the properties of biomass and its building blocks. A detailed description on pyrolysis process and pyrolysis reactor is presented. The characterisation of pyrolysis products and the key factors that influence their formation are discussed in the following section. Next, Chemistry and reactions in biomass pyrolysis are introduced. *Ab initio* thermochemical protocols, the theoretical approach for mechanism investigation is then reviewed. Finally, key research gaps are identified and research objectives are established.

2.2 Structures and main characteristics of biomass

2.2.1 Lignocellulose

The structure of lignocellulose material spans eleven orders of magnitudes (10^{-10} to 10^{1} m) from bonds, cell, fibres to tree [11]. The major biopolymers are cellulose, hemicellulose and lignin. Cellulose is the major structural component in the primary cell wall while micro-fibrils are formed by the cellulose chain,

connected with hydrogen bonds. Hemicellulose intersects with pectin, forming a network of cross-linked fibers. Lignin provides strength to the cell, filling the space in the cell wall.

In Table 2-1, the range and content of typical lignocellulose content are given based on the different types of feedstock [12].

Table 2-1 Variation range of composition of different feedstocks [12] (data on dry basis)

Feedstock	Cellulose (%)	Hemicellulose (%)		Lignin (%)
		Hexoses	Pentoses	
Softwood	40-48	12-15	7-10	26-31
Hardwood	30-43	2-5	17-25	20-25
Cereal Straw	38-40	2-5	17-21	6-21
Maize Straw	35-41	2	15-28	10-17
Rape Straw	38-41	n/a	17-22	19-22
Recovered Paper	50-70	n/a	6-15	15-25

2.2.2 Cellulose

Cellulose is the most common compound on Earth and the most abundant biopolymer synthesized by nature, approximately 10^{11} tons per year [12]. Cellulose is an important structural component of the primary cell wall of green plants and algae. Cellulose is mainly used to produce paperboard and paper.

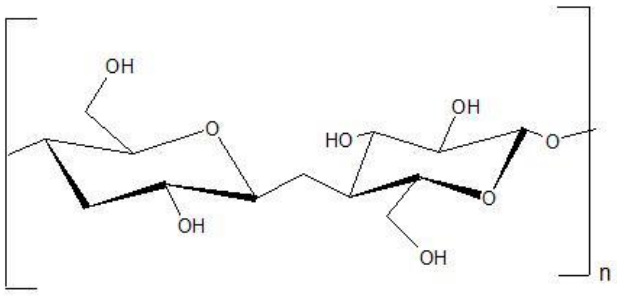

Figure 2-1 Cellulose atomic structure model

Cellulose is a linear polymer of D-glucopyranose units linked with together by β-1,4-glycosidic bonds as shown in Figure 2-1 [13]. The D-glucopyranose units are connected to form long, straight chains of 5000 – 10000 units which vary according to the sources of biomass [10, 14]. The multiple hydroxyl groups in each unit forms intramolecular and intermolecular hydrogen bonds within the same cellulose chain or a neighbor chain, leading to formation of a crystalline supermolecular structure. Due to its crystalline structure and degree of polymerisation, microcrystalline cellulose is completely insoluble in normal aqueous solutions. The configuration of cellulose makes it more resistant to thermal degradation than hemicellulose.

2.2.3 Hemicellulose

Hemicellulose is the second major component in biomass, which presents along with cellulose in almost all plant cell walls [15]. While cellulose is strong and crystalline, the structure of hemicellulose is amorphous and randomly arranged with little strength.

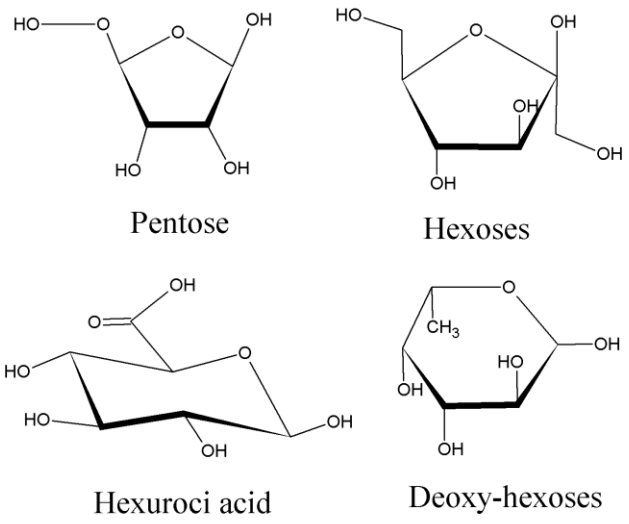

Figure 2-2 Main hemicellulose components

Hemicellulose is a mixture of various polymerised monosaccharides which can be divided into four general classes of structurally different cell-wall polysaccharide types, including xylans, mannans, β-glucans with mixed linkages and xyloglucans [16]. The main components are shown in Figure 2-2 [13]. The length of the chain of hemicellulose is in the order of 150 compared with 10^4 of cellulose and the chain sometimes presents side-chain branches while cellulose is unbranched. Hemicellulose is thermally less stable than cellulose.

2.2.4 Lignin

Lignin is the third major component in biomass which fills spaces in the cell wall between cellulose, crosslinking different polysaccharides and conferring mechanical strength to the cell wall [17].

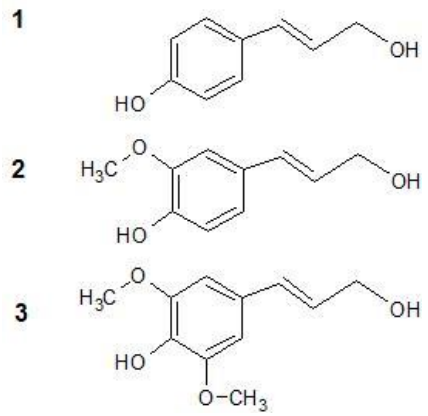

Figure 2-3 Main lignin components: monolignols: paracoumaryl alcohol (1), coniferyl alcohol (2) and sinapyl alcohol (3)

Lignin is a cross-linked racemic macromolecule with molecular weight over 10000u. There are three monolignol monomers, methoxylated to various degrees: *p*-coumaryl alcohol, coniferyl alcohol, and sinapyl alcohol. These monolignols shown in Figure 2-3 [17] are incorporated into lignin in form of the phenylpropranoids p-hydroxyphenyl (H), guaiacyl (G) and syringyl (S), respectively. The degree of polymerisation in nature is difficult to measure, since it is fragmented during extraction. The

heterogeneous nature of lignin and its strength is also reflected in its thermal stability as lignin reacts over a much broader range of temperature.

Klein described the structure of lignin as groups of single-rings aromatics with two attributes. The first is the type of propanoid side chain attached to the aromatic ring [18]. The second is the number and position of methoxyl groups attached to the aromatic ring [19].

Table 2-2 Different types of linkages in lignin

Model	Glasser et al. [20]	Erickson et al. [21]	Nimz et al. [22]
Linkage per C9 Units			
β carbon-oxygen-4 aromatic carbon	55	49-51	65
α carbon-oxygen-4 aromatic carbon		6-8	
β carbon-5 aromatic carbon	16	9-15	6
β carbon-1 aromatic carbon	9	2	15
5 aromatic carbon-5 aromatic carbon	9	9.5	2.3
4 aromatic carbon-oxygen-5 aromatic carbon	3	3.5	1.5
β carbon-β carbon	2	2	5.5
β carbon-β carbon forming a furanic structure	N/A	N/A	2
α and γ carbon-oxygen-γ carbon	10	N/A	N/A
α carbon-β carbon	11	N/A	2.5
β carbon- 6 aromatic carbon	2	4.5-5	N/A
6 aromatic carbon-5 aromatic carbon	1-5	N/A	N/A
1 aromatic carbon-oxygen-4 aromatic carbon	N/A	N/A	N/A
1 aromatic carbon-5 aromatic carbon	N/A	N/A	N/A
Total	118-123	85.5-96	99.8

The most common types of linkages in softwood lignin are presented in Table 2-2, while a brief comparison between softwood lignin and hardwood lignin [23] is shown in Table 2-3. The complexity of monomers indicates the heterogeneity of lignin and the difficulties in understanding its structure [24].

Table 2-3 Bond distribution in softwood and hardwood lignin

Type of linkage	Softwood lignin	Hardwood lignin
Arglycerol-β-aryl ether (β-O-4)	46	60
Phenylcoumaran (β-5)	11	6
Noncyclic benzyl aryl ether (α-O-4)	7	7
Biphenyl (5-5)	10	5
Diaryl ether (4-O-5)	4	7
1,2-Diarylpropane (β -1)	7	7
Resinol (β - β)	2	3
Others	13	5

2.3 Biomass pyrolysis

2.3.1 Pyrolysis

Pyrolysis is an irreversible thermochemical decomposition of biomass at elevated temperatures under very deficient oxygen conditions which involves multiphase changes such as gas phase diffusion and thermal conduction [25]. This process generally produces numerous chemical products in the form of pyrolysis volatiles and solid residue. The condensation of pyrolysis volatiles yields dark brown colored liquid called pyrolysis liquid. The non-condensable portion of pyrolysis volatiles consists of gaseous products such as CO, CH_4, H_2 and CO_2. Solid residue produced from pyrolysis is called as biochar which is formed through repolymerisation and dehydration reactions.

2.3.2 Pyrolysis reactors

Depending on the heating rate, pyrolysis technologies can be categorised into two groups: conventional pyrolysis and fast pyrolysis.

Table 2-4 Overview the characteristics of pyrolysis reactors

Reactor Type	Heat Transfer Rate	Mode of Operation	Heating Medium	Particle size	Pyrolysis oil yield
Fixed-bed	Slow	Batch	Furnace surface and gas	Chips, Fine particles	66 wt.%
Bubbling fluidised-bed	Fast	Continuous	Sand and gas	Fine particles	75 wt.%
Circulating fluidised-bed	Fast	Continuous	Sand and gas	Fine particles	75 wt.%
Rotary kilns	Slow	Continuous	Furnace surface and gas	Large particles	45 wt.%
Rotating cone	Fast	Continuous	Furnace surface, sand and gas	Chips, fine particles	70 wt.%
Cyclone reactor	Fast	Continuous	Furnace surface and gas	Fine particles	74 wt.%
Ablative reactor	Fast	Continuous	Furnace surface	Large particles	75 wt.%
Auger screw		Continuous	Furnace surface	Fine particles	51 wt.%
Entrained flow	Fast	Continuous	Furnace surface and gas	Fine particles	60 wt.%

Conventional pyrolysis is typically used to modify solid material and minimize oil and gas yields. Normally conventional pyrolysis occurs with temperatures, residence time and heating rate ranging from 673 to 773 K, 5 to 30 min and 10K•min^{-1} to 10K•s^{-1}, respectively. In conventional pyrolysis, the heating rate can be as low as 10 K•min^{-1}. Such a process is mainly utilized for char production. During slow heating, the residence time could be as long as 30 minutes, which enhances the secondary reactions in the vapor phase.

The initial fast pyrolysis research was carried out at the University of Waterloo (1979-1985), where an atmospheric fluidised-bed reactor was developed [26]. Since then, various reactors have been developed for fast pyrolysis to optimise the pyrolysis process and improve the quality of products. Each reactor has its own characteristics (as illustrated in Table 2-4). The advantages and limitations are also discussed as followed.

Fixed-bed reactor

The fixed-bed reactor system consists of a reactor with a fixed bed of feedstock and a condensation system for product sampling [27]. This technology is simple, reliable and has proven effective for biomass feedstock with uniform particle size. This type of reactor is mainly used for small-scale heat and power application. The main limitation of fixed-bed reactor is its batch nature.

Bubbling fluidised-bed reactor

Bubbling fluidised-bed reactor is one of the most popular configurations for biomass pyrolysis both in the laboratory and in industry. Fluidised-bed contains a fluidisation vessel, a continuous feeder system, solid discharge, dust separator, gas distributor and gas supply [28]. The feedstock particles are fed into

the fluidised-bed at the bottom and travel through the heated inorganic particles-often sand. Bubbling fluidised-bed reactor enables a better control of temperature and vapour residence time, provides high heat transfer rate, good solids-to-gas contact and storage capacity. After pyrolysis, the char is removed by a cyclone separator and the vapour is condensed by a quenching system. Small biomass particle size (less than 2-3mm) is required by bubbling fluidised-bed reactors to achieve high biomass heating rates.

Circulating fluidised-bed reactor

Circulating fluidised-bed reactors (CFBs) are very similar in operation to bubbling fluidised-bed reactors. However, CFBs employ a second fluidised-bed unit to combust the char contained in the inorganic heat carrier to produce heat which could provide heat to the first fluidised-bed unit for pyrolysis reaction [29]. CFBs are particularly useful when the inorganic heat carrier has catalytic effects that cause the char to adhere to the catalyst surface.

Rotary kilns

The basic components of a rotary kiln are the shell, the refractory lining, support tyres and rollers, drive gear and internal heat exchangers [30]. The kiln is a cylindrical vessel, which rotates slowly about its axis. The feedstock is fed into the upper end of the cylinder and gradually moves down towards the lower end with a certain amount of mixing and stirring.

Rotating cone reactor

In the rotating cone reactor, biomass particles mixed with inorganic heat carriers are injected into the bottom of the reactor which rotates at a high rpm. The centrifugal force moves the solids toward the lips

of the cone, enabling a better heat transfer between heat carrier and biomass particles. Pyrolysis vapours are normally directed to a condenser whereas the char and sand are sent to a combustor [31].

Cyclone reactor

Cyclone reactor, used worldwide for gas-solid separation, is also employed for pyrolysis reactions. The particles enter tangentially into the reactor and then flow against the heated wall where they are heated and pyrolysed. The solid residues are collected at the bottom while the vapour and gas leave the reactor at the top [32, 33].

Ablative reactor

Compared to other reactors, the ablative reactor is substantially improved in terms of heating methods. In the ablative reactor, the biomass particles are heated from the hot reactor wall and become "melting" under pressure in contact with reactor surface. The biomass particles are then moved away mechanically and pyrolysis vapours are condensed in a quenching system. The advantage of this reactor is that it doesn't require an excessive grinding and it allows larger particles than the fluidised-bed reactors [34].

Auger screw reactor

In auger screw reactor, biomass feedstock is moved by auger and passes through a heated tube whereby the feedstock is pyrolysed. The pyrolysed vapours are drawn off into a condenser system to form liquid and the auger transports the char to the end for collection [35]. The design of this reactor provides a good control of biomass residence time and has little or no gas carrier requirements but the mechanical maintenance of wear and tear could be complex.

Entrained flow reactor

In entrained flow reactor, biomass particles entrained in the carrier gas are down-fed into the reactor tube [36]. Heat transferred from the reactor tube's walls and carrier gas pyrolyses the biomass particles as they flow along the tube. With the particles sufficiently separated in the carrier gas, a better heat transfer and a higher heating rate can be achieved [37]. The pyrolysis vapours are collected in a condensation system in which pyrolysis liquid is formed.

2.4 Identification and characterisation of pyrolysis products

2.4.1 Established methodology and approaches

Researchers have developed various analytical techniques to study the biomass decomposition reactions and analyse the pyrolysis products. Van Passen *et al.* proposed a guideline for tar sampling and analysis consisting of gas preconditioning, particle filter, tar collection, and volume metering which is accepted as "European Tar Protocol" [38]. However, this method could only collect the final products as it is not the real-time analysis. A molecular beam mass spectrometry (MBMS) has been developed, observing three groups of pyrolysis products: primary products from vaporisation from biomass, secondary products depolymerised from the primary products, and polycyclic aromatic hydrocarbons [39]. Although this technique could offer a real-time detection, the amount of molecule fragments generated by electron ionisation makes it difficult for the identification and separation of specific products [40]. Some online optical measurement techniques have also been developed. G. Di Nola integrated a heated wire mesh reactor with an in-situ FTIR spectrometry, carrying out simultaneous detection for gaseous products [41]. Laser-induced fluorescence (LIF) measurement was used to provide both spectrally-resolved and time-resolved data of pyrolysis volatiles [42]. Nevertheless, the spectra were so complicated that only limited information about certain functional groups could be speculated.

Table 2-5 Main characteristics of established approaches

Measurement method	Measurement way	Advantages	Disadvantages
Tar protocol	Offline	Pyrolysis oil can be thoroughly trapped by condensation.	Cannot give any information on any individual compound.
MBMS	Online	Real-time analysis: time-dependent mass spectrum.	Electron ionisations causes too many fragments of molecules.
FTIR	Online	Real-time analysis: infrared spectrum of absorbance or transmittance.	Hard to determine the unknown compounds only with information of functional groups.
LIF	Online	Fluorescence spectrum.	Hard to determine the unknown compounds only with information of functional groups.
GC/MS	Offline	Separation of the mixture and corresponding mass spectrum.	Long-time separation makes it hard to identify intermediates.
SVUV MS	Online	Fragment-free mass spectrum.	Certain species' IEs are unknown or too close to distinguish.
EPR	Offline	EPR spectrum of radicals	Hard to determine the unknown compounds only with information of functional groups.

A. Dufour used GC/MS to quantify the products from wood chips pyrolysis, observing a linear relations between the molar production of between CH_4 and all quantified tars [43]. Although gas chromatography is an effective method to separate and identify the final products of biomass pyrolysis, the long-time separation hinders our recognition of the unstable intermediates. A. Dufour *et al.* recently applied synchrotron vacuum ultraviolet photoionisation mass spectrometry (SVUV MS) which could provide fragment-free mass spectra under different ionisation energies (IEs) to cellulose pyrolysis, proposing a new intermediate compound to be the precursor of furanone-based species [44]. However, as the ionisation energies of certain compounds are either too close to each other or unknown, not all

intermediates and final products could be determined using this technique. Wang *et al.* [45] studied the effect of temperature on the EPR properties of oil shale pyrolysate. Thermal bitumen was found to be the intermediate product in the oil shale pyrolysis process.

2.4.2 Effect of operating parameters on pyrolysis process

The mechanism of pyrolysis reactions are influenced by various operating variables, such as raw material, temperature, pressure and heating rate. The effects of these factors on pyrolysis process are summarised as followed.

Table 2-6 Typical lignocellulose content of plant materials (data on dry basis)

Plant material	Cellulose	Hemicellulose	Lignin
Orchard grass[10]	32.0	40.0	4.7
Rice straw[10]	34.0	27.2	14.2
Birchwood[10]	40.0	25.7	15.7
Poplar[12]	31.0	43.0	23.0
Oak[12]	32.0	35.0	26.0
Wheat straw[12]	37.0	32.0	18.0
Cotton[46]	0.8	91.2	0.4
DDGS[47]	13.5	16.0	N/A

Raw materials

A considerable amount of research efforts have been undertaken to investigate the pyrolysis reactions with different raw materials including chicken litter, corn stalk, pine wood, poplar, switch grass, etc. [48-54]. From Table 2-6 where typical lignocellulose contents of some plant materials are shown, we can see that the proportion of cellulose, hemicellulose and lignin is around 80%. Current research suggests

the speciation of the pyrolysis products doesn't change much whereas the product distribution [26] did vary depending on the properties of raw materials.

Temperature

Another key factor influencing the pyrolysis mechanism is temperature. Various reactions such as polymerisation, dehydration and decarboxylation could be involved in different temperature regions. For instance, in cellulose pyrolysis, Tang and Bacon [55] classified the cellulose pyrolysis mechanism based on the following four temperature zones.

Paul and Besler [56] investigated the effect of temperature on pyrolysis in a static batch reactor, showing that as the pyrolysis temperature increased, the percentage mass of solid char decreased, while gas and liquid products increased. The conventional viewpoint is that biomass pyrolysis with the temperature over 673K could maximise the yield of pyrolysis liquid.

Table 2-7 Four temperature zones for cellulose pyrolysis

Temperature range	Reaction zones
298-423K	Physical desorption of water
423-513K	Dehydration from cellulose unit
513-673K	Thermal cleavage of the glycosidic linkage and scission of other C-O bonds and some C-C bonds via a free radical reaction
673K	Aromatisation

At the molecular level, SVUV PIMS was employed to study the pyrolysis of pine wood and poplar [48, 49]. The mass spectra at different photo energies, temperature, and time-evolved profiles of selected species during the pyrolysis process were measured. For pyrolysis of pine wood, as pyrolysis temperature

increased from 573 to 973 K, a decrease of oxygen content in high molecular weight species was observed as high molecular oxygen content products are easier to undergo thermal degradation. In poplar pyrolysis, it was observed that as pyrolysis temperature increased from 573 to 973 K, syringyl subunits of lignin underwent an increase firstly and then a decrease whereas guaiacol subunits decreased continuously.

Pressure

Pressure has a profound impact on biomass pyrolysis. William and Michael reported that high pressure and low flow rate decreased the heat of pyrolysis and thus promoted the char formation [57, 58]. They further proposed that the char was not produced through primary reaction. The same promotion of char formation was also observed when Ramesh V. Pindora, et al [59] studied the pyrolysis of eucalyptus using a two-stage fixed-bed reactor. With increasing pressure, pyrolysis products were observed to become more aromatic and less oxygenated.

Heating rate

Heating rate is another important parameter. However, it is so hard to define the real heating rate and temperature within the reactant particles so that we normally use the external heating rate and temperature instead.

The variation of heating rate was found to affect the formation of pyrolysis products. The effect of heating rate on the yields of pyrolysis products was studied in a static batch reactor [56]. The result showed that higher heating rates led to lower yields of char and higher yields of gaseous and liquid products. A more detailed study using CDS-Pyroprobe was performed to understand the influence of heating rate on each compound formed during the pyrolysis process. Twenty-eight compounds were

quantified while phenols and toluene concentrations was found to increase with the increase of pyrolysis temperature. The quantity of each compound was affected by heating rate [60]. Thermogravimetric analysis on pyrolysis was conducted using TGA-DSC. It was found that the increase in heating rate led the peaks of DTG curve to higher temperatures [61]. And the production of aromatic fragments was found to be favored by a synergistic relationship with high heating rate [62].

Heating rate also affects product properties. Brunner and Roberts [63] reported that a low heating rate enhanced microscope volume, surface area and the density of char in the expense of the O/C ratio. All those research findings indicated that heating rate plays an important role in pyrolysis.

Residence time

Residence time is a very important factor that influences the pyrolysis process. A shorter residence time is believed to suppress the secondary reactions [64-66] as the primary volatiles are rapidly quenched after they are released from sample particles. A longer residence time could increase the chance of the interactions within pyrolysis products [9].

Many researchers [9, 67, 68] have found that a longer residence time (normally from 1s to 1 min) could contribute to promoting the secondary reactions, which lead to a lower yield of pyrolysis liquids and a higher yield of gaseous products. Lin *et al.* [69] proposed a kinetic model based on the results of cellulose pyrolysis using a Pyroprobe. The kinetic model is consisted of the formation of levoglucosan, isomerisation of levoglucosan into other anhydrosugars, oligomerisation of anhydrosugars into oligomers and decomposition of anhydrosugars. However, the residence time in Pyroprobe system could be several seconds or even longer which makes it hard to be controlled. Recently D.K Shen et al [70] studied the cellulose pyrolysis product distribution in a fluidised-bed reactor with residence time ranging

from 0.44s to 1.32s and found that a part of 5-hydroxymethyl furfural is generated from the levoglucosan degradation which led to the production of furfural. Patwardhan *et al.* claimed [9] that oligomerisation of levoglucosan and decomposition of 5-hydroxymethyl furfural and 2-furaldehyde were the major secondary reactions occurring in the fluidised-bed reactor when the residence time was around 1s. This result was based on the difference of the yields of cellulose pyrolysis products in a micropyrolyser and a fluidised-bed reactor as the latter one has a longer residence time. It should be noted that this variation in product yields might also be caused by the difference of reactor configurations and feedstock particle sizes rather than the difference of residence time [7].

Particle size

Particle size is also an essential factor in the pyrolysis process. A larger particle could hinder the process of heat transfer and mass transfer while a smaller particle could enable the transfer process to be completed in transient.

Researchers have employed various methodologies [71-73] to study the effect of particle size (normally a range from 0.18-5.00 mm) on biomass pyrolysis process. It was found that as particle size increased, a decrease in the formation of gaseous products was observed with an increase in the formation of char and pyrolysis liquids. The effect of particle size on the pyrolysis products from biomass was not as significant as the pyrolysis of coal and oil shales when particle size exceeds certain threshold [72].

2.4.3 Effect of extractives and inorganic minerals on pyrolysis process

In biomass, there are some amounts of extractives. Extractives are non-structural components as they do not constitute cell walls or cell layers. The extractive in lignocellulosic biomass mainly includes resins, fats, waxes, sugars, tannins, etc. The amounts of extractives mainly depends on the type of biomass and

its location of the plant. However, the extractives did have considerable impact on the pyrolysis process when extractive-rich biomass is being pyrolysed.

Table 2-8 Effect of main inorganic minerals on the pyrolysis process

Inorganic minerals	Effects
Na^+	NaCl accelerated the decomposition of carbohydrate to small fragmented molecules [74] and suppressed the formation of levoglucosan [75].
K^+	KCl reduced the activation energy up to 50kJ•mol^{-1} [76] and suppressed the formation of levoglucosan [77].
Ca^{2+}	$CaCl_2$ favoured the formation of furans and levglucosenone and has less inhibition of levoglucosan formation than K^+ and Na^+ [78].
Mg^{2+}	$MgCl_2$ suppressed the formation of glycolaldehyde but favoured 5-hydroxymethylfurfual and levoglucosenone [78] while dramatically improving dehydration reactions [79].
Zn^{2+}	Zn^{2+} catalysed the breakdown of C-C and C-O bonds and promoted the formation of char and gas at the expense of liquids [80, 81].
Fe^{3+}	Fe3+ catalysed the conversion of cellulose into anhydrosugars [82].

It was found that the presence of extractives assisted the decomposition process. The activation energy for pyrolysis of raw Mongolian pine and Manchurian ash were 104 kJ•mol^{-1} and 85kJ•mol^{-1}, respectively while the activation energy increased to 119 kJ•mol^{-1} and 109 kJ•mol^{-1} after removing extractives [83]. The formation of pyrolysis products were also influenced by the presence of extractives [84, 85]. The increase of extractive content improved the yields of liquids and lowered the yields of char and gas. For

liquids, higher extractive contents lead to higher yields of levoglucosan and furans. For gas, lower extractive contents leads to higher yields of CO_2, CO, and aldehydes, and lower yields of acids and alkanes.

Inorganic minerals are another important species in lignocellulosic biomass, which mainly include calcium, sodium, magnesium, phosphorous, sulphur, chlorine, etc. Table 2-8 gives a brief summary on the effect of main inorganic minerals (Na, K, Ca, Mg, Zn, and Fe) on the pyrolysis process.

2.5 Chemistry and reactions in biomass pyrolysis

2.5.1 Depolymerisation

In cellulose pyrolysis, the depolymerisation process is a cleavage of 1, 4-glycosidic bond through a homolytic or heterolytic process which occurs at the very beginning of cellulose pyrolysis. Typically, the degree of polymerisation (DP) of cellulose ranges from 2000 to 4000. After depolymerisation, DP is decreased and smaller molecules are generated [86]. It has been observed that DP reached 200-400 before any noticeable weight loss. The substantial decrease in DP suggested that cellulose was decomposed into "cellulose" with a lower degree of polymerization which is called as "active cellulose" in the literature [87].

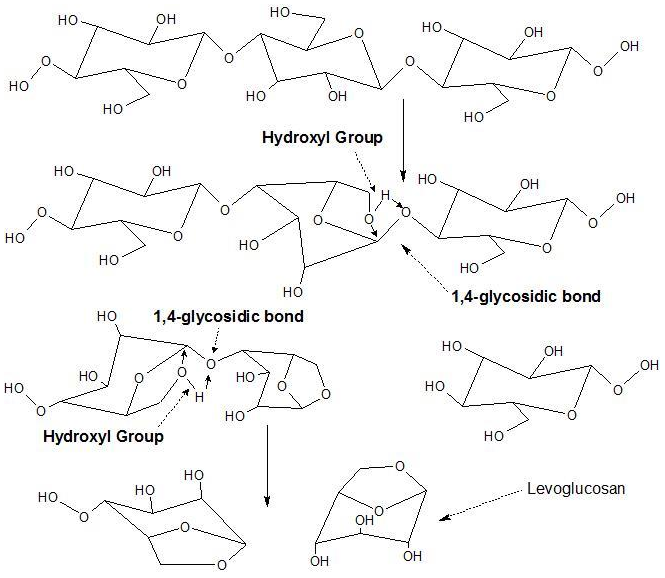

Figure 2-4 Scheme of cellulose chain cleave (adapted from [43])

An example of depolymerisation is transglycosylation for the generation of anhydrosugars. The 1, 4-glucosidic bond is presumably cleaved by the acetal reaction between C-1 and C-6, evolving the hydroxyl radical from C-6, then the free hydroxyl radical coalesces with the disrupted glucosidic bond on C-4 to form levoglucosan [39]. The free hydroxyl radicals and chemical structure rearrangement is similarly initiated among other anhydrous hexoses, such as anhydro-D-mannose and 1, 6-anhydro-glucofuranose. A detailed scheme is shown in Figure 2-4.

In hemicellulose pyrolysis, when temperature ramps to around 525K, the glycosidic linkages between monomers become very unstable which leads to depolymerisation and the formation of different anhydrosugars and furan derivatives. In the pyrolysis of glucomannan, it can be found that levoglucosan, levomannosan and levogalactosan are produced [88, 89] whereas in the pyrolysis of xylan, anhydroxylopyranose, dianhydro xylopyranose are detected. Several reaction pathways which are similar to cellulose depolymerisation were proposed [90]. It should be noted that in the pyrolysis of xylan,

the xylosyl cation cannot lead to the formation of a stable anhydride due to the absence of C-6 and O-4. Under this circumstance, the xylosylcation could undergo subsequent glycosidic bond cleavage and dehydration to form dianhydro xylopyranose [91].

2.5.2 Dehydration reactions

In cellulose pyrolysis, dehydration reactions refer to the chemical loss of water occurring from 493 to 823 K, while physical loss of water happens when temperature is below 493K [92]. According to Broido [93], dehydration is the first reaction in the degradation of cellulose and leads to the formation of anhydrosugars. The dehydration can be categorised into two kinds, namely intra-ring and inter-ring dehydration.

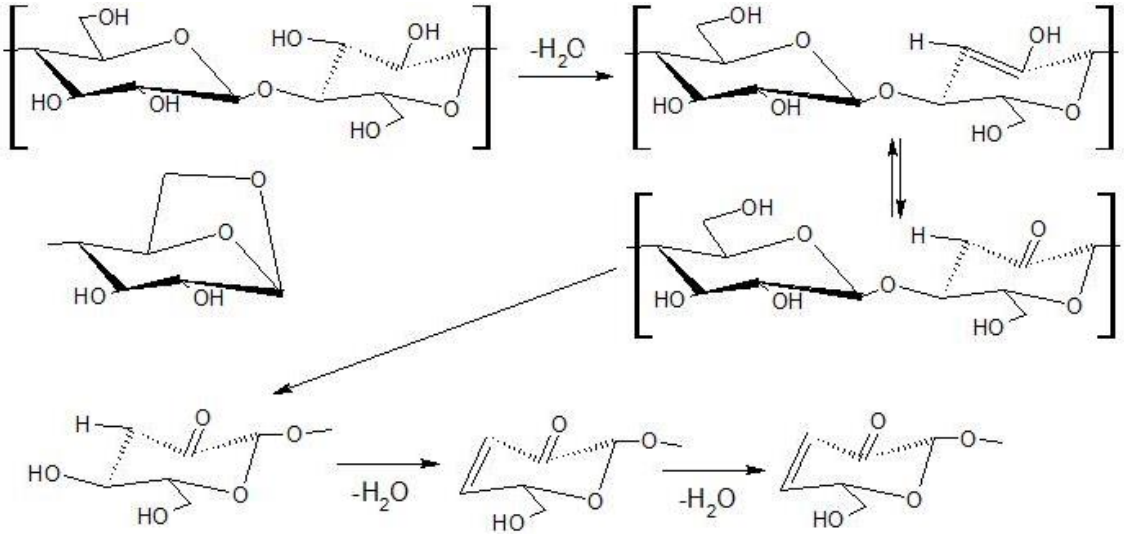

Figure 2-5 Scheme of intra-ring dehydration reaction (adapted from [76])

Figure 2-5 shows the pathways of the intra-ring dehydration which occurs at the –OH group on C-3 and leads to unsaturation within the pyranose ring or a ketone species [92]. Figure 2-6 shows the pathways of inter-ring dehydration proposed by Klizer and Broido [93]. The inter-ring dehydration is believed to

the dominant pathway over the intra-ring dehydration and in part responsible for the formation of cross-linked structures and furanic ends.

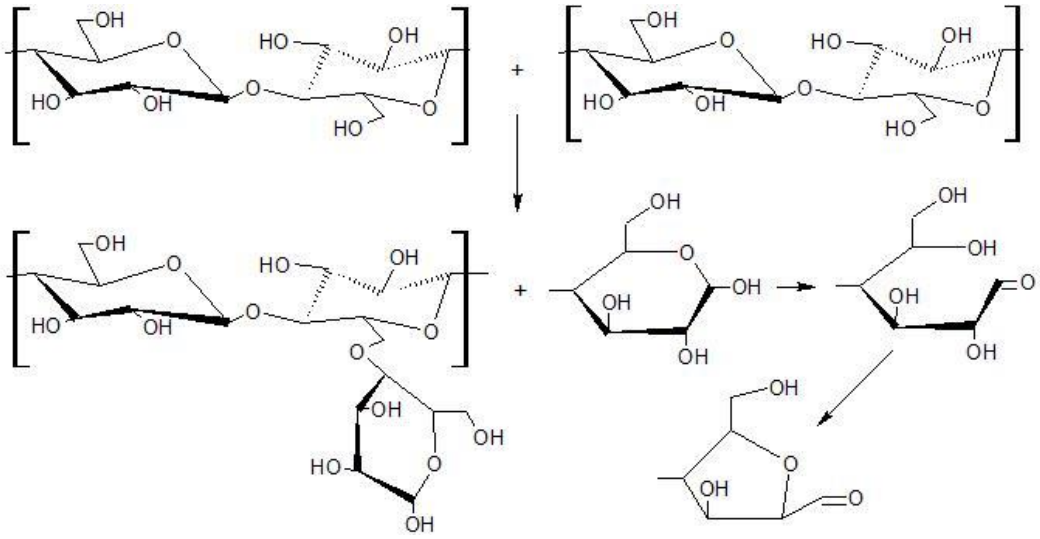

Figure 2-6 Scheme of inter-ring dehydration reaction (adapted from [77])

In hemicellulose pyrolysis, the release of H_2O became significant at 473K [94, 95]. A theoretical calculation of the water production suggested that about 15 wt.% was produced during hemicellulose pyrolysis. However, it is not possible to find any proposed reaction pathways of dehydration in hemicellulose pyrolysis.

2.5.3 Formation of levoglucosan

Levoglucosan is the major product from cellulose pyrolysis [82]. The formation of levoglucosan has attracted numerous research efforts. Two hypotheseses were proposed to understand its formation: (1) subsequent dehydration after complete depolymerisation of carbohydrates, and (2) initial partial depolymerisation. If levoglucosan was formed via subsequent dehydration, the pyrolysis glucose should produce a higher yield of levoglucosan. However, a wide range of experimental results of carbohydrates

pyrolysis showed that it was not the case [83, 226, 227]. Therefore, it is believed that levoglucosan was produced during depolymerisation.

Different mechanisms were proposed based on the experimental results focusing internal unit cleavage and chain decomposition. In one proposed mechanism, a hydrolysis step was needed to form the non-reducing levoglucosan end unit. Yet, water was found to promote cross-linking reactions to generate more char and other cross-linked products rather than levoglucosan. This mechanism might be a source of levoglucosan in the low temperature region, in which both inter- and intra- ring dehydration are active [96].

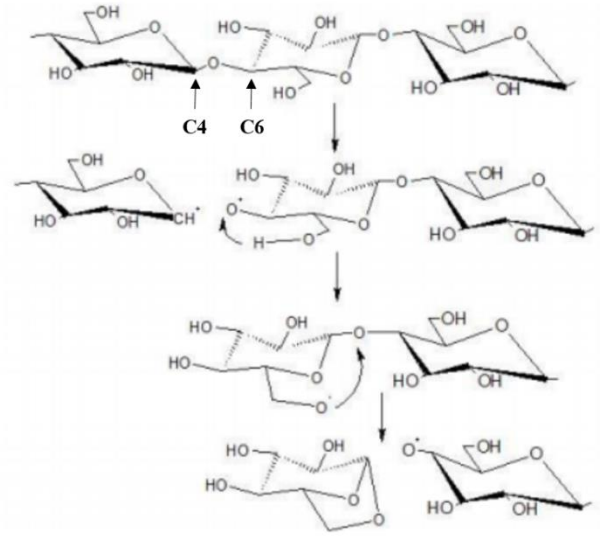

Figure 2-7 Scheme of radical-chain decomposition of cellulose (adapted from [83])

As levoglucosan is considered to be generated during the depolymerisation, Golova [97] suggested another radical mechanism (shown in Figure 2-7), which starts from an active end of cellulose chain and consequently splits off the cellulose unit to form levoglucosan until the whole chain was decomposed. In this scheme, an active end at C-4 produced by cleavage was transferred to C-6, which later weakened

the glycosidic bond and thus tore the cellulose unit off to form the levoglucosan, transferring the active end to the adjunct unit in the cellulose chain. Recently, Mayes and Broadbelt [98] used density functional theory methods and implicit solvents to compare the likelihood of forming either radical or ionic intermediates.

2.5.4 Formation of levoglucosenone

The formation of levoglucosenone during pyrolysis has been studied both theoretically and experimentally [99-106]. However, the molecular mechanisms underlying the formation of levoglucosenone during pyrolysis of cellulose and biomass are still largely unknown. A number of precursors for the formation of levoglucosenone were proposed and investigated [99, 101, 102, 107]. In an early experimental study it was suggested that levoglucosan is a precursor of levoglucosenone [99]. More recently, Assary and Curtiss [101] proposed a detailed scheme of reaction pathways for the conversion of levoglucosan to levoglucosenone using density functional theory (DFT) and high-level *ab initio* procedures. They found that a water molecule could catalyse this transformation with an activation barrier of $\Delta H^{\ddagger}_{298}$ = 56.6 kcal mol^{-1} at the G4 level. Qiang Lu *et al.* studied the reaction pathways for the formation of levoglucosenone from *β*-D-glucopyranose and cellobiose at the B3LYP/6-31+G(d,p) level of theory [102]. They found that the enol-to-keto tautomerisation is the rate-determining step (RDS) both from *β*-D-glucopyranose and cellobiose with barriers of $\Delta H^{\ddagger}_{298}$ = 69.5 kcal mol^{-1} and $\Delta H^{\ddagger}_{298}$ = 62.7 kcal mol^{-1}, respectively.

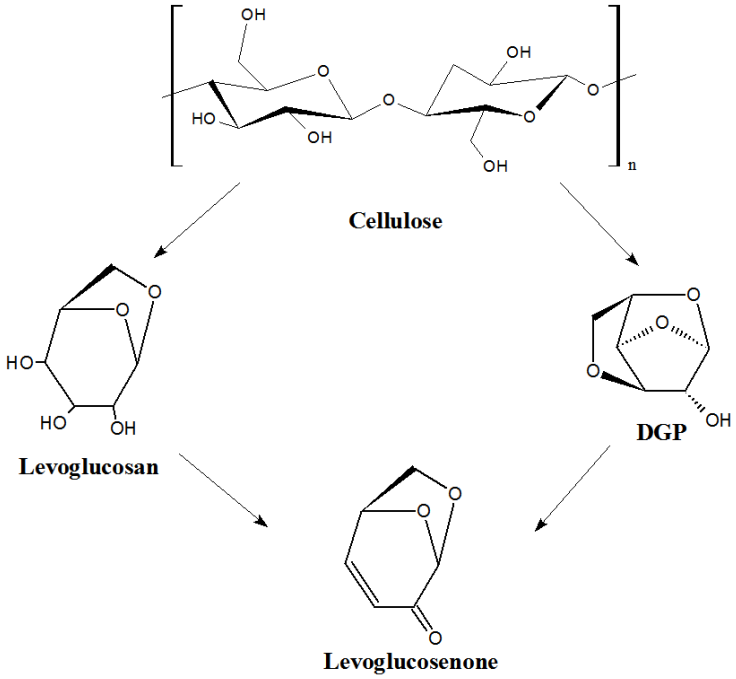

Figure 2-8 A schematic illustration of the two possible pathways for the conversion of cellulose to levoglucosenone

In a recent computational investigation, Satorri [107] investigated the reaction mechanism for the conversion of levoglucosan to levoglucosenone, and suggested that 1,4:3,6-dianhydro-α-D-glucopyranose (DGP) – an important anhydrosugar product (3.3 wt.% [69]) from cellulose pyrolysis – might be a possible precursor for the formation of levoglucosenone. However, the reaction mechanism for the DGP-to-levoglucosenone conversion was not investigated. Figure 6-1 summarises the two pathways for the conversion of cellulose to levoglucosenone. Nearly four decades ago Shafizadeh *et al.* [108] showed that pyrolysis of DGP under acidic conditions generated significant amounts of levoglucosenone. They proposed a general reaction scheme for the formation of levoglucosenone from DGP. This scheme is illustrated in Figure 6-2. This scheme involves diol, triol, and tetraol intermediates, however the reaction mechanisms leading to their formation were not discussed.

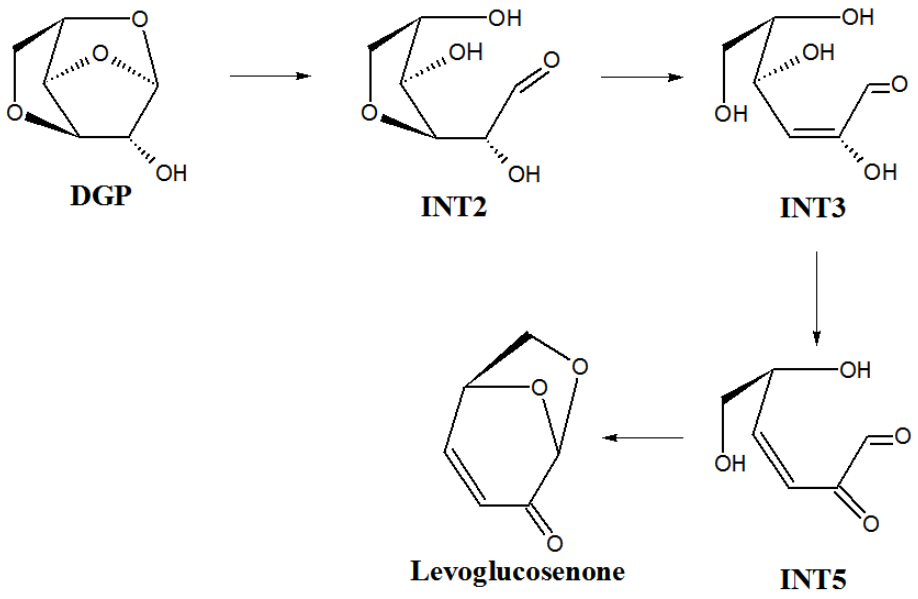

Figure 2-9 Scheme for the conversion of levoglucosenone to DGP proposed by Shafizadeh *et al.* [108]. For the sake of consistency the labels of the intermediates are taken from Figure 6-1

.2.5.5 Fragmentation— the formation of low molecular weight compounds

Besides levoglucosan, some smaller compounds could also be found in cellulose pyrolysis, such as acetol, acetic acid, glycolaldehyde and 5-HMF. The reactions producing these small compounds are called fragmentation reactions, which means that they are generated from the ring scission or the cleavage of cellulose to produce compounds with less than 5 carbons. These reactions are believed to compete with levoglucosan production (depolymerisation) and lead to a lower yield of levoglucosan [70]. Shafizadeh [109] first proposed a mechanism to illustrate the fragmentation reactions which starts from levoglucosan (shown in Figure 2-10), arguing that levoglucosan was first decomposed to glycopyranose and then into the production of glycolaldehyde. Recently, Gu et al. [70] suggested a different pathway, where small molecules could either be directly converted from the cellulose chain or formed by the secondary decomposition of levoglucosan.

In hemicellulose pyrolysis, the yield of the low molecular weight compounds such as formic acid, furan derivatives, CO and CO_2 was about 50 wt.%. Patwardhan *et al.* [91] argued that these species could be attributed to the branched, amorphous structure and low degree of polymerisation of hemicellulose. The formation of CO_2 and formic acid was proposed to be due to the decarboxylation of the glucoronic acid groups, a monomeric sugar having carboxylic acid functionality contained in hemicellulose. An overall primary reaction scheme of hemicellulose pyrolysis was proposed, consisting of depolymerisation, dehydration to furan and pyran ring derivatives and furanose and pyranose ring-break-age to light oxygenated species [91].

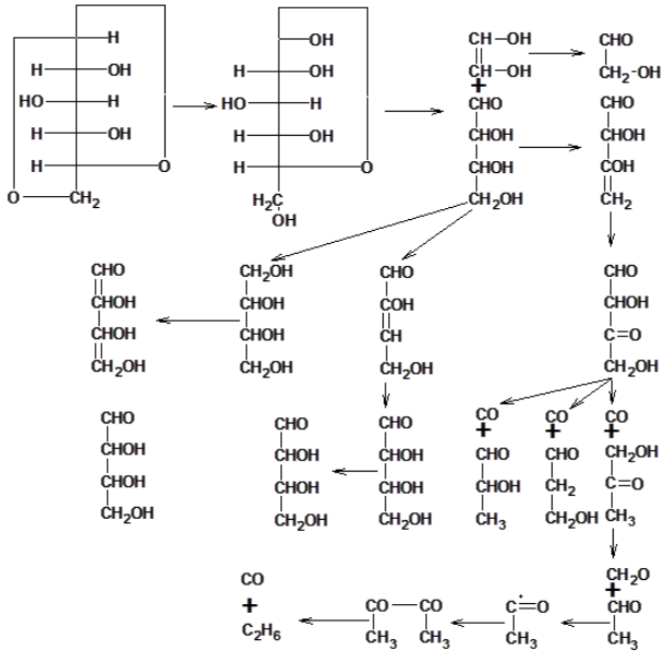

Figure 2-10 Scheme of levoglucosan fragmentation (adapted from [86])

2.5.5 Charring process (polymerisation)

Products of cellulose pyrolysis are highly reactive and tend to further react by either fragmenting into small compounds or growing in size for carbonization. The latter reaction is usually called polymerisation. Levoglucosenone was proposed as one of the important intermediates to form the

polymerised carbonised residue [96]. Kawomoto *et al.* [110] also studied the mechanism of char formation and proposed a pathway shown in Figure 2-11. They argued that the polymerisation reaction of anhydromonosaccharides played a key role for carbonised char formation.

In hemicellulose pyrolysis, the char yield reported in different experiments was significantly different. Yang et al [29] reported char yield of 22 wt.% from commercially purchased birchwood xylan and Shafizadeh [111] reported char yields of about 31 wt.% from the pyrolysis of synthetic xylan and galactoglucomannan, while Patwardhan *et al.* [91] reported char yield of 10.7 wt.%. The differences in the yield char in those studies could likely be attributed to the differences in heating rate and raw material. As for the charring, Patwardhan *et al.* claimed [91] that xylosyl cation could undergo a transglucosylation reaction with other polymeric xylosyl anions leading to the formation of longer polymers, which eventually underwent dehydration leading to the formation of char.

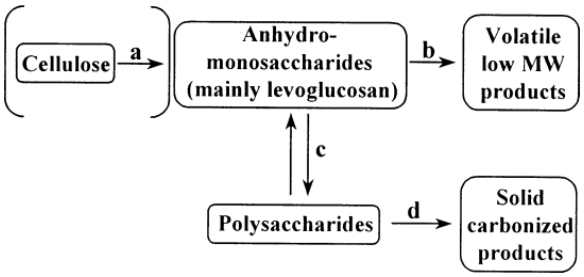

Figure 2-11 Scheme of cellulose pyrolysis pathway via anhydromonosaccharide (adapted from [87])

2.5.6 Lignin pyrolysis

Compared with cellulose and hemicellulose pyrolysis, which has been extensively studied, lignin pyrolysis is still poorly understood. The complexity of lignin structure hinders a better understanding on lignin pyrolysis. Currently, the main research efforts focus on a) the depolymerisation reactions

responsible for the formation of the lignin oligomers, b) the cross-linking reactions, and c) the polymerisation leading to the formation of char.

Table 2-9 lists the main reactions occurring during lignin pyrolysis with the corresponding temperature region [112].

Table 2-9 Temperature regions for lignin pyrolysis reactions

Temperature region	Reactions/Cleavage of bonds
Around 473K	Dehydration
423K─573 K	Cleavage of α- and β- aryl-alkyl-ether linkages
Around 573 K	Aliphatic side chains splitting off from aromatic rings
643-673K	Cleavage of carbon-carbon linkage between lignin units

Although the complexity of the structure of lignin itself hinders an in-depth understanding of the pyrolysis process, researchers have employed various model compounds (including monomeric, dimeric and trimetric compounds as listed in Table 2-10) to approach a better understanding of the degradation of lignin pyrolysis. Also the mechanisms of phenolic monomer and oligomer formations are discussed.

2.5.6.1 Mechanisms of phenolic monomer and oligomer formations

The mechanisms of phenolic monomer and oligomer formation are still unclear and widely debated. Thermal-mechanical ejection [113] is one of the most commonly cited models, arguing that phenolic oligomers are formed by partially cracked lignin fragments. Several studies [114, 115] also proposed the randomness of the formation of primary pyrolysis-products. It should be noted that among previous studies, the pyrolysis products collected might be the results of secondary reactions as quench vessels were quite downstream from the reactor. Recently, several researchers [92-95] have utilized different

online and quenching approaches to study the formation of phenolic monomers and oligomers. Zhou et al. [116] employed a wire-mesh reactor to pyrolyse lignin and trapped the pyrolysis products for analysis. As the results showed that the trapped products were almost phenolic oligomers, the authors argued that the primary products of lignin pyrolysis were phenolic oligomers while phenolic monomers were derived from the secondary reactions and repolymerisation. In the method [117, 118] with a micropyrolyser coupled to gas chromatograph and mass spectrometer (Py-GC/MS), twenty different kinds of monomers were detected and identified as the primary products while the larger molecular weight compounds such as phenolic oligomers and other heavy compounds could not be detected. Patwardhan *et al.* [119] found that pyrolysis products quenched after longer distances from the reactor had higher molecular weight which is opposite to the hypothesis suggested by Zhou *et al.* [116] A molecular beam mass spectrometer was utilized to approach an online detection of high molecular weight compounds. However, although numerous peaks were observed from the online spectra, indicating the complexity of the pyrolysis, only very limited peaks were deeply investigated. It is still far away from characterising the unknown species. Nevertheless, in this study, high molecular peaks (over 200 Daltons) were widely studied and possible structures were proposed [114, 120, 121]. In order to complete a more comprehensive understanding of the composition of pyrolysis products, high resolution mass spectrometer was also employed. Xianglan Bai [122] collected the pyrolysis products and subjected them to FT-ICR MS and Orbitrap MS. The experimental results showed that 569 phenolic compounds with MW less than 504 Da were found and phenolic monomers were the most abundant products followed by dimer, trimmer and tetramer. The authors suggested that a considerate amount of primary products were monomers while oligomers were formed from the reoligomerisation of phenolic monomers. Using imaging photoelectron phtoion coincidence with VUV synchrotron radiation [123], radical fragments such as the hydroxyclopentadienyl radical in guaiacol decomposition, was identified by mass-selected threshold photoelectron spectra in

excellent agreement with the Frank-Condon simulation. A lumped scheme of the thermal degradation of lignin shown in Figure 2-12 depicts the whole pyrolysis pathways of lignin [124].

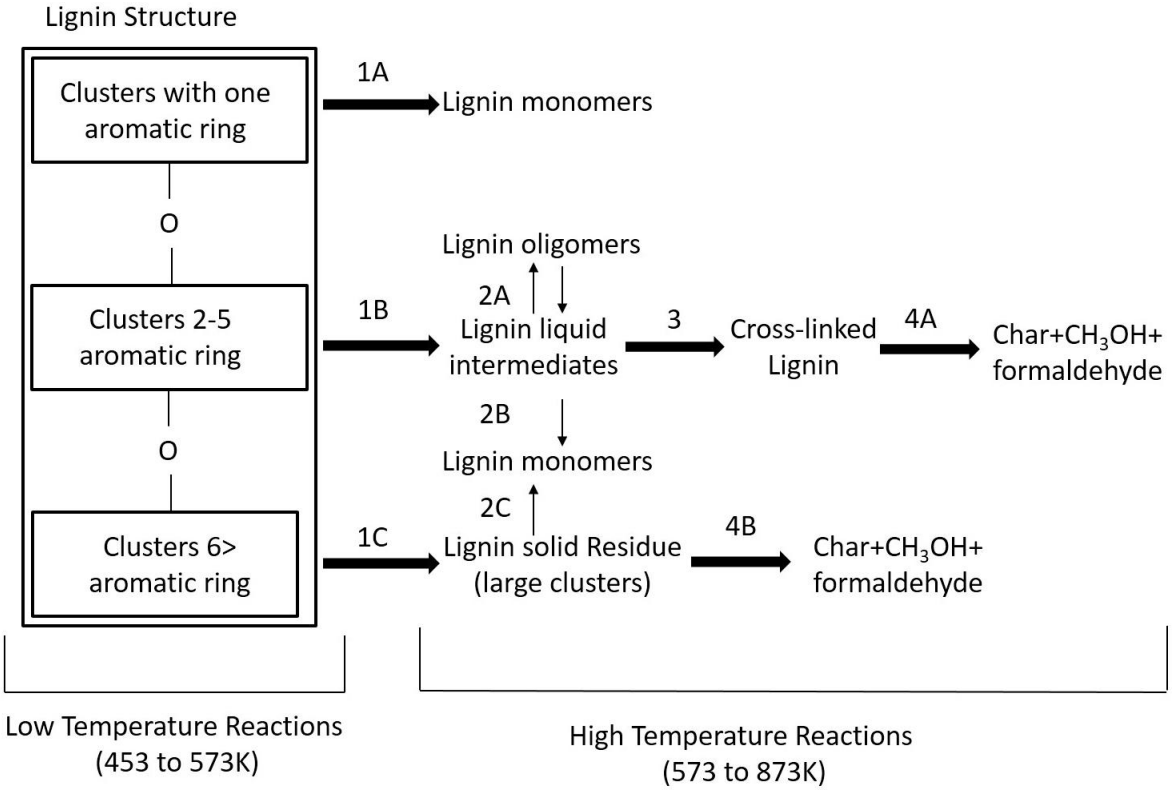

Figure 2-12 Scheme of lumped lignin pyrolysis mechanisms (adapted from [101])

2.5.6.2 Pyrolysis of phenolic monomeric compounds

Various monomeric products have been identified from the pyrolysis of lignin and wood [39, 125, 126]. Studying the pyrolysis of phenolic monomeric compounds is very important to understand the thermal behaviour and stability of the intermediate compounds from lignin pyrolysis. Current research efforts mainly focus on monomeric compounds such as guaiacol, anisole, syringol and coniferyl alcohol.

Klein [127] studied the guaiacol pyrolysis at 623K in a small batch reactor, proposing that the demethylation of guaiacol led to the formation of catechol, CO_2 and phenol. The influence of the group

functionalities on the thermal behaviour of the aromatic unit was also studied by Klein. It was found that substitution in the guaiacylic ring had little impact on the pyrolysis mechanism of the studied compounds (syringol, isoeugenol, vanillin, anisole). Chao Liu *et al.* [125] studied the guaiacol pyrolysis mechanism based on density function theory, proposed five pyrolytic pathways of guaiacol and calculated standard thermodynamic and kinetic parameters . The results ranked the five reactions pathways, indicating that the energy barrier of guaiacol demethoxylation could be reduced if a hydrogen radical was coupled to the carbon atom in the benzene ring where the methoxyl group was located.

Anisole pyrolysis was found to generate to a wider range of products than the guaiacylic model compound, indicating a higher reactivity of guaiacol provided by the phenolic HO-group substituent. In anisole pyrolysis, a possible pathway for the production of benzaldehyde, toluene and phenol was proposed by Schlosberg et al [128]. It proposed that the free radical produced from anisole pyrolysis either went through rearrangement to benzaldehyde or stabilization to the formation of benzylachohol.

Asmadi *et al.* [129] studied and compared the thermal reactions of guaiacol and syringol in a closed ampoule reactor (Pyrex glass). The authors claimed that the O-CH3 bond homolysis occurring over 400℃ was the rate-determining step and the two methoxyl groups in syringols induced the double opportunity of the radical rearrangements. Pyrolysis reactions of coniferyl alcohol were also studied by Kotake [130]. It was found that polymerisation was more important than the evaporation and side-chain conversion while coniferyl alcohol was found to be much more reactive than other side-chain conversion products.

2.5.6.3 Pyrolysis of phenolic dimeric and trimetric compounds

Dimeric and trimetric compounds containing a variety of functional groups such as carbonyl, hydroxyl and carboxyl units have been used by several researchers to study the thermal stability and behaviour of different bonds in lignin.

Table 2-10 List of dimers investigated along with a schematic representation of the structures.

Dimers	Structure
2-phenethyl phenyl ether	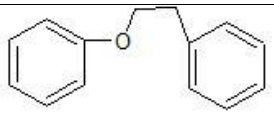
Benzyl phenyl ether	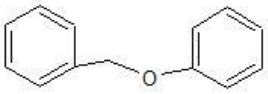
Diphenyl ether	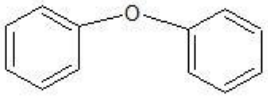
Biphenyl	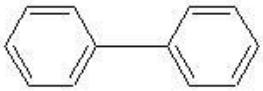
1,3-Diphenylpropane	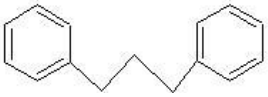
Benzyl ether	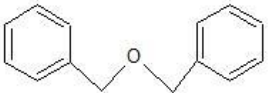
Guaiacylglycerol-*β*-guaiacyl ether	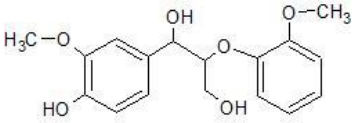
2,2 biphenol	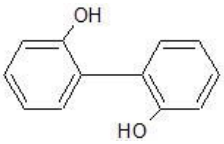

Klein [127] performed the pyrolysis of five dimers (listed in the Table 2-10) to investigate the interactions of C-C and C-O bonds thermal behaviour. 2-phenethyl phenyl ether is the simplest dimer

for the investigation of the thermal behaviour of β-ether bonds. The thermal behaviour of α-ether bond were studied by using benzyl phenyl ether whereas aromatic C-O bond studied by using phenyl ether. Carbon-carbon linkages were simulated using biphenyl and biphenol compounds. By comparing the pyrolysis of 1, 3-diphenylpropane and benzyl phenyl ether, Gilbert and Gajewski [131] found that the degradation reaction was accelerated by the existence of thermally unstable compounds like benzyl phenyl ether. Simmon and Klein [132] proposed three possible mechanisms of pyrolysis of dibenzyl ether: a free radical mechanism, a concerted reaction, and a combined concerted free radical reaction. Guaiacylglycerol-β-guaiacyl ether and veratrylglycerol-β-guaiacyl ether were also pyrolysed for further investigation [133]. The results showed dimers preserving the β-ether bonds were identified in the volatile products and indicated it as a result of a HO-group elimination.

Kawamoto *et al.* [134] studied the influence of C_γ-OH on pyrolytic cleavage mechanisms of β-ether bond in phenolic dimers with various p-substituted dimers. The authors found low temperature C_β-O bond homolysis via quinone methide and radical chain mechanism starting from the direct C_β-O bond homolysis while relatively small extent of radical chain reaction observed in nonphenolic C_γ-deoxy dimers. More specifically, the β-O-4 bond is the major type of linkage which occupies 46%-60% of the total linkages depending on the type of wood. The pyrolysis behaviour of β-O-4 type dimers has been widely studied. Britt *et al.* [135] further studied the fast vacuum pyrolysis of phenethyl phenyl ether (PPE) and argued that the reactions were dominated by free-radical reactions, molecular rearrangements, and concerted eliminations. A computational study of PPE was done by Beste *et al.* [136-138], investigating oxygen-carbon bond dissociation enthalpies, phenyl-shift, hydrogen abstraction and substituent effects. Recently, Sheng Chu *et al.* [139] studied the pyrolytic behaviour of a β-O-4

oligomeric lignin model compound, identifying twenty five volatile compounds and proposing a free radical reaction pathway (shown Figure 2-13).

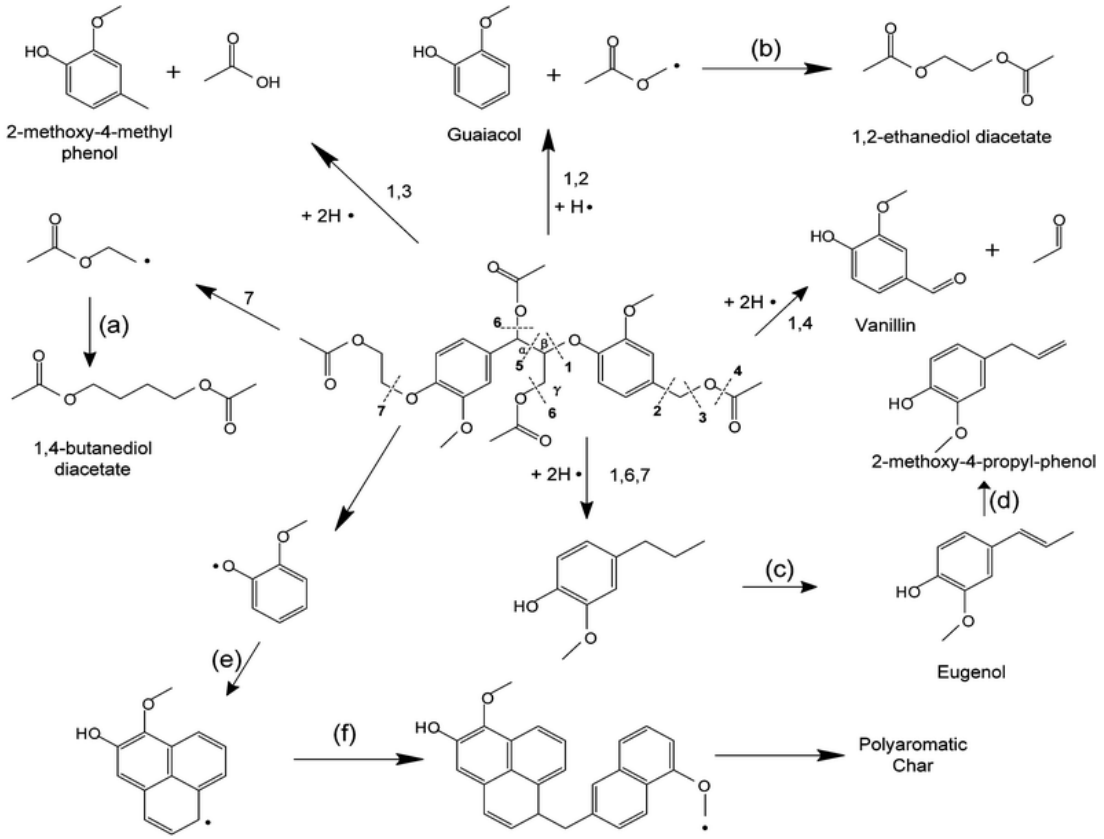

Figure 2-13 Scheme of reaction pathways of pyrolysis of lignin oligomeric compound (adapted from [115])

2.6 The interactions among cellulose, hemicellulose and lignin during pyrolysis

Normally, cellulose, hemicellulose, and lignin are the three main building blocks in all biomass covering 40-60, 20-40, 10-25 wt.% (dry basis), respectively which have very different thermal behaviours [140]. Cellulose and hemicellulose pyrolysis form anhydrosugars, furans, aldehydes, ketones and carboxylic acids as their volatile products, while the volatiles from lignin pyrolysis mainly are consisted of low molecular weight aromatic compounds with guaiacyl-units or phenolic-units. To date, many researchers proposed that the pyrolysis behaviour of cellulose, hemicellulose and lignin could be regarded as

independent so that any lignocellulosic biomass can be described as the superposition of the three main building blocks and the complexity of various kinds of biomass can be simplified [141-144]. Yang *et al.* [29, 145] investigated the pyrolysis characteristics of the three components and their synthesized samples (mixture of these components in different ratios) and found negligible interactions among the three components. A computational approach was made to predict the weight loss of a synthesized biomass from its composition in cellulose, hemicellulose and lignin and to predict the proportions of the three components of a biomass. The results calculated for the weight loss of the synthesize mixture are quite consistent with the experimental observations. However, results for predicting the composition of the biomass in terms of cellulose, hemicellulose and lignin were not very satisfactory. Wang *et al.* [146] observed cellulose-lignin and hemicellulose-lignin interactions under syngas, respectively and reported that hemicellulose and lignin did not affect the pyrolysis characteristics of cellulose as they could not affect each other in the pyrolysis process. Qu *et al.* [147] also found that under the assumption of no significant interactions of the three components, the additivity law can predict reasonably the trend of product yields of typical biomass sample (rice straw, corn stalk, and peanut vine) based on their composition of cellulose, hemicellulose and lignin.

From the morphological view of the plant cell-wall, the main components (cellulose, hemicellulose and lignin) would not perform independently without any intrinsic interactions during the pyrolysis process. In order to have a better understanding of the pyrolysis mechanism of biomass and optimise the efficiency of pyrolysis process, the interactions among the chemical components of biomass during pyrolysis have recently attracted growing research efforts. In a TG-MS study [95], significant interactions between cellulose and lignin were observed which suppressed the formation of liquid products and promoted the yield of char. Hosoya *et al.* [148] investigated cellulose-hemicellulose and

cellulose-lignin interactions during pyrolysis at gasification temperature of 1073K for 30s at a tube reactor. It showed that cellulose-hemicellulose interaction is not significant in gas, liquid and char yields whereas cellulose-lignin interactions could affect liquid composition. The vapor phase carbonisation of lignin-derived products inhibited the formation of anhydrosugars and promoted the formation of lignin-derived compounds. To reveal the vapor-phase and solid-liquid phase interactions, Hoyosa *et al.* [149] also studied the interaction between cellulose and lignin in two types of reactors. The research results showed that solid/liquid phase interaction in the early stage of pyrolysis enhanced the liquid formation instead of water and char. Fushimi *et al.* [150] studied the interaction among the major biomass components during gas and liquid evolution using a continuous cross-flow moving bed reactor. It was found that the initial decomposition of lignin was hindered by the interaction with cellulose pyrolysis. The interactions suppressed the evolution of levoglucosan and significantly increased the evolution rate of 5-methylfurfural. These findings were different from the ones from Hoyosa *et al* [149].. Wang *et al.* [151] studied the characteristics of biomass using a TGA coupled with FTIR. The biomass component didn't act independently as from 623K to 773K, cellulose-lignin interactions promoted the formation of 2-furfural and acetic acid and cellulose-hemicellulose interactions enhanced the formation of 2,6-dimenthoxy.

We have to acknowledge that the interactions among the components of biomass (cellulose, hemicellulose and lignin) during pyrolysis are insufficiently investigated in the literature. Further research concerning the interactions among the three components need to be addressed in order to gain a better understanding of the pyrolysis mechanism: 1) the effect of temperature on the interactions among the components during pyrolysis; 2) the effect of interactions on the reaction kinetics of pyrolysis process, 3) the effect of interactions on the formation of pyrolysis products.

2.7 *Ab initio* thermochemical protocols

Ab initio thermochemical protocols have been widely used in numerous mechanism study including biomass pyrolysis and are one of the most powerful approach to unravel complicated chemistry. This section outlines the theoretical framework used in *ab initio* thermochemical protocols. Section 2.7.1 to 2.7.7 describe the theoretical framework of ab initio methods including Hartree-Fock, Møller-Plesset perturbation theory and Coupled-Cluster theory. Section 2.7.8 to 2.7.9 describe basis sets and other energetic contribution such as relativistic effects, spin-orbit coupling and zero-point vibration energy. Section 2.7.10 briefly describes composite methods including Gn theory and W1 theory which are employed in this thesis work.

2.7.1 The Schrödinger equation

Quantum chemistry explains how entities like electrons have both particle-like and wave-like characteristics. The Schrödinger equation[152, 153] describes the wave function of a particle:

$$\left\{\frac{-h^2}{8\pi^2 m}\nabla^2 + V\right\}\psi\left(\vec{r},t\right) = \frac{ih}{2\pi}\frac{\partial\psi\left(\vec{r},t\right)}{\partial t} \tag{1.1}$$

In this equation, Ψ is the wave function, m is the mass of the particle, h is Planck's constant, and V is the potential field in which the particle is moving. The product of Ψ with its complex conjugate ($\Psi^*\Psi$, often written as) is interpreted as the probability distribution of the particle.

In the case for a collection of particles, Ψ would be a function of the coordinates of all the particles in the system as well as t. The energy and other properties of the particle and system can be obtained by solving the Schrödinger equation subject to specific boundary conditions.

The equation in Hamiltonian form is as follows:

$$\hat{H}\Psi_i\left(\vec{x}_1,\ldots,\vec{x}_N,\vec{R}_1,\ldots,\vec{R}_M\right)=E\Psi_i\left(\vec{x}_1,\ldots,\vec{x}_N,\vec{R}_1,\ldots,\vec{R}_M\right) \quad (1.2)$$

where $\hat{H}$ is the Hamiltonian operator, Ψ is the wave function, E is the energy of the system. $\vec{x}_N$ describes the positions of the electrons, N and $\vec{R}_M$ describes the positions of the nuclei M. A knowledge of Ψ allows the properties of the system to be deduced.

2.7.2 The Born-Oppenheimer approximation

The Born-Oppenheimer (BO) approximation[154] decouples the motion of the nuclei (vibrational, rotational and translational) and of the electrons based on the premise that the mass of nuclei are much heavier than electrons and the electronic velocities far exceed those of the nuclei [155]. Then we have the so-called electronic Hamiltonian ($\hat{H}_{elec}$),

$$\hat{H}_{elec}=-\sum_{i=1}^{N}\frac{1}{2}\nabla_i^2-\sum_{i=1}^{N}\sum_{A=1}^{M}\frac{Z_A}{r_{iA}}+\sum_{i=1}^{N}\sum_{j>i}^{N}\frac{1}{r_{ij}}. \quad (1.3)$$

The electronic wave function corresponds to the electronic Hamiltonian ($\hat{H}_{elec}$),

$$\Psi_{elec}=\Psi_{elec}\left(r_i,R_A\right). \quad (1.4)$$

which describes the motion of the electrons. Apart from the electronic (r_i) and the nuclear coordinates (R_A), a spin (w) is assigned to specify an electron.

The total energy can be written as,

$$E_{tot}=E_{elec}+\sum_{A=1}^{M}\sum_{B>A}^{M}\frac{Z_AZ_B}{R_{AB}}. \quad (1.5)$$

The difficulties in solving Eq. (1.3) lies in the electron-electron interaction $\frac{1}{r_{ij}}$. Many approximation methods have been developed for solution. The Slater determinant as a fundamental tool, will be introduced first before we step into specific methods.

2.7.3 Slater determinants

Based Pauli Exclusion Principle[156], the electron wave function should be satisfy the antisymmetric condition as follows,

$$\Phi\left(x_1,\cdots x_i,\cdots x_j,\cdots x_N\right)=-\Phi\left(x_1,\cdots x_j,\cdots x_i,\cdots x_N\right). \tag{1.6}$$

In a general N-electron system, the Slater determinant[157] can be expressed as,

$$\Phi\left(x_1,\cdots x_i,\cdots x_j,\cdots x_N\right)=\left(N!\right)^{-1/2}\begin{vmatrix}\chi_i\left(x_1\right) & \chi_j\left(x_1\right) & \cdots & \chi_k\left(x_1\right)\\ \chi_i\left(x_2\right) & \chi_j\left(x_2\right) & \cdots & \chi_k\left(x_2\right)\\ \vdots & \vdots & & \vdots\\ \chi_i\left(x_N\right) & \chi_j\left(x_N\right) & \cdots & \chi_k\left(x_N\right)\end{vmatrix} \tag{1.7}$$

A short notation for a Slater determinant with the diagonal elements shown is expressed as,

$$\Phi\left(x_1,x_2,\cdots,x_N\right)=\left|\chi_i\left(x_1\right),\chi_j\left(x_2\right)\cdots\chi_k\left(x_N\right)\right\rangle \tag{1.8}$$

2.7.4 Hartree-Fock theory

The Hartree-Fock method[158] is one of the most prominent computational approach among the approximate ways for the determination of the wave function in the Schrödinger equation. One of the most difficulties in solving the Schrödinger equation is to determine the energies of each electron. Based Born-Oppenheimer approximation, we assume that the positions of the nuclei are fixed. Another approximation used in Hartree-Fock theory is that the energy of each electron is calculated in the average static field of the other electrons.

In the Hartree-Fock method, the Hamiltonian can be divided into two parts: a core Hamiltonian $H^c{}_i$ describing the kinetic energy and the electron-nuclei attraction potential and a part describing the electron-electron repulsion:

$$H = \sum_i \left[H^c(i) + \sum_{j>i} \frac{1}{r_{ij}} \right] \text{ with } H^c(i) = -\frac{1}{2}\nabla_i^2 - \sum_A \frac{Z_A}{r_{iA}} \tag{1.9}$$

The core Hamiltonian can be exactly solved whereas the electron-electron repulsion part can only be approximated, i.e. each electron is considered to be moving independently of the others in an average field created by other electrons.

The wave function is expressed in the form of a Slater Determinant and the related energy is obtained by minimization of its expression with respect to the molecular orbitals χ_i. This leads to the Hartree-Fock eigenvalue equation where the Fock operator $\hat{F}$ acts on the orbitals χ_i to generate the same orbital function multiplied by constant ε_i, which represents the energy of each corresponding orbital:

$$\hat{F}_i \chi_i = \varepsilon_i \chi_i \tag{1.10}$$

The negative of the eigenvalue of the Fock operator associated with the spin orbital, $-\varepsilon_i$. An initial guess of orbitals is proposed and the calculation of the system's energy which is done based on initial electron field configuration, is iterated until convergence. Hartree-Fock calculation have been employed in many applications and is sufficiently accurate in many chemical problems [159-162].

2.7.5 The electron correlation problem

The difference between the Hartree-Fock energy and the full Schrödinger equation is defined as the correlation energy:

$$E_{corr} = E - E_{HF} \tag{1.11}$$

It was found that correlation energy is of great importance to determine the properties of a system. The missing electronic correlations in Hartree-Fock leads to great deviations compared with experimental results. A number of methods referred as post Hartree-Fock Methods, have been proposed to address the electron correlation issues, which has three categories, namely, full Configuration-Interaction, Møller-Plesset Perturbation Theory and Coupled-Cluster method.

The full Configuration-Interaction method gives the best solution as all the correlations among electrons and orbitals are considered in linear combinations. However, the computational cost required by full Configuration-Interaction method make it infeasible for most chemical systems.

2.7.6 Møller-Plesset perturbation theory

Møller-Plesset perturbation theory[163] is one of the major *ab initio* post-Hartree-Fock methods. Based on Rayleigh- Schrödinger Perturbation Theory, it expands the reference wave function and its corresponding energies as a Taylor's series of the perturbation parameter λ $(0 < \lambda < 1)$, which allows the excitations truncated to be considered. This allows to obtain meaningful properties such as heat of formation, activation energy, and an accurate relative energies along the Potential Energy Surface.

The principle of perturbation theory in general is to start from a simple model which has been solved exactly or approximately and gradually add the small "perturbation" to this simple model. The unperturbed Hamiltonian (H^0) as equal to the sum of the one-electron Fock operators:

$$H^0 = \sum_{i=1}^{N} F_i \tag{1.12}$$

Where the superscript describe the correction-order, N is the number of electrons in the system. The MP_n equation may be written as

$$(H^0 + \lambda H^{'})\left|\Psi_0\right\rangle = \varepsilon\left|\Psi_0\right\rangle \tag{1.13}$$

where the subscript 0 denotes the ground state.

In a form of Taylor series expansion, (1.10) can be written as:

$$(H^0 + \lambda H^{'})\left|\Psi^0 + \lambda\Psi^1 + \lambda^2\Psi^2 + \cdots\right\rangle = \varepsilon^0 + \lambda\varepsilon^1 + \lambda^2\varepsilon^2\left|\Psi^0 + \lambda\Psi^1 + \lambda^2\Psi^2 + \cdots\right\rangle \tag{1.14}$$

where $\Psi^1 = \frac{\partial\Psi^0}{\partial\lambda}, \Psi^2 = \frac{\partial\Psi^0}{\partial\lambda^2}$, etc.

The operator $H^{'}$ is incorporated in the perturbation theory to correct the wave function. As the first order MP does not improve energy beyond HF level, MP2, MP3, etc. are used for the optimization.

It should be noted that the second order (MP2) is the most common used level with MP4 used as the next common. MP2 is a very efficient method with a computational cost of N^5, and offers analytical gradient and Hessians for PES exploration[164]. For higher orders, some unpredictable convergence behaviors[165] such as slow, erratic, oscillatory could cause computational problems, which are not applicable to excited states.

2.7.7 Coupled Cluster methods

The coupled cluster method was introduced by Čížek [166] in the 1960's and became the most reliable, yet computational affordable method for the approximate solution of the electronic Schrödinger and the prediction of molecular properties[167-169]. In coupled cluster method, a wave function is derived

from Hartree-Fock wave function and multi-electron wave function is built using a so-called exponential cluster operator for electron correlation.

The coupled cluster wave function is written as,

$$\Psi_{cc} = e^{T}\Phi_0 \tag{1.15}$$

where the cluster operator T is the sum of connected operator T_i and the exponential operator e^T is expanded as a Taylor series.

The Schrödinger equation using the coupled cluster wave function is given as,

$$\hat{H}e^{T}\Phi_0 = Ee^{T}\Phi_0 \tag{1.16}$$

Multiplying Φ_0^* and expand out the exponential in Eq. (1.16), we get

$$E = \left\langle \Phi_0 \left| \hat{H}\left(1 + T + \frac{1}{2}T^2 + \frac{1}{6}T^3 \cdots\right)\right| \Phi_0 \right\rangle \tag{1.17}$$

Then we could obtain the truncation of the coupled cluster energy equation

$$E = \left\langle \Phi_0 \left| \hat{H}\left(1 + T + \frac{1}{2}T^2 + \cdots\right)\right| \Phi_0 \right\rangle \tag{1.18}$$

Expansion of the cluster operator T up to T_N would mean all possible excited states are considered. However, a truncation of T must be performed in approximation. So the lowest level starts from T_2 as T_1 does not improve anything upon Hartree-Fock. With N as the number of basis functions in the calculation, CCSD calculation has an expensive scale of N^6, and to go beyond CCSD could make calculation extremely demanding. A widely known approach CCSD(T)[170] is employed for the triple excitation in a perturbative manner.

2.7.8 Basis sets

Hartree Fock. Perturbation and Couple Cluster theory have revealed us the pathway from Schrödinger equation to a set of solvable equation. Each molecular orbital is constructed from linear combination of basis functions to represent the wave function. Essentially, almost all electronic structure methods rely on an expansion on the unknown wave function in terms of a set of basis functions. If the basis set were complete, i.e., it involved an infinite number of basis functions, then the wave function would be no longer approximate. Any type of basis functions may in principle be used such as exponential, Gaussian, spline, Slater type orbitals and etc. The computational cost and the accuracy of the capture of physics problems are two main issues being considered when selecting basis functions. We will now discuss in more details on basis sets.

2.7.8.1 Gaussian type orbitals

From the early days, Slater type orbitals (STOs) were universally used in quantum chemistry calculations because of the similarity of the exact solution of the Schrödinger equation for the hydrogen atom. However, four-center two electron integrals involving STOs makes the calculation extremely complicated and has no analytical form. Therefore, in modern quantum chemistry, the Slater orbitals are normally only applied in atomic and diatomic systems.

$$\phi_i(\zeta, n, l, m, r, \theta, \psi) = Nr^{n-1}e^{-\zeta r}Y_{lm}(\theta\phi) \tag{1.19}$$

where Y are the spherical harmonic functions, N is the normalization constant. n , l and m are the quantum numbers: principal, angular momentum, magnetic, respectively. ζ is called the "exponent".

Boys[171] proposed that all integrals in SCF calculation could be evaluated analytically if a Gaussian function is presented. Numerous quantum chemistry codes employ Gaussian functions as basis sets. The Gaussian functions type orbitals (GTO) has the following form in Cartesian coordinates:

$$g\left(\zeta, l_x, l_y, l_z, x, y, z\right) = Ne^{-\zeta r^2} x^{l_x} y^{l_y} z^{l_z} \tag{1.20}$$

GTOs are usually employed because of their attractive integration properties, which means that all the required integrals can be calculated analytically. Several primitive Gaussian functions are normally grouped into one Gaussian function known as contracted Gaussian function to alleviate the slow convergence of GTO.

The origins of the exceedingly slow convergence of GTO lie in the orbital approximation leading to poor description of the short-range correlated motion of the electrons. A practical approach is the combination of very large Gaussian basis set with extrapolation techniques. Before stepping into extrapolation techniques, it is essential to understand the meaning of Pople style basis set and the correlation consistent basis sets of Dunning *et.al* [172-174].

2.7.8.2 Pople style and correlation consistent basis sets

For Pople style basis set, take 6-31G and 6-311G basis set as an example. A 6-31G basis set is a double split valence basis set, with core orbitals described by one contracted Gaussian function consisting of six primitive Gaussians and valence orbital being split into two contracted Gaussians, one consisting of three primitive Gaussians and the other just one primitive Gaussians. A 6-311G basis set is a triple split valence basis set. The core orbitals are described by a contraction of six primitive Gaussians whereas the valence is split into three parts which are contractions of three, one and one primitive Gaussians, respectively.

Further improvements can be achieved by adding so-called polarization or diffuse functions. In order to better describe the distortions in molecule's electron density, some basis sets with additional functions with larger angular momentum are added. Normally an asterisk represents the polarization function in the basis set like 6-31G*. Diffuse functions are sometime also included to improve the description at large distances from the nuclei, which is important for anions as the additional electrons are loosely bound to nuclei.

The correlation consistent basis sets are designed to systematically recover the correlation energy with the increasing size of the basis sets. In previous basis set function, there is not a clear way to achieve continuous improvements with increasing the basis functions, which sometimes lead to the convergence problem and uncertainties in the choosing process. The correlation basis set choose the basis function based on the contributions to the correlation energy from each function whereas the function type is not considered. For instance, 2d and 1f function belong to the same group. For the first- and second-row atoms, the basis sets are cc-pVNZ where N = D, T, Q, 5, 6,… (D = double, T =triples, etc.) The 'cc-p' represents 'correlation-consistent polarized' whereas the 'V' suggests that they are valence-only basis sets. Example of several widely used correlation-consistent basis sets are: cc-pVDZ (Double-zeta) and cc-pVTZ (Triple-zeta). As Pole style basis sets, diffuse functions can be added, with a new prefix of aug: aug-cc-pVXZ (X = D, T, Q and 5). In correlation-consistent basis sets, core functions can be added for geometric and nuclear properties calculations whereas diffuse functions are augmented for electronic excited-state calculations and long-range interactions. It should be noted that extrapolation methods have been developed based on the correlation consistent basis set to systematically improve the basis set size.

2.7.8.3 Basis set extrapolation

When atoms interact, the basis sets allocated to each of them will overlap. This overlapping give electrons greater freedom to localise and can result in a reduction of energy. This reduction is due to the incompleteness of the basis sets and an artifact of working with limited basis sets. This is called the basis set superposition error (BSSE) [175]. There are schemes to correct for BSSE. The most common is the so-called Counterpoise correction [176]. However, these schemes are not sufficient to guarantee high accuracy because of the incompleteness of the basis sets. In order to address this, extrapolation schemes are developed to alleviate basis set incompleteness errors based on correlation-consistent basis sets.

Several extrapolation schemes for the correlation energies [177-181] have been proposed. These work are either based on the motivation from helium-like system [182-185] or empirical studies [186, 187]. For example, the following asymptotic dependence of the correlation energy (E^{corr}) on $L_{\max}$ is suggested:

$$E_{L_{\max}}^{corr} = E_{\infty}^{corr} + AL_{\max}^{-\alpha} \tag{1.21}$$

where *corr* denotes the particular contribution to the correlation energy. With two cardinal number X and X+1, Eq. (1.31) could extrapolate to the basis set limit from a simple two-point geometric formula:

$$E_{\infty} = E\left(X+1\right) + \frac{E\left(X+1\right) - E\left(X\right)}{\left(\frac{X+1}{X}\right)^{-\alpha} - 1} \tag{1.22}$$

Another popular three-parameter extrapolations scheme is,

$$E_X^{corr} = E_{\infty}^{corr} + CX^{-3} + DX^{-5} \tag{1.23}$$

where E_X^{corr} is the corresponding electron correlation energy for a given cardinal number (X) and E_{∞}^{corr} is the electron correlation energy at the CBS. C and D are the fitting parameters.

2.7.9 Other energetic contributions

2.7.9.1 Relativistic effects

Relativistic effects [188-191] are important for heavier elements with high atomic numbers which could contribute at the kcal/mol range. In the periodic table, these elements are shown in the lower area, such as lanthanides and actinides because electrons in these elements attain relativistic speeds. In this case, the four-component Dirac equation [192] is solved instead of non-relativistic Schrödinger equation to treat the relativistic effect theoretically. In order to obtain the Dirac equation, several relativistic contributions are considered, including modification of the potential operator, coupling between the electronic and positronic states, magnetic interactions and the velocity-dependent mass of electron. However, due to the severe computational demand, many approximation methods were proposed instead of solving the full four-component relativistic Dirac equation, such as RESC [193] and ZORA [194].

2.7.9.2 Spin-orbit coupling

The spin-orbit coupling is an interaction of a particle's spin with its motion. The energy levels are affected by the electromagnetic interaction between the spin and the magnetic field generated by the electron neat the nucleus. For example, Zeeman Effect is detectable as a result of spin-orbit coupling. It should be noted that spin-orbit coupling is not considered in the nonrelativistic Schrödinger equation. To account this effect, a spin-orbit coupling term (H_{so}) is added to the Hamiltonian operator.

2.7.9.3 ZPVE (zero-point vibrational energy)

The zero-point vibrational energy is the lowest possible energy that a molecular system have at absolute zero temperature and is the energy of the ground state at 0 K. The energy of the ground vibrational state

is referred as ‘zero-point vibrational energy’ as the system has zero rotational energy but nonzero vibrational energy.

There are several methods to calculate the zero-point vibrational energy (ZPVE):

1. Take an average of the theoretical and experimental ZPVEs [195] as the theoretical approach always overestimates the ZPVE and experimental approach leads to an underestimate [196]
2. For simple monatomic and diatomic molecule system, accurate experimental ZPVEs are available from high-resolution measurements
3. Use accurate theoretical harmonic frequencies combined with cubic and quartic corrections
4. Use an empirical scaling factor to scale frequencies to obtain an estimate for the theoretical ZPVE. Many benchmark efforts have been done to derive scale factors for various thermodynamic properties.

It should be noted that the size of the system and the magnitude of the ZPVE could strongly affect the accuracy. For instance, the errors in B3LYP/pc-2 scaled ZPVES are 0.2, 0.4, and 0.5 kcal mol^{-1} for methane, ethane and propane. However, for n-pentane, the ZPVE is around 100 kcal mol^{-1} and 1% error leads to a 1kcal mol^{-1} error and some isodesmic reactions are employed to improve the accuracy [197].

2.7.10 Composite methods

Thermochemical properties such as zero-point vibrational energy (ZPVE), ionization potentials (IP), electron affinities (EA), enthalpies of formation (H_f°), heat capacities (C_p°), total atomization energies (TAE) and standard molar entropies (S°) are of great value in the investigation on chemical transformations. However, it is the fact that these properties of relevant compounds are widely

unavailable due to the difficulties in the experimental measurements especially for free radicals and intermediates. Composite methods are developed to reach a high accuracy with a combination of several calculations, aiming to reach chemical accuracy within 1kcal mol^{-1} of the experimental value. Methods with a high level of theory and a small basis set are combined with methods employing lower levels of theory with larger basis sets to calculate thermodynamic properties. Two main categories will be introduced: (i) empirically corrected methods (Gn methods [198-206]), (ii) nonempirical extrapolation methods (Wn methods [187, 207, 208]).

2.7.10.1 Gn methods

The Gaussian-*n* (G*n*) theories have been developed to approach exact molecular energies using a set of calculations based primarily on *ab initio* molecular orbital theory with different levels of accuracy and basis sets. The approach used in the Gn theories is a composite approach, where the combination of a very high-level correlation method such as QCISD(T) and CCSD(T) based on a mid-size basis set such as 6-31(d) and energies from lower level calculations (MP2, MP4) with larger basis sets is employed.

This first Gaussian-n theory, G1, was developed in 1989 by Pople et al [198], which has an accuracy of over 2 kcal mol^{-1} compared with experimentally measured ionization potentials, atomization energies and proton affinities of 31 molecules. The second generation of Gaussian-n theory, G2, improved the accuracy to 0.5 kcal/mol in mean absolute deviation for 39 first row compounds [200]. Reduced Møller-Plesset orders was also incorporated to reduce computational cost and minimise the compromise in accuracy [201, 203, 205]. The third generation of Gaussian-n theory, G3 [202], was developed in 1998. Some improvements compared to its predecessors include the G3 large basis set, high level correction term, core correlation effects. The mean absolute deviation using G3 theory for the G2/97 test set and for the 147 neutral enthalpies of formation is 0.99 kcal mol^{-1} and 0.91 kcal mol^{-1}, respectively[203]. The

most current Gaussian-n theory, G4 [204], was developed in 2007. The overview of Gaussian-4 theory and Gaussian-4 theory using reduced order perturbation theory (G4(MP2) theory) is as follows.

Gaussian-4 theory

Gaussian-4 theory has several features which are not available in G3 theory and leads to the performance improvement. The features include extrapolations to the HF limit, calculation of coupled cluster energies, density functional geometries, high level correction terms and improved polarization functions. Gaussian-4 theory uses a sequence of calculations based on *ab initio* molecular orbital to obtain a total energy shown including seven steps:

1. The equilibrium structure is obtained at the B3LYP/6-31G(*2df,p*) level.
2. The ZPVE is obtained by scaling B3LYP/6-31G(*2df,p*) with a factor of 0.9854.
3. The Hartree-Fock energy limit E(HF/limit) is calculated using a linear two-point extrapolation scheme and aug-cc-pVnZ basis sets.
4. A series of single point energy is calculated as

$$\Delta E\left(\text{diffuse}\right) = E\left[MP4/6-31+G\left(d\right)\right] - E\left[MP4/6-31G\left(d\right)\right] \tag{1.24}$$

$$\Delta E\left(\text{polarization}\right) = E\left[MP4/6-31G\left(2df,p\right)\right] - E\left[MP4/6-31G\left(d\right)\right] \tag{1.25}$$

$$\begin{aligned}\Delta E\left(\text{G3largeXP}\right) = {} & E\left[MP2\left(\text{full}\right)/\text{G3largeXP}\right] - E\left[MP2/6-31G\left(2df,p\right)\right] \\ & -E\left[MP2/6-31+G\left(d\right)\right] + E\left[MP2/6-31G\left(d\right)\right]\end{aligned} \tag{1.26}$$

$$\Delta E\left(CC\right) = E\left[CCSD(T)/6-31G\left(d\right)\right] - E\left[MP4/6-31G\left(d\right)\right] \tag{1.27}$$

5. The MP4/6-31G(d) base energy and four single point energies combined also with the Hartree-Fock and a spin-orbit correction, ΔE(SO):

$$E' = E\left[MP4/6-31G(d)\right] + \Delta E(\text{diffuse}) + \Delta E(\text{polarization}) + \Delta E(\text{G3largeXP}) + \Delta E(\text{CC}) + \Delta E(\text{HF/limit}) + \Delta E(\text{SO}) \quad (1.28)$$

6. A high-level correction term is taken into account.

$$E(G4) = E' + E(\text{HLC}) \quad (1.29)$$

$$E(\text{HLC}) = -An_{\beta} - Bn_{\alpha} \quad (1.30)$$

where A, B, n_{β}, n_{α} are the empirical parameters.

In the full G3/05 test set (including enthalpies of formation, ionisation potentials, electron affinities *et al.*), the mean absolute deviation using G4 theory is 0.83 kcal mol^{-1}, which improved significantly compared to the 1.13 kcal mol^{-1} for G3 theory. Specifically, the mean absolute deviation of various thermodynamic properties such as enthalpies of formation, for hydrocarbons or non-hydrocarbons have specific improvements [209].

G4(MP2) theory

G4(MP2) theory [205] is developed based on G4 theory with the elimination of the MP3 and MP4 large basis set calculations, which enables less computational cost. G4(MP2) theory uses a sequence of calculations based on *ab initio* molecular orbital to obtain a total energy shown including seven steps:

1. Equilibrium structure optimization and frequency calculation at the B3LYP/6-31G(2df,p) level of theory
2. Zero-point vibrational energy is scaled by a factor of 0.9854

3. The base energy calculation is at the triples-augmented coupled cluster level of theory, CCSD(T), with the 6-31G(d) basis set: E[CCSD(FC,T)/6-31G(d)] where FC denotes that frozen core is used in the calculation.
4. A series of single point energies correlation is as follows:

a. The correction at the second order Møller-Plesset level (MP2) is

$$\Delta E\left(MP2\right)=\left[E\left(MP2\left(FC\right)/\text{G3MP2LargeXP}\right)\right]-\left[E\left(MP2\left(FC\right)/6-31G\left(d\right)\right)\right] \quad (1.31)$$

b. The Hartree-Fock energy limit E(HF/limit) is

$$\Delta E\left(\text{HF}\right)=\left[E\left(\text{HF/limit}\right)\right]-\left[E\left(\text{HF/G3MP2LargeXP}\right)\right] \quad (1.32)$$

c. The high level correlation energy is

$$E(\text{HLC})=-Cn_{\beta}-Dn_{\alpha} \quad (1.33)$$

where C, D, n_{β}, n_{α} are the empirical parameters.

5. The G4(MP2) energy (E(G4(MP2)) is calculated along with the consideration of spin-orbit coupling ΔE(SO)

$$\begin{aligned} E\left(G4\left(MP2\right)\right)=E\left[CCSD\left(FC,T\right)/6-31G\left(d\right)\right]+\Delta E\left(MP2\right) \\ +\Delta E\left(HF\right)+\Delta E\left(SO\right)+E\left(HLC\right)+E\left(ZPE\right) \end{aligned} \quad (1.34)$$

It was found that G4(MP2) gives significant improved results compared to G3(MP2) and are also more accurate than the full G3 theory with a less cost. G4(MP2) theory has an average absolute deviation of 1.04 kcal/mol for the G3/05 test set. Overall, G4(MP2) provide a more accurate and economical method[205].

2.7.10.2 W1 theory and W1-F12 theory

A detailed description and discussion of Wn theory is given in other references [187, 210, 211]. Here a brief overview of W1 theory and W1-F12 theory will be given as follows.

W1 theory [187] is developed by Martin and co-workers in order to an accuracy at ±1 kcal mol^{-1} without employing the empirical parameters derived from experiments. The following components are combined together in the energy calculation in W1 theory: (1) HF-SCF component; (2) valence CCSD correlation component, (3) valence (T) component; (4) inner-shell correction; (5) scalar relativistic effects; (6) first order spin-orbit coupling; and (7) zero-point vibrational energy. The specific protocol for Weizmann-1 theory is as followed:

1. Geometry optimization at the B3LYP/VTZ +1 level of theory
2. Zero-point vibrational point calculated from B3LYP/VTZ +1 frequencies with a scale factor of 0.985
3. CCSD(T)/AVDZ+2d single-point calculation and CCSD(T)/AVTZ+2d1f single-point calculation
4. CCSD/AVQZ+2d1f single-point calculation
5. TAE is extrapolate from SCF/AVDZ+2d, SCF/AVTZ+2d1f and SCF/AVQZ+2d1f components of TAEs
6. The CCSD valence correlation component is extrapolated from the three valence correlation energies from CCSD(T)/AVDZ+2d and CCSD(T)/AVTZ+2d1f calculations
7. The valence (T) component is extrapolated from valence (T) component from from CCSD(T)/AVDZ+2d and CCSD(T)/AVTZ+2d1f calculations
8. Inner-shell correction is from CCSD(T)/MT small calculation

9. Scalar relativistic and spin-orbit coupling is from ACPF/MT small calculation

It is worth noting that the CCSD(T) (W1 theory) energies depends on the combination of large Gaussian basis sets with extrapolation techniques, which leads to an significant computational cost. For instance, for systems consisting of over nine nonhydrogen atoms, the computational cost caused by the most economical W1 theory is prohibitively expensive based on the current server capability. W1 theory has a mean absolute error of 0.30 kcal mol^{-1} and contains a single, molecule-independent, empirical parameters which is not derived from the experiments, but form the results.

In order to extend the applicability of W1 theory, explicitly correlated version of W1 theory, namely W1–F12 theory [212] has been developed. It was shown that CCSD–F12 basis set convergence is faster than the conventional calculation. In the W1–F12 theory, all the CCSD correlation energy was obtained using the explicitly correlated CCSD(F12) method. The benchmark work suggested that W1–F12 theory has an excellent performance for systems with only first-row elements, attaining a root mean square deviation of 0.19 kcal mol^{-1} against all-electron, relativistic CCSD(T) reference atomization energies at infinite basis set limit. Furthermore, W1–F12 was applied to large system such as benzene, naphthalene, anthracene and DNA bases adenine, cytosine, etc., where good agreements were shown.

2.7 Conclusions and gaps

Fundamental understanding of the thermal decomposition of biomass during pyrolysis is crucial both for science and industry. However, the multiscale of biomass feedstock and the multiphase of the pyrolysis hinder us to reveal the chemistry of biomass pyrolysis. For biomass, length scales within lignocellulosic biomass span eleven orders of magnitude, from bond to biopolymer, wood cell, wood fibre and tree.

During degradation, variation is occurring at all levels, rendering fundamental prediction a challenge. For pyrolysis, a serious of simultaneous reactions such as depolymerisation, dehydration, polymerisation, fragmentation and carbonisation are undergoing as well as interacting with each other, making the whole process exceedingly complicated. One key problem is the lack of the identification and characterisation of the pyrolysis reaction products which is significant for the understanding of product formation characteristics and mechanisms. Previous research efforts mainly focused on reactor development, kinetic models and the parametric influence on the product distribution. Due to the complexity of biomass pyrolysis and the absence of well-established analytical techniques, mechanistic understanding has remained fairly obscure.

2.8 Specific research objectives

To address the research gaps identified in the above section, this thesis aim at understanding the identification and characterisation of pyrolysis intermediates and the mechanism of their transformations and interactions. A detailed network of the proposed methodology in this research is depicted in Figure 2-14. The specific objectives are:

1. To characterise the products from pyrolysis of cellulose, hemicellulose and lignin, respectively and investigate their interactions during pyrolysis.
2. To identify and characterise cellulose pyrolysis products at different scales using a TGA, a micropolyser and a fixed-bed reactor.
3. To assess the effect of residence time and temperature on the formation of cellulose pyrolysis products in a micro fixed-bed reactor and investigate the transformations among important products from cellulose pyrolysis.

4. To propose possible formation and decomposition pathways in cellulose pyrolysis, use *ab initio* thermochemical protocols to simulate, study the energy profiles and identify the rate-determining step.
5. To apply *ab initio* thermochemical protocols in thermochemistry calculations for the determination of heat formation of C_{60}.

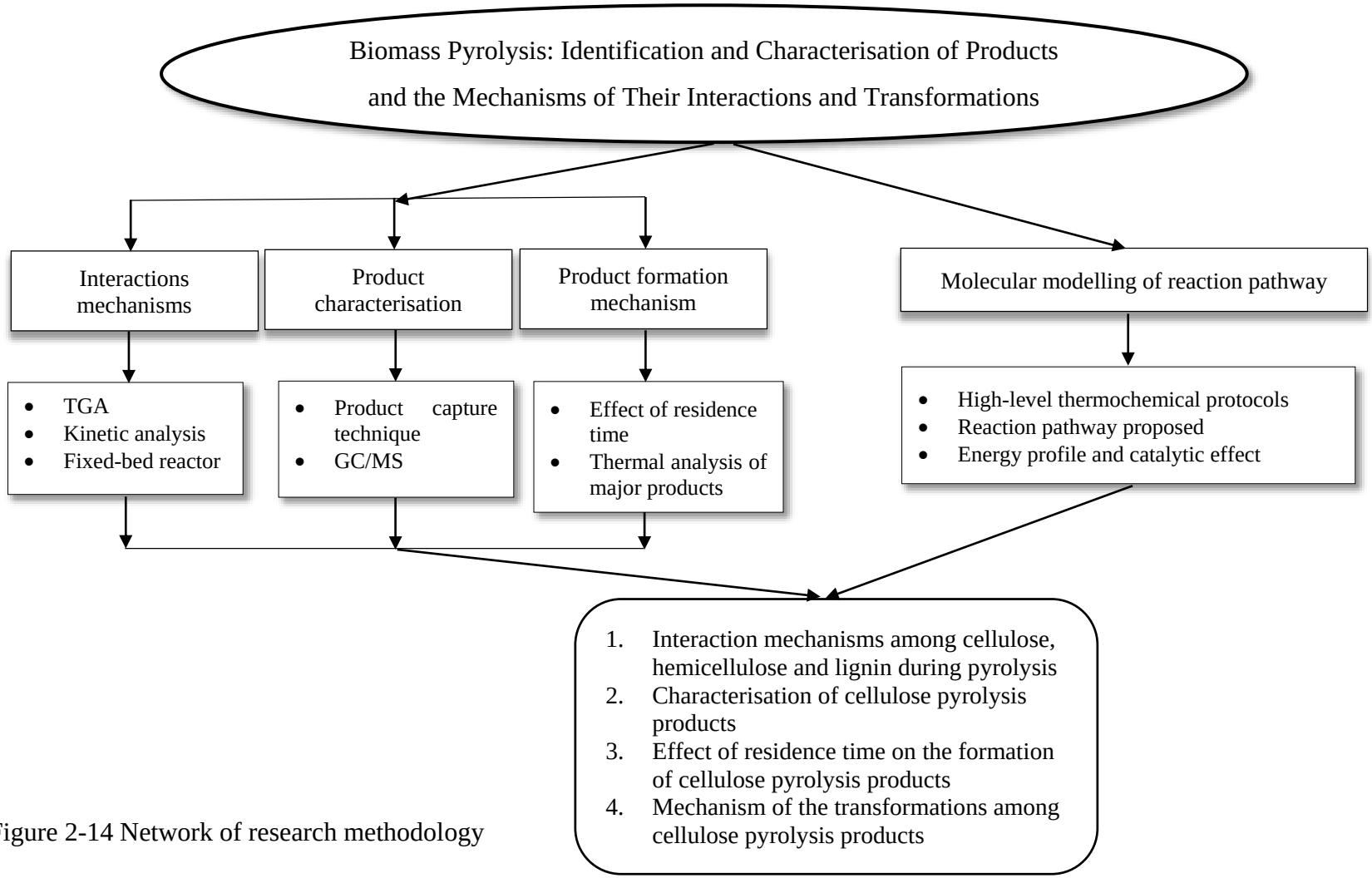

Figure 2-14 Network of research methodology

Chapter 3. Investigation into the Interactions between Cellulose, Hemicellulose, Lignin during Pyrolysis

3.1 Introduction

Chapter 2 reported that literature findings regarding the interactions between the biomass components (cellulose, hemicellulose and lignin) during pyrolysis were varied and sometimes contradictory. Against this backdrop, the present work aims to understand how cellulose, hemicellulose and lignin interact during pyrolysis. The effect of temperature on the interactions was investigated. Furthermore, the effects of the interactions on reaction kinetics and product formation were quantitatively studied. The pyrolysis experiments of cellulose, hemicellulose, lignin and their mixture were first carried out in a thermogravimetric analyser (TGA) where the basic thermal degradation characteristics were identified and the pyrolysis kinetics was discussed. The experiment was then carried out in a fixed-bed reactor to fully characterise the pyrolysis product composition and yields under various reaction conditions and to investigate the interactions between cellulose, hemicellulose and lignin at a molecular level.

3.2 Methodology and experimental details

3.2.1 Non-isothermal pyrolysis in TGA

The three components (cellulose, hemicellulose and lignin) were purchased from Sigma-Aldrich. Cellulose is in powder fibrous film, and lignin is in brown powders whereas xylans in yellow powder film was used as a representative component of hemicellulose.

Cellulose, hemicellulose (xylan), lignin and sample mixture (cellulose, xylan, lignin mixed with a ratio of 1:1:1) samples were pyrolysed in a TGA (SDT Q5000, TA Instruments). A thin layer of the sample (ca. 5.7mg) was distributed evenly in a ceramic crucible and placed in the TGA. The sample was then heated at a desired heating rate to the final temperature of 1023 K in nitrogen at a flow rate of 150

ml•min^{-1}. The non-isothermal pyrolysis experiments were performed at different heating rates, namely, 3 K•min^{-1}, 15 K•min^{-1}, 30 K•min^{-1}, 60 K•min^{-1}, and 90 K•min^{-1}, from room temperature to the desired 1023 K.

3.2.2 Kinetic analysis using the Friedman method

The TGA data of the pyrolysis of cellulose, hemicellulose, lignin and sample mixture in this experiment was subjected to kinetic analysis using the Friedman method [213]. The single step reaction model is commonly used in pyrolysis studies [214] as it is independent of heating rates to estimate the reaction kinetics. The rate of solid-state degradation or conversion, $d\alpha / dT$, can be described by

$$\frac{d\alpha}{dT} = \frac{1}{\beta} k(T) f(\alpha) = \frac{1}{\beta} A \exp\left(\frac{-E}{RT}\right) f(\alpha) \tag{3.1}$$

where T is the particle temperature (K), α the degree of conversion, β the heating rate (K•min^{-1}), $k(T)$ the temperature-dependent rate constant, $f(\alpha)$ the differential conversion function, A the pre-exponential factor (min^{-1}), E the activation energy (kJ•mol^{-1}) and R is the universal gas constant (8.314JK^{-1}mol^{-1}), respectively.

The degree of conversion, α is determined from Eq.(3.2).

$$\alpha = \frac{m_0 - m_t}{m_0 - m_f} \tag{3.2}$$

where the m_0 is the initial mass, m_f the final mass and m_t is the mass at time t.

Rearranging the Eq. (3.1) based the Friedman could lead to

$$\ln\left[\beta\left(\frac{d\alpha}{dT}\right)_\alpha\right] = -\frac{E_\alpha}{RT_\alpha} + \ln\left[A_\alpha f(\alpha)\right] \tag{3.3}$$

For a given value of α, the plot of $\ln\left[\beta\left(d\alpha/dT\right)\right]$ vs. $1/T_\alpha$ is a straight line with the slope being $-E_\alpha/R$, from which the activation energy can be calculated.

3.2.3 Pyrolysis in a fixed-bed reactor

A schematic diagram of the fixed-bed reactor system [215, 216] is shown in Figure 3-1. A cellulose sample of 0.75 g was weighed, placed into a crucible and then inserted into the cold zone of the reactor before the pyrolysis started. The system was purged with nitrogen at 500 ml•min^{-1} after the furnace reached the required temperature. The sample was then pushed into the reaction zone using a stainless steel pushing pod and kept there for 15 minutes for pyrolysis. The condensable volatiles known as pyrolysis liquid, were then collected using a two-stage cold system, which consisted of a U tube and 4-meter long PFA cooling coil immersed in a salt-ice cooling bath (253 K) and ethanol-dry ice cooling bath (195 K), respectively. The liquid was stored properly after each experiment for further analysis. The non-condensable volatiles, known as pyrolysis gas, were collected in a gas collection bottle. Solid products remaining in the crucible were regarded as the char. The weight of solid residue and liquid were taken by the increases of weights of the crucible and cooling coils, respectively.

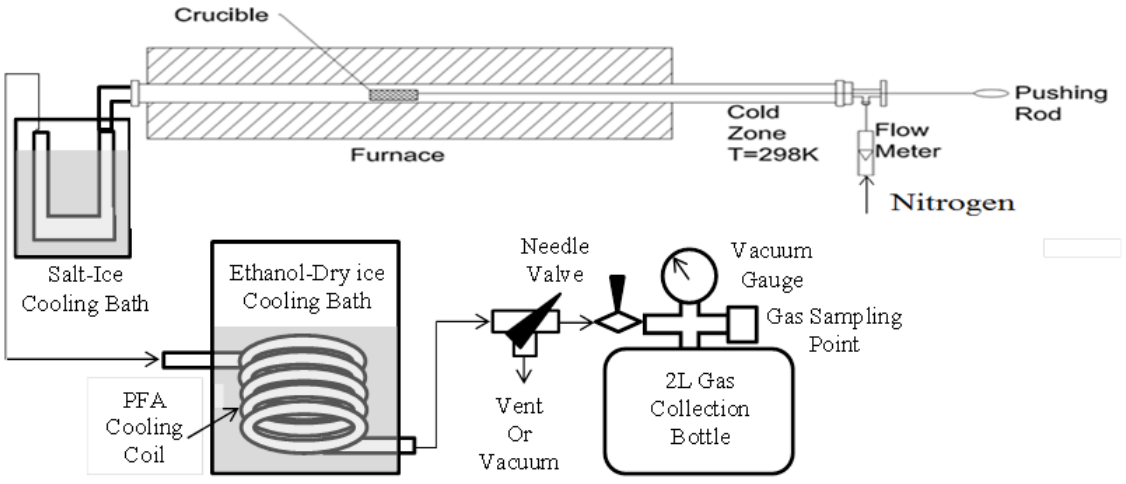

Figure 3-1 A schematic diagram of a fixed-bed reactor setup

The yields of char (w_c), pyrolysis liquid (w_l) and pyrolysis gas (w_g) were then calculated from the experimental data using the following equations:

$$w_c = \frac{m_c}{m_o} * 100\% \quad (3.4)$$

$$w_l = \frac{m_l}{m_o} * 100\% \quad (3.5)$$

$$w_g = (1 - w_c - w_l) * 100\% \quad (3.6)$$

where m_c, $m_l$and m_o are the weights of the char, pyrolysis liquid and the initial weight of the cellulose sample used, respectively.

Pyrolysis experiments were carried out at 823 K, 873 K, 923 K, 973 K, and 1023 K, respectively. Each experiment was repeated three times and the results reported were the average data of the three measurements. A Gas Chromatography - Mass Spectrometer (Agilent 7890A GC - 5975C MS) using a Restek RTX 65 column (30m in length and 250μm i.d. and 0.1 μm film thickness) was configured to analyse the pyrolysis liquid products. The inlet and the GC-MS interface were kept at 648K and 573 K, respectively. The initial temperature of the column, 313K was maintained for 2 minutes and was subsequently increased to 573 K at 5 K•min^{-1}. The final temperature was maintained for 6 minutes. External standard method was used for the quantification of pyrolysis products. For each identified product, the average results of the peak area and peak area% were calculated and used for analysis. Due to the complexity of cellulose pyrolysis products, a quantitative analysis of all liquid compounds was not conducted. However, the chromatographic peak area of a compound is considered linear with its quantity, and the peak area% is linear with its content. Therefore, for each product and category, its average peak area value obtained under different reaction conditions can be compared to reveal the changing of the yields, and the peak area% value can be compared to show the changing of its relative content among the detected products.

3.3 Results and discussion

3.3.1 Kinetic analysis

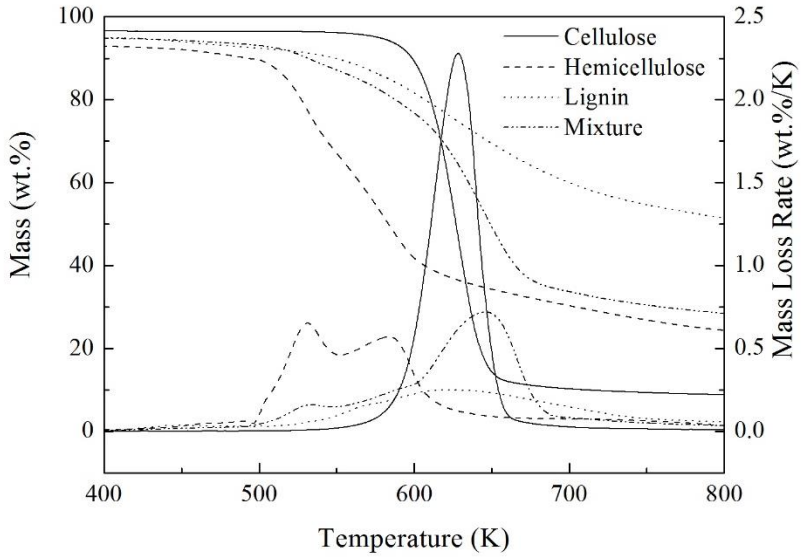

Figure 3-2 Pyrolysis mass loss and mass loss rate of cellulose, hemicellulose, lignin and sample mixture in a TGA at a heating rate of 30 K•min^{-1}

The mass loss and mass loss rates of cellulose, hemicellulose, lignin and sample mixture pyrolysed in the TGA at the heating rate of 30 K•min^{-1} are presented in Figure 3-2. The pyrolysis of cellulose occurred between 500 K and 700 K with the maximal mass loss rate (2.2 wt.%•K^{-1}) at ca. 630 K and 0.1 wt.% of solid residual left. The pyrolysis of hemicellulose started at 500 K and completed at around 650 K during which the mass loss was about 65 wt.% and two loss peaks identified at ca.523 K and ca. 573 K. After 650 K, the mass loss rate is low (ca. 0.085 wt.%•K^{-1}) and the amount of solid residue left is still high (ca. 20 wt.%). Compared to cellulose and hemicellulose, the pyrolysis of lignin has a very slow mass loss rate (less than 0.25 wt.%•K^{-1}) from 500 K to 800 K with ca. 60 wt.% of solid residual left. This might be due to the polymerisation reactions during lignin pyrolysis, leading to char production [217]. The pyrolysis of sample mixture mainly occurred from 500 K to 700 K in which two distinguished peaks of

mass loss can be identified. The first peak is located at 523 K whereas the second peak is located at 650 K. The remaining solid residue is ca. 30 wt.%. Consistent with the previous study [29], these two peaks can be accounted for by the decomposition of hemicellulose and cellulose, respectively. And the addition of lignin strongly decreased the mass loss rate due to the effect of polymerisation reactions.

In order to further investigate the pyrolysis kinetic of the three components and sample mixture, the TG data was analysed according to the Friedman method to investigate the model-free activation energy. Figure 3-3 shows the plot of $\ln\left[\beta\left(d\alpha/dT\right)\right]$ against $1/T$ as a function of conversion from 0.2 to 0.75. The model-free activation energy at each conversion was obtained from the slope of each linear regression line in Figure 3-3. The calculated squares of the correlation coefficient, R2, corresponding to the linear fitting used in the Friedman method were in the range from 0.98 to 1. The calculated activation energy as a function of conversion is depicted in Figure 3-4.

The activation energy of cellulose remained relatively constant with $E_{\alpha.cellulose}$ = 260.42 kJ•mol^{-1} whereas the activation energy of hemicellulose, lignin and sample mixture changed as the reaction proceeded. The activation energy of hemicellulose fluctuated around 300 kJ•mol^{-1} when the conversion was around 40% but overall steadily increased from 280 kJ•mol^{-1} to 375 kJ•mol^{-1}. For the lignin, the activation energy was around 265 kJ•mol^{-1} as the conversion was less than 35% and then increased to ca. 360 kJ•mol^{-1} when the conversion was greater than 40%. This is expected as cellulose is a uniform polymer of D-glucopyranose units while hemicellulose, lignin are consisted of various monomers with complex functional groups and bonding structures. However, the activation energy of sample mixture had a different trend compared to cellulose, hemicellulose and lignin. It increased as the conversion increased till 40% and then decreased when the conversion exceeded 40%. This difference in activation energy

showed that the activation energy of pyrolysis of sample mixture cannot be simply regarded as the superposition of the pyrolysis of the three building components, which indicates non-negligible interactions between cellulose, hemicellulose and lignin during pyrolysis.

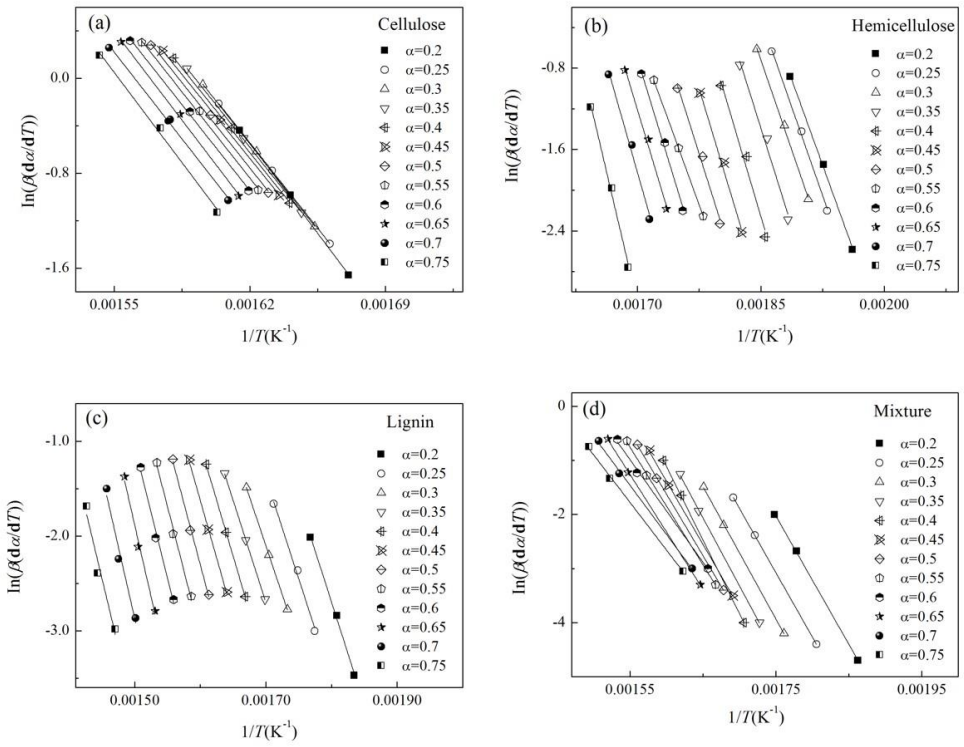

Figure 3-3 The Arrhenius plots for pyrolysis of cellulose, hemicellulose, lignin and sample mixture using the Friedman method

3.3.2 Pyrolysis in a fixed-bed reactor

In order to understand the effect of the interactions of the three components on the yields and compositions of pyrolysis products at a molecular level, pyrolysis experiments of cellulose, hemicellulose, lignin and sample mixture in the fixed-bed reactor were carried out at temperatures of 823 K, 873 K, 923 K, 973 K, and 1023 K. The yields of pyrolysis products including gas, liquid and char

are shown in Figure 3-5 and a detailed characterisation of pyrolysis liquid compounds is illustrated in Figure 3-6.

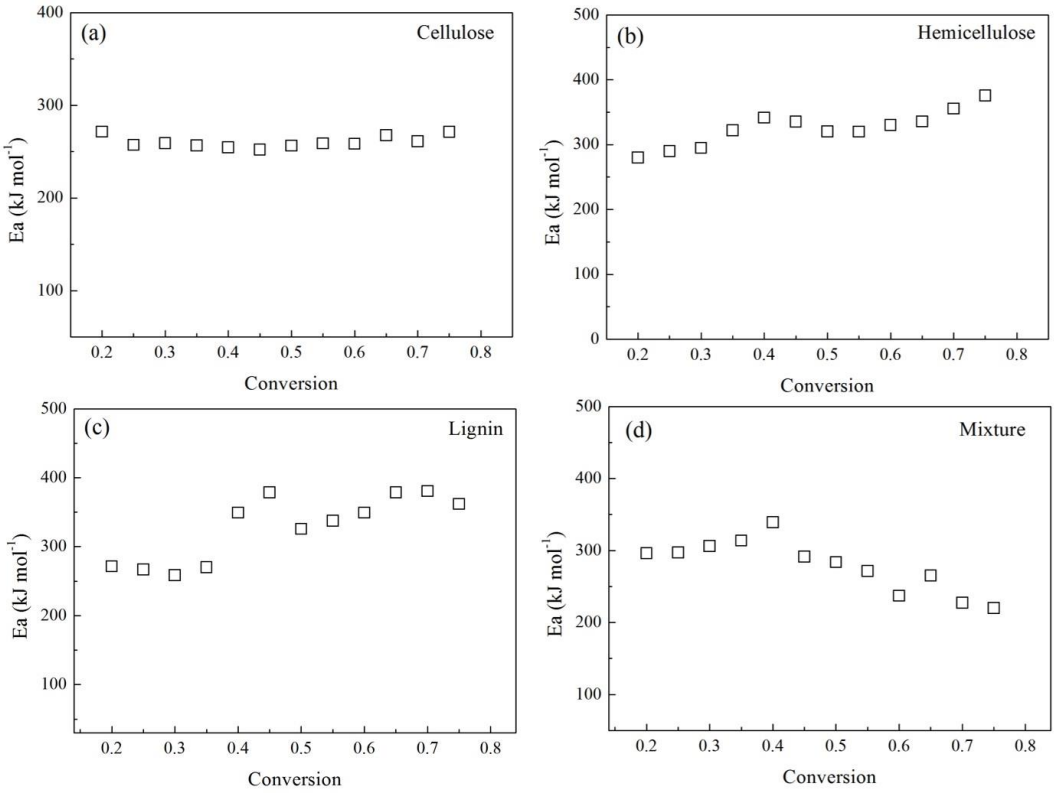

Figure 3-4 Plots of activation energy as a function of conversion for cellulose, hemicellulose, lignin and sample mixture

3.3.2.1 Yields of pyrolysis gas, liquid and char

The yields of gas, liquid and char from pyrolysis of cellulose, hemicellulose, lignin, sample mixture and calculated average (calculated average of the three components based on the superposition assumption) at different temperatures are shown in Figure 3-5. In pyrolysis of cellulose, hemicellulose and lignin, the yield of gas increased and the yield of char decreased as temperature increased from 823 K to 1023 K. The yield of liquid increased with temperature increasing, then reached a maximum at 923 K and then decreased after 923 K. Among the three components, lignin has the lowest yield of gas and highest yield

of char. From 823 K to 923 K, hemicellulose had the highest yield of gas whereas cellulose had the highest yield of liquid. After 923 K, hemicellulose and cellulose had similar product yields. This can be attributed to the fact that hemicellulose has a random amorphous structure whereas cellulose is a very long polymer of glucose units. Thus, hemicellulose is easier to be decomposed at the lower temperature than cellulose.

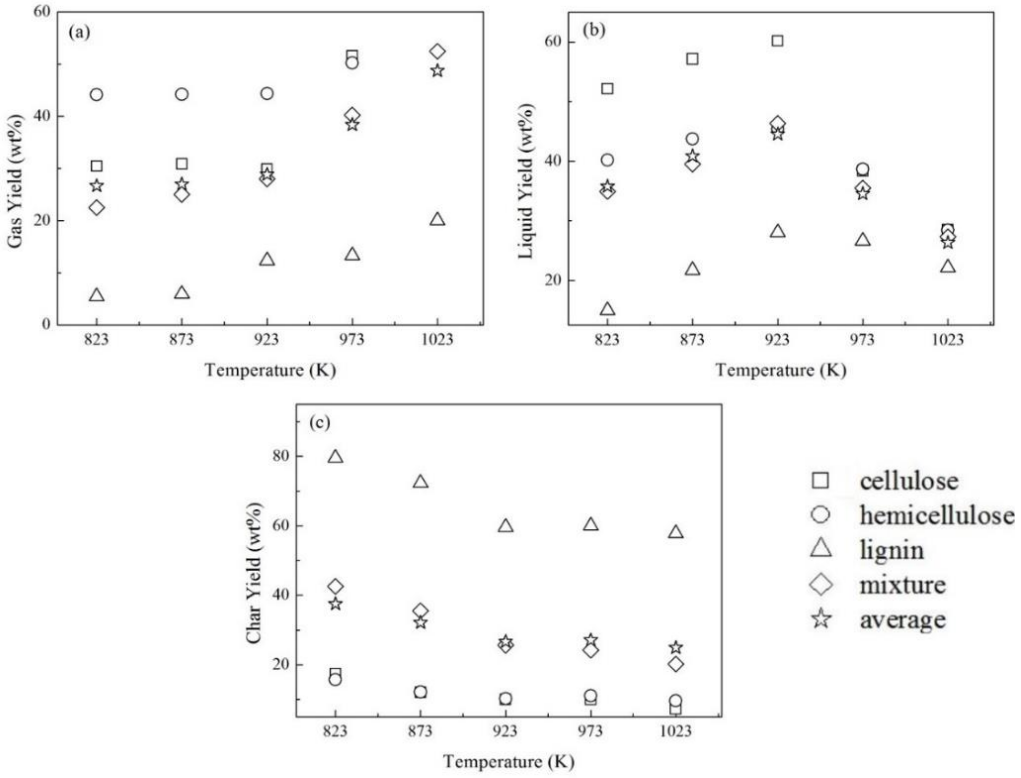

Figure 3-5 Yields of gas (a), liquid (b) and char (c) in pyrolysis of cellulose, hemicellulose, lignin, sample mixture and calculated average as a function of temperature in a fixed-bed reactor

In Figure 3-5, the yields of gas, liquid and char in pyrolysis of sample mixture and calculated average were also shown. At all temperatures from 823 K to 1023 K, the yield of liquid from mixture pyrolysis was very close to the calculated average. The yield of gas in pyrolysis of sample mixture was higher than

the calculated average and the yield of char in pyrolysis of sample mixture was lower than the calculated average as temperature increased from 823 K to 923 K. However, when the temperature exceeded 923 K, the yield of gas from mixture pyrolysis was higher than the calculated average and the yield of char in pyrolysis of sample mixture was lower than the calculated average. This indicates that in the interactions of the three components during pyrolysis, the reactions for char production such as polymerisation and oligomerisation [122, 218] were more favored at temperature from 823 K to 923 K whereas the cracking reactions [219, 220] were more favored at higher temperatures from 923 K to 1023 K.

3.3.2.2 Yields and composition of pyrolysis liquid compounds

In order to investigate the interactions of cellulose, hemicellulose, and lignin during pyrolysis at a molecular level, pyrolysis liquids were analysed using GC-MS. A variety of compounds were detected and classified as anhydrosugars, furans, ketones, acids, aldehydes, esters, phenols, benzenes and others [147, 221]. Anhydrosugars such as levoglucosan and levoglucosenone were the main products in cellulose pyrolysis whereas smaller oxygenated molecules such as ketones, acids were the main products in hemicellulose pyrolysis. In lignin pyrolysis, the production of phenols dominated in all temperatures while no anhydrosugars were detected and a small amounts of ketones, acids and esters were produced. These differences are because of the chemical structure of the three components. In general, the formation of anhydrosugars is mainly produced by cellulose via glycosidic bond cleavage and intramolecular hydrogen rearrangements [92]. Ketones and acids are mainly derived from the decomposition of hemicellulose via the breakage of the acetyl groups and uronic acid side chains. Phenols are produced in the lignin pyrolysis as the lignin basic units (p-coumaryl alcohol, coniferyl alcohol, and sinapyl alcohol [222]) are all phenols. In pyrolysis of cellulose, hemicellulose and lignin,

the increase of temperature promoted the production of phenols and benzenes. For all oxygenated compounds such as anhydrosugars, ketones and furans, their yields steadily increased as temperature increased from 823 K to 923 K but significantly decreased when temperature exceeded 923 K.

In Figure 3-6, the compositions and their relative peak areas of pyrolysis liquid from sample mixture and calculated average (superposition of cellulose, hemicellulose and lignin products assuming no interactions) were also shown. It can be seen that the relative peak areas% of all oxygenated compounds in pyrolysis of sample mixture remained relatively constant around 56% from 823 K to 923 K but decreased to 25.68% when the temperature reached 1023 K. The relative peak areas% of all oxygenated compounds in the calculated average was about 6% higher than the relative peak areas% of the mixture at all temperatures. The relative peak areas% of phenols and benzenes from pyrolysis of sample mixture increased from 38.37% to 72.58% when the temperature increased from 823 K to 1023 K. The relative peak areas% of phenols and benzenes in the calculated average were lower than the relative peak areas% in pyrolysis sample mixture at all temperatures and the gaps increased from 4% to 10% as temperature increased. This indicates that in the pyrolysis of sample mixture, the formation of lignin derived compounds was promoted while the formation of cellulose derived and hemicellulose derived compounds was suppressed. At 1023 K, no anhydrosugar compounds were detected in pyrolysis of sample mixture.

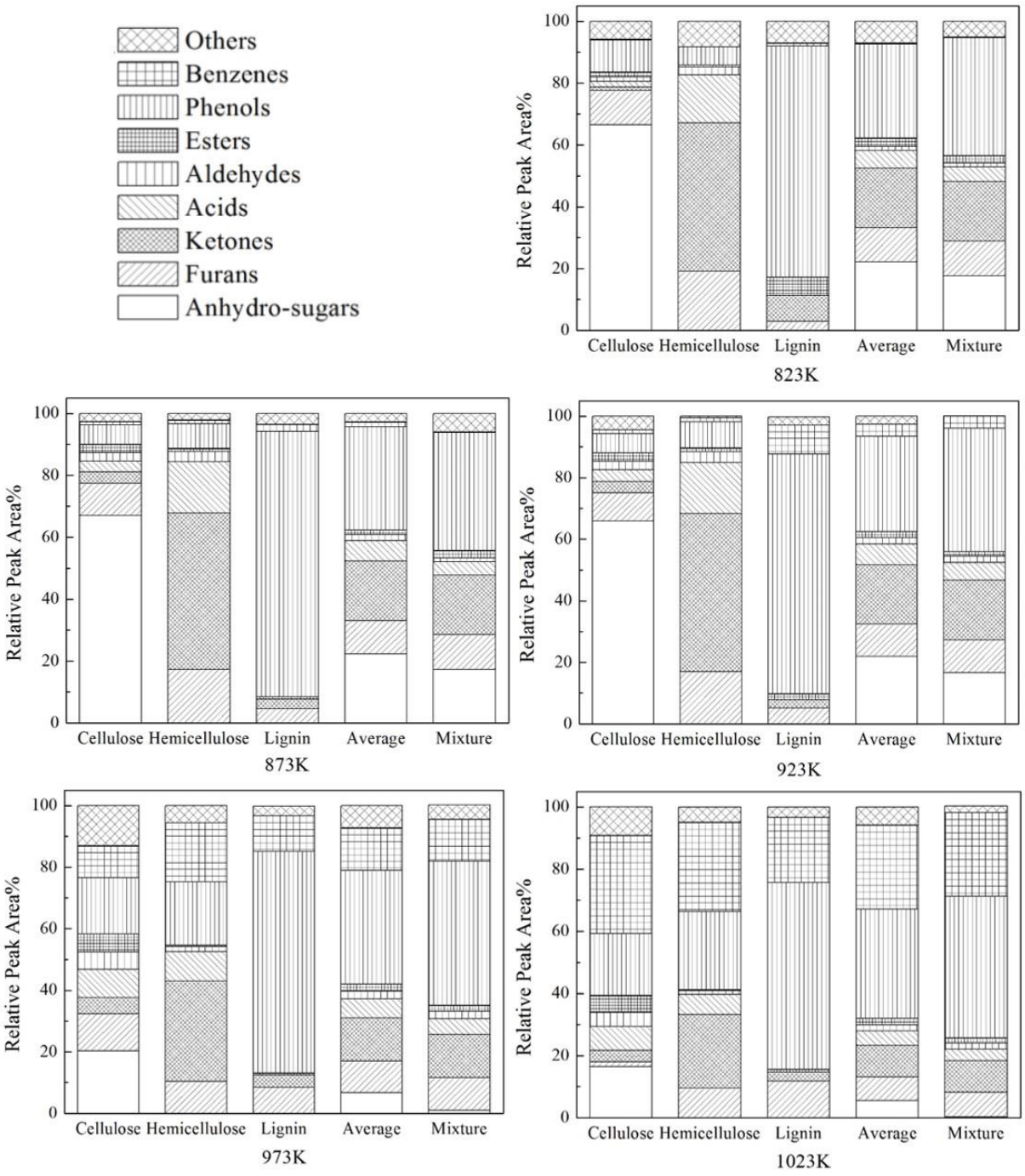

Figure 3-6 Variations of composition and relative peak areas of pyrolysis liquid compounds as a function of temperature in a fixed-bed reactor

3.4 Conclusions

In order to assess how cellulose, hemicellulose and lignin interact during pyrolysis, the pyrolysis experiments of cellulose, hemicellulose, lignin and their sample mixture were studied experimentally using thermogravimetric analyser (TGA) and in a fixed-bed reactor (FBR) at various pyrolysis temperatures. The following conclusions have been drawn from the present work. Kinetic analysis based on TGA experiments showed that the activation energy of cellulose remained relatively constant around 260.42 kJ•mol^{-1} whereas the activation energy of hemicellulose and lignin both increased from 250 kJ•mol^{-1} to 375 kJ•mol^{-1} as the conversion increased. The activation energy of their sample mixture showed a decreasing trend as the conversion decreased. This opposite trend indicates that the interactions of cellulose, hemicellulose and lignin play an important role during pyrolysis. As a result of the interactions between cellulose, hemicellulose and lignin, the yield of char increased from 823 K to 923 K while the yield of gas increased from 923 K to 1023 K. The formation of lignin derived compounds were promoted whereas the formation of cellulose derived and hemicellulose derived compounds were inhibited.

Chapter 4. Identification and Characterisation of Cellulose Pyrolysis Products

4.1 Introduction

Cellulose is the most abundant component in all kinds of biomass, which makes up to 30-50% by dry mass of a plant [12]. Cellulose is a linear polymer of D-glucopyranose units linked by β-1,4-glycosidic bonds [13]. As discussed in Chapter 2, reactions in cellulose pyrolysis such as depolymerisation, dehydration, fragmentation and charring have been extensively studied in literature. The most widely accepted kinetic scheme was developed by Shafizadeh [223] in which an initial step formed "active cellulose", which subsequently decomposed by two competitive reactions, one yielding volatiles and the other forming char and gas. Capart *et al.* [224] proposed that the cellulose decomposition occurred directly via two competitive channels, one ascribed to the formation of levoglucosan and char, the other to the light gas. However, none of these models described the decomposition mechanism or product formation in detail.

Recently, research efforts have shifted toward understanding the pyrolysis chemistry combined with analytical techniques [39, 44, 60, 70, 104, 225-227]. In most of the studies reported [70, 225-227], pyrolysis products were collected in the downstream of the pyrolysis reactor in a condensation system and then subjected to further analysis such as GC-MS and HPLC. However, it should be noted that the condensation system was some distance downstream from the reactor and the residence time was at least around 1s [70, 225, 226]. Thus, the product volatiles were able to circulate freely in the system with the possibility for secondary reactions to occur. Several researchers [60, 104] directly analysed the pyrolysis products using a micropyrolyser coupled with a gas chromatograph-mass spectrometer (Py-GC-MS) in

order to minimise the effects of secondary reactions. The major disadvantage of this technique is that the heavier compounds could be hardly detected by the Py-GC-MS. To overcome this disadvantage, a molecular beam mass spectrometer [39, 44] was employed enabling the detection of high-molecular-weight compounds. A few peaks with high intensity was investigated [117, 228]; however, the majority of GC-MS non-detectable compounds remain unknown because of the limitation of mass spectrometer. Such studies have provided valuable insights into cellulose pyrolysis reactions, but a lack of an in-depth speciation and charaterisation of the pyrolysis products hinders a better understanding of the mechanism of cellulose pyrolysis.

The present work was aimed at understanding cellulose pyrolysis characteristics and pyrolysis product characterisation under various reaction conditions to reveal the pyrolysis mechanism. Cellulose pyrolysis experiments were first carried out in a TGA to identify the basic thermal decomposition characteristics. Cellulose was then pyrolysed in a micropyrolyser with the pyrolysis products being quenched immediately to minimise secondary reactions to investigate the formation of primary products. Lastly, pyrolysis experiments were conducted in a fixed-bed reactor to investigate the effect of pyrolysis temperature on the yields and compositions of cellulose pyrolysis products including pyrolysis liquid, gas and char.

4.2 Methodology and experimental details

Figure 4-1 shows the schematic diagram of a micropolyser for cellulose pyrolysis in the micropolyser. The pyrolysis experiments were carried out using a commercial CDS Pyroprobe (model 5200, CDS Analytical Inc. Oxford, PA). For each test, approximately 8 mg of cellulose sample (powder fibrous form, Sigma-Aldrich) was placed in the middle of the quartz tube (25 mm long, 1.9 mm i.d.) of the Pyroprobe

and then the quartz tube was heated to the final pyrolysis temperature at a heating rate of 20 K•ms^{-1}. The pyrolysis was performed at three different final temperatures, namely 823 K, 923 K and 1023 K and at each pyrolysis temperature, the pyrolysis time was held at the final pyrolysis temperature for 60 s. The pyrolysis products were then captured using a liquid nitrogen quenching method. An upside-down vial is placed on the top of the heating filament of the Pyroprobe while a nitrogen flow (250 ml•min^{-1}) was introduced through a union tee to sweep the pyrolysis products into the vial. Once the pyrolysis products entered the vial, the products condensed onto the inner surface of the vial as the surface temperature was low enough for quenching with the surrounding liquid nitrogen positioned in the gap between the inner surface and outer shell. It is believed that this setup can help to suppress the occurrence of secondary reactions as the pyrolysis products were immediately quenched. The pyrolysis products collected were then dissolved in 200 μl of acetone for further analysis.

Anhydro-oligosaccharides were proposed to be the primary products in many studies [229, 230]. However, due to the low volatility and high molecular weight of anhydro-oligosaccharides [231, 232], an in-depth understanding of their structure and formation still remains ambiguous. In order to have a more comprehensive characterisation of cellulose pyrolysis products, silylation of pyrolysis products was conducted, as the silyl derivatives were less polar and more thermal stable, making it possible to be analysed by GC-MS [233, 234]. The silylation procedure was as followed: the solution was first evaporated under a soft stream of nitrogen at ambient temperature and then dissolved in 10μl of pyridine/dichloromethane and reacted with 10 μl of N-methyl-N-(trimethylsilyl)trifluoroacetamide (MSTFA, Thermo Fisher Scientific), at 40 K for 30 minutes. All experiments were repeated three times and the reported data in the following section was the average of the three measurements.

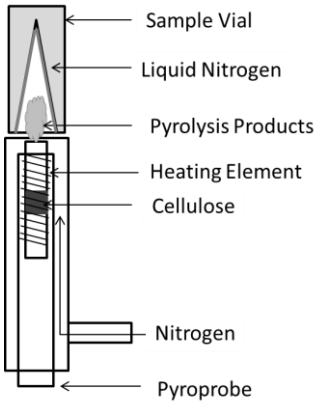

Figure 4-1 A schematic diagram of a micropolyser setup

A Gas Chromatography - Mass Spectrometer (Agilent 7890A GC - 5975C MS) using a Restek RTX 65 column (30 m in length and 250 μm i.d. and 0.1 μm film thickness) was configured to analyse the pyrolysis products. The inlet and the GC-MS interface were kept at 648 K and 573 K, respectively. The initial temperature of the column, 313 K was maintained for 2 minutes and was subsequently increased to 573 K at 5 $K \cdot min^{-1}$. The final temperature was maintained for 6 minutes. External standard method [60] was used for the quantification of pyrolysis products. A Gas Chromatography (Agilent 7890 GC) with two thermal conductivity detectors (TCD1 for H_2 detection with N_2 as carrier gas and TCD2 for CO, CO_2 and N_2 detection with He as carrier gas) and one flame ionization detector (FID for hydrocarbon detector with He as carrier gas) was configured to analyse the pyrolysis gas. The operational parameters were the same as the GC-MS system.

Cellulose samples were also pyrolysed in a TGA and a fixed-bed reactor as described elsewhere (Chapter 3). In the TGA, the non-isothermal pyrolysis experiments were performed at different heating rates, namely 3 $K \cdot min^{-1}$, 15 $K \cdot min^{-1}$, 60 $K \cdot min^{-1}$, and 90 $K \cdot min^{-1}$, from room temperature to 1023 K. In the fixed-bed reactor, pyrolysis experiments were conducted at 823 K, 873 K, 923 K, 973 K and 1023 K.

The pyrolysis liquid was analysed by GC-MS system aforementioned whereas the pyrolysis gas was analysed by GC-FID/TCD system.

4.3 Results and discussion

4.3.1 Non-isothermal cellulose pyrolysis in TGA

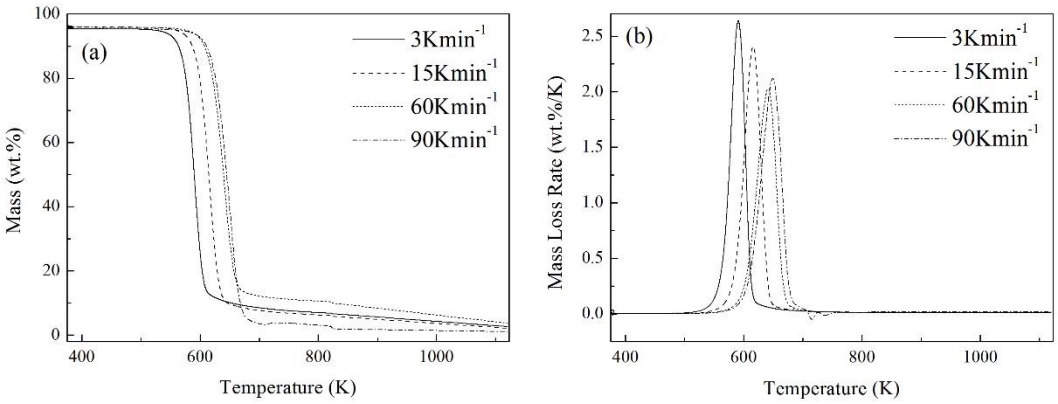

Figure 4-2 Cellulose pyrolysis in TGA at heating rate of 3, 15, 60, and 90 K•min^{-1} with a final temperature of 1123 K; (a) TG curves and (b) DTG curves

Figure 4-2 shows the mass loss and mass loss rate of cellulose heating from ambient temperature to 1123 K at the heating rate of 3, 15, 60 and 90 K•min^{-1} in TGA. Taking the case with the heating rate of 3 K•min^{-1} for example, before ca. 523 K, no obvious weight loss was observed. Moisture evaporation and possible desorption of very light hydrocarbons might occur at temperature below 523 K. The obvious mass loss (about 80 wt.%) started from 523 K and completed at 653 K between which one distinct peak appeared on the pyrolysis DTG curve of cellulose as shown in Figure 4-2(b) at ca 593 K. From 653 K to 1123 K, the mass loss observed was approximately 10 wt.%. It can be seen that from 523 K to 653 K, the majority of cellulose was pyrolysed in TGA whereas from 653 K to 1123 K, slightly thermal cracking [235] and decarbonisation [236] might occur .

As shown in the mass loss profiles of cellulose at all tested heating rates, the DTG curves shifted towards higher temperatures. The liberation of products from cellulose sample during pyrolysis was achieved when the pressure of the volatile products exceeded that of the ambient partial pressure. At lower heating rates volatile products were given sufficient time to diffuse and escape from the cellulose sample. When heating rates increased, the diffusion of volatile products was prohibited and the relatively light hydrocarbons volatilized at a higher temperature [237, 238]. As a result, DTG curves shifted to higher temperatures at higher heating rates as shown in Figure 4-2(b). Based on the understanding of cellulose pyrolysis behavior studied in TGA, further micropolyser and fixed-bed reactor experiments were conducted in the present research to reveal the mechanism underlying cellulose pyrolysis.

4.3.2 Cellulose pyrolysis in the micropolyser (CDS Pyroprobe)

4.3.2.1 Characterisation of cellulose pyrolysis products

The pyrolysis experiments of cellulose in CDS pyroprobe were carried out at temperature of 823 K, 923 K and 1023 K to investigate the effect of temperature on the yields and compositions of primary products and to reveal the mechanism of cellulose pyrolysis. The fast heating rate of CDS Pyroprobe and the downstream capture of products using liquid nitrogen provide a new insight into the formation of cellulose primary products. Figure 4-3 shows the ion chromatograph of products from cellulose pyrolysis at 823 K, 923 K and 1023 K, respectively, and Table 4-1 summarises the major compounds identified using GC-MS. The identified compounds were classified into five groups, namely furans, anhydro-sugars, ketones, and others [60, 70]. Not all pyrolysis products have been captured but the only most important ones. At 823 K, the identified compounds mainly consisted of furans and anhydro-sugars, while the ketones was in the trace amounts. The main furan and the anhydro-sugar compounds were furfural, levoglucosan and levoglucosenone. At 923 K, the identified compounds were similar to that at

823 K except that the 2, 3-andro-d-mannosan and D-Allose were also produced at relatively high concentrations. It suggests that the generations of furfural, levoglucosan and levoglucosenone were the main reactions occurring at 823 K and 923 K and as the temperature increased, more anhydro-sugar compounds were produced. As the pyrolysis temperature further increased to 1023 K, more than twenty five pyrolysis compounds were identified. Many compounds were not identifiable at lower temperatures. It is worth noting that 2, 3-andro-d-mannosan was only produced at 923 K while it disappeared at 1023 K, indicating that it might be decomposed at 1023 K.

Figure 4-4 shows the ion chromatograms of silyl derivatives of levoglucosan, cellobiose and cellulose pyrolysis products obtained at 823 K, 923 K and 1023 K. Due to the similarity of the volatility and molecular weight, levoglucosan and cellobiose (purchased from Sigma-Aldrich) were used as standards for the identification of monosaccharide and disaccharides in the pyrolysis products. In the chromatograms, the silyl derivatives of levoglucosan had one peak occurred at 23.5 minute with major mass fragments being at m/z of 204 and 217 whereas the silyl derivatives of cellobiose had two peaks, appearing at 38.7 and 39.7 minutes with major mass fragments being at m/z of 204 and 316.

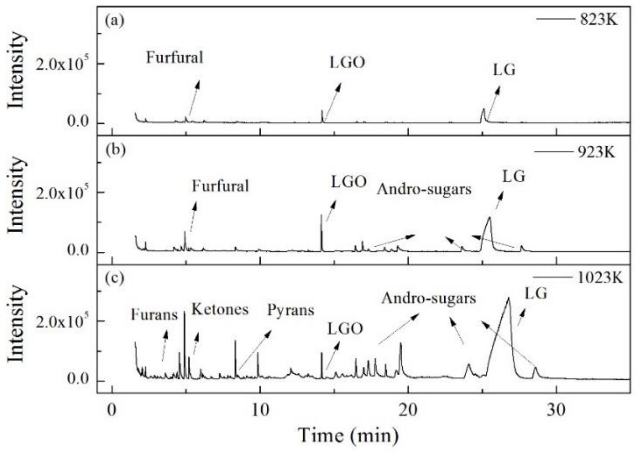

Figure 4-3 The ion chromatograph of cellulose pyrolysis products obtained at 823 K (a), 923 K (b) and 1023 K (c) in a micropolyser

Table 4-1 Identification of cellulose pyrolysis products at 823 K, 923 K and 1023 K in a micropolyser

	823 K	923 K	1023 K
Anhydro-sugars	levoglucosenone; levoglucosan	levoglucosenone 1,4:3,6-dianhydro-π d-glucopyranose D-Allose levoglucosan 1,6-anhydro-π d-glucofuranose 2,3-andro-d-mannosan	levoglucosenone; 1,4:3,6-dianhydro-π d-glucopyranose D-Allose levoglucosan 1,6-anhydro-π d-glucofuranose
Furans	furfural	furfural	furfural furan,2-methyl furan, 2.5-dimethyl 2(5H)-furanone 2(3H)-furanone, dihydro-4-hydroxy- 2-furancarboxaldehyde, 5-methyl 2(3H)-furanone, dihydro; 2-furancarboxaldehyde, 5-(hydroxymethyl)-
Ketones	Trace amount	Trace amount	2,3-butanedione 2-propanone, 1-hydroxy- 2H-Pyran-2,6(3H)-dione 2-cyclopenten-1-one, 2-hydroxy-
Others	Trace amount	Trace amount	2-cyclohexen-1-ol cis-1,2-cyclohexanediol phenols toluene

It can be found that in Figure 4-4(d), there were several peaks in the ion chromatograms of cellulose pyrolysis products appearing at the similar retention time to the silyl derivatives of cellobiose and the major mass fragments were also at the m/z of 204 and 316. Therefore, although the specific molecular structures that peaks 1 to 5 represented were unknown, based on the retention time and major mass fragments, it indicates that these compounds were disaccharides. It is also worth noting that the yields of disaccharides significantly increased as pyrolysis temperature increased from 823 K to 1023 K.

4.3.2.2 Formation of furfural, levoglucosan and levoglucosenone

As furfural, levoglucosenone and levoglucosan are believed to be the three major products of cellulose pyrolysis [104, 239], Figure 4-5 shows the variations of relative yields of furfural, levoglucosenone and levoglucosan as a function of pyrolysis temperature. The relative yield is calculated as the ratio of the quantified mass of the identified compound to the original mass of cellulose used. It is evident that the yields of levoglucosan and furfural increased with increasing pyrolysis temperature whereas the yield of levoglucosenone increased from 823 K to 923 K and then decreased as temperature continued to increase to 1023 K. This suggests that the formation of levoglucosenone was inhibited at elevated pyrolysis temperature while high temperature favored the formation of furfural and levoglucosan [104]. At high pyrolysis temperature, it is believed that levoglucosenone might be decomposed into low molecular weight compounds at 1023 K.

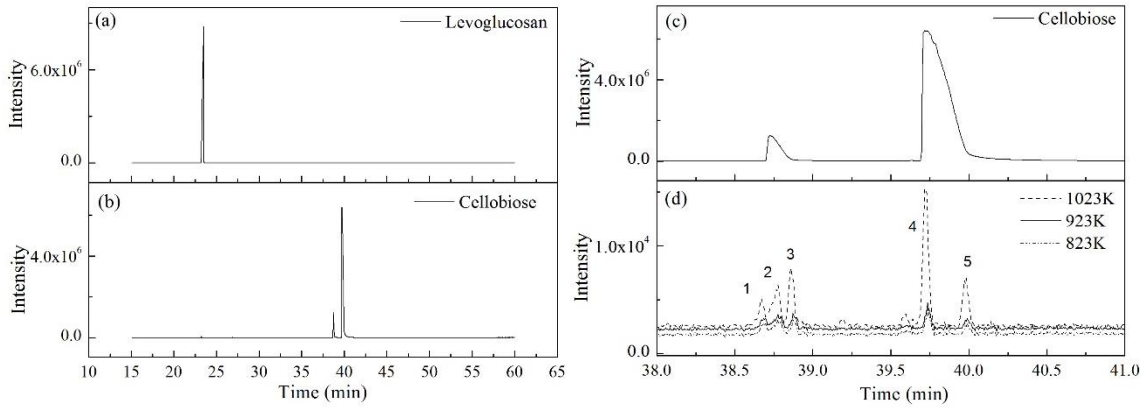

Figure 4-4 The ion chromatograms of silyl derivatives of levoglucosan (a), silyl derivatives of cellobiose (b and c), and silyl derivatives of cellulose pyrolysis products obtained at 823 K, 923 K and 1023 K (d) in a micropolyser

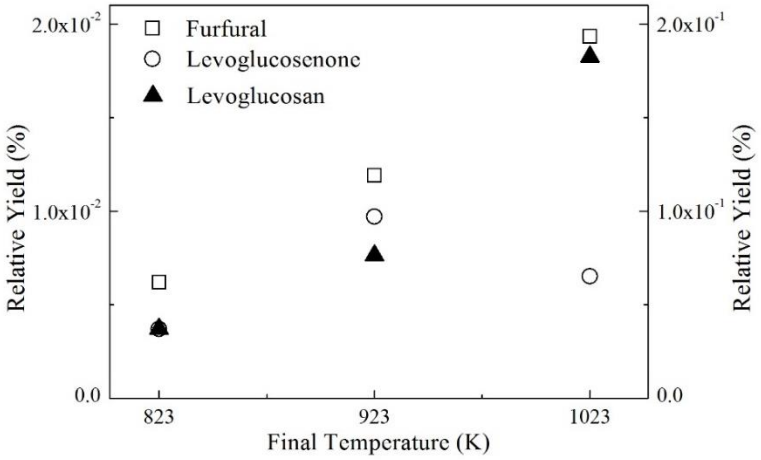

Figure 4-5 Yields of furfural, levoglucosenone and levoglucosan as a function of pyrolysis temperature in the micropolyser

4.3.3 Cellulose pyrolysis in a fixed-bed reactor

Cellulose pyrolysis in a fixed-bed reactor was carried out at temperatures of 823 K, 873 K, 923 K, 973 K and 1023 K to investigate the effect of temperature on the yields and compositions of pyrolysis liquid, gas and char, and to investigate cellulose pyrolysis mechanism.

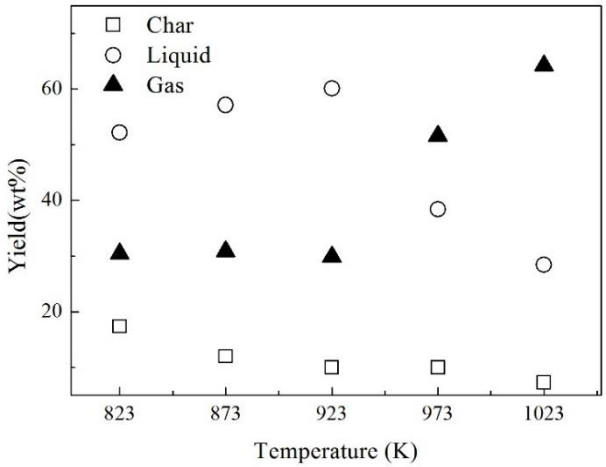

Figure 4-6 Yields of gas, liquid and char from cellulose pyrolysis as a function of temperature in a fixed-bed reactor

4.3.3.1 Yields of pyrolysis gas, liquid and char

The yields of cellulose pyrolysis liquid, gas and char at studied temperatures are shown in Figure 4-6. It was seen that the main products were pyrolysis liquid and gas while the char only accounts for a small fraction. Increasing the pyrolysis from 823 K to 923 K saw an increase in the amount of liquid whereas the amount of gas remained relatively constant. As the temperature further increased from 923 K to 1023 K the production of gas was significantly promoted whilst the production of liquid was inhibited. The increase in gas yield with increasing temperature was likely due to the increased rate of cracking at higher temperatures [219]. Furthermore, it has been argued that higher gas yield and declining liquid yield at temperatures greater than 923 K are the results of secondary cracking of liquid products at a greater rate at higher temperatures. The yield of char decreased as the temperature increased from 823 K to 1023 K.

Although it was argued that re-polymerization of cellulose pyrolysis products occurred to promote the formation of pyrolysis char, the thermal cracking reaction was the dominant process with the increasing temperature.

4.3.3.2 Yields of pyrolysis liquid compounds

As described in Chapter 3, all the detected liquid compounds were classified into eight categories. The eight groups were anhydro-sugars, furans, ketones, acids, aldehydes, esters, phenols and benzenes. Figure 4-7 and Table 4-2 show the effect of temperature on the peak area and peak area% of each group. The sum of the peak area% was not equal to 100% due to the small amount of other unidentified peaks on the chromatograms. It can be seen that the peak area and peak area% of each group was remarkably influenced by the pyrolysis temperature.

Among all liquid products, anhydro-sugar compounds were the dominant products in cellulose pyrolysis from 823 K to 923 K. With temperature further increasing to 1023 K, the peak area and peak area% of sugars both significantly decreased, indicating that sugar compounds were decomposed in the secondary cracking reactions at higher temperatures. Furans is a group of compounds which contains a furan oxygenated ring and is less thermal stable than sugar compounds [240]. Similar to anhydro-sugars, the production of furans was inhibited as the temperature increased from 823 K to 1023 K whereas the peak area% of furans remained relatively constant (around 20%) from 823 K to 973 K and significantly dropped to 1.66% at 1023 K. Ketones, acids, aldehydes and esters are groups of smaller fragmented oxygenated compounds. The peak area of these compounds all increased from 823 K to 873 K and decreased from 873 K to 1023 K. However, in the liquid compounds the peak area% of all these groups increased as the temperature was promoted. This indicates that all these small oxygenated compounds

were decomposed at a smaller rate than other larger oxygenated compounds such as sugars and furans. The peak area of phenols decreased from 823 K to 1023 K whereas the peak area% remained relatively constant from 823 K to 923 K and significantly increased to 19.96% when temperature reached 1023 K. The formation of benzenes was significantly promoted as temperature increased from 823 K to 1023 K. It should be noted that benzenes compounds are relatively close to the tar definition in European tar protocol [241] and the characteristics of benzenes formation are in consistent with previous finding that the yield of tar compounds was promoted by the elevated temperature [242] as the tar compounds were more thermally stable. This is also consistent with the DFT calculation results [243-245] that as temperature increases, OH groups in phenols are either expulsed or replaced by redundant H atoms.

4.3.3.3 Yields of pyrolysis gas compounds

The gas compounds from cellulose pyrolysis mainly consist of carbon monoxide (CO), carbon dioxide (CO_2), hydrogen (H_2), methane (CH_4), ethane (C_2H_6), ethylene (C_2H_4), and acetylene (C_2H_2). Table 4-2 lists the yields of the major gas compounds produced from cellulose pyrolysis at different temperatures.

As can be seen from Table 4-2, the concentrations of CO, H_2, CH_4, C_2H_6, C_2H_4 and C_2H_2 remained relatively constant from 823 K to 923 K. The dominant gas compounds were CO, CO_2 and H_2 and the proportion of all light hydrocarbons including CH_4, C_2H_6, C_2H_4 and C_2H_2 was trivial. As the temperature increased to 1023 K, the concentration of H_2, CH_4, C_2H_6, C_2H_4, and C_2H_2 significantly increased whilst the concentration of CO decreased from 51.55 mol% to 46.37 mol% and CO_2 from 31.69 mol% to 17.34 mol%. It indicates that the secondary cracking reactions of hydrocarbons occurred at a greater rate after 923 K.

4.4 Conclusions

Cellulose pyrolysis was studied experimentally using a thermogravimetric analyser (TGA), in a micropolyser and in a fixed-bed reactor (FBR) at various pyrolysis temperatures. The following conclusions have been drawn from the present work. TGA experiments showed that cellulose pyrolysis mainly occurred from 523 K to 623K. At 823 K and 923 K the primary products captured in the micropolyser were furans and anhydro-sugars but at 1023 K became more complex, consisting furans, anhydro-sugars, ketones and disaccharides. The formation of levoglucosenone and 2, 3-andro-mannosan was favored at temperatures of 823 K and 923 K but inhibited at the pyrolysis temperature of 1023 K. In the FBR, eight groups of pyrolysis liquid products were produced namely, anhydro-sugars, furans, ketones, acids, aldehydes, esters, phenols and benzenes, while CO, CO_2, H_2, CH_4, C_2H_6, C_2H_4, C_2H_2 were the main pyrolysis gas products. With temperature increasing, the yields of oxygenated liquid compounds, including anhydrosugars, furans, ketones, acids, aldehydes, and esters, were inhibited while the yields of phenols and benzenes were promoted. CO and CO_2 were the dominant gas products at temperatures from 823 K to 923 K, whereas the concentrations of H_2, CH_4, C_2H_6, C_2H_4 and C_2H_2 were significantly promoted as the temperature increased from 923 K to 1023 K.

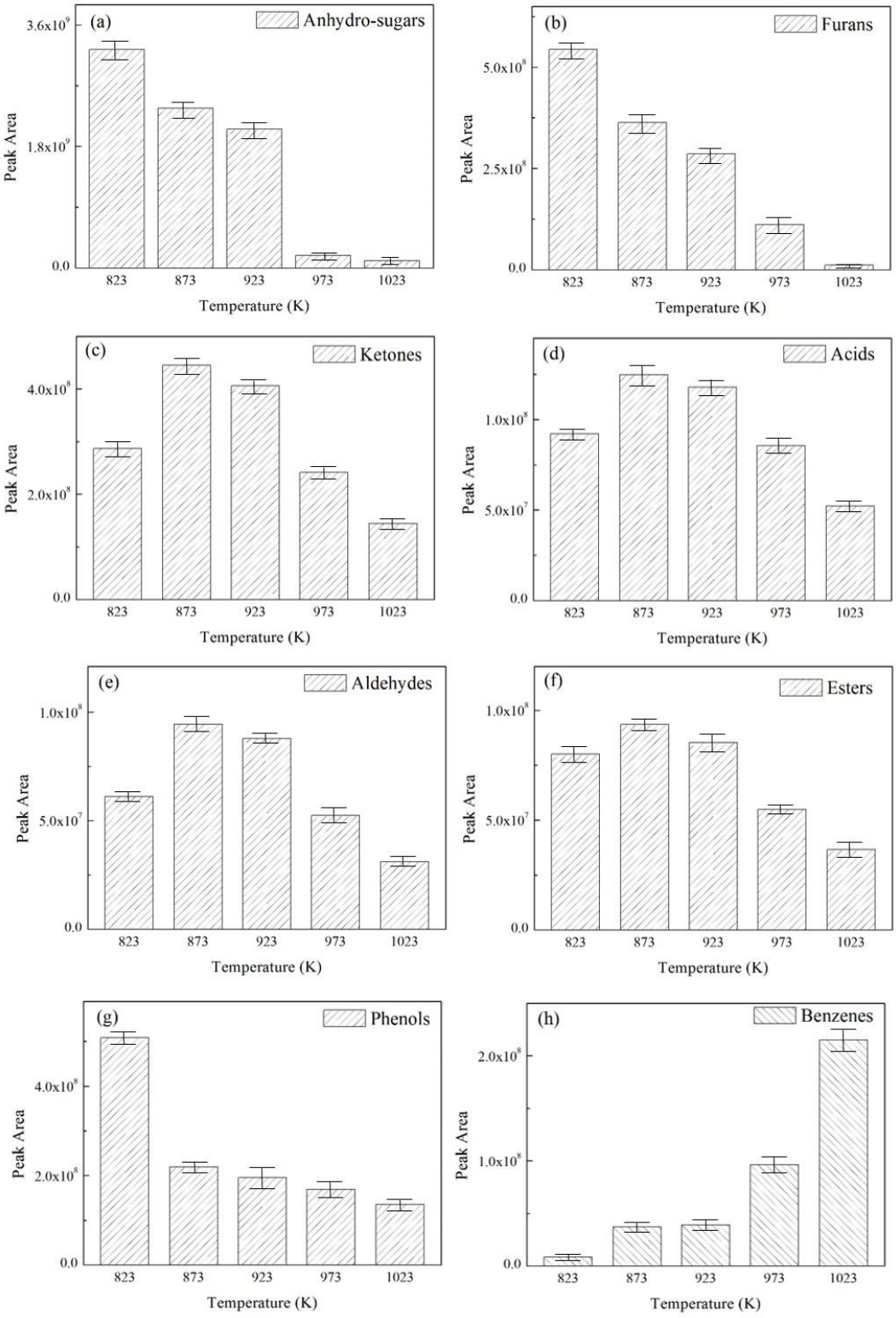

Figure 4-7 Peak area of anhydro-sugar (a), furans (b), ketones (c), acids (d), aldehydes (e), esters (f), phenols (g) and benzenes (h) as a function of pyrolysis temperature in a fixed-bed reactor

Table 4-2 Yields and compositions of cellulose pyrolysis products in a fixed-bed reactor at different pyrolysis temperatures

Cellulose products	Temperature				
	823 K	873 K	923 K	973 K	1023 K
Liquid (wt.%)	52.16	57.13	60.17	38.40	28.48
Compounds (Peak Area%)					
Anhydro-sugars	66.47	67.07	65.91	20.31	16.36
Furans	11.17	10.32	9.17	12.00	1.66
Ketones	1.10	3.75	3.67	5.26	3.65
Acids	1.89	3.54	3.78	9.22	7.69
Aldehydes	1.26	2.68	2.82	5.64	4.58
Esters	1.65	2.65	2.74	5.91	5.36
Phenols	10.46	6.24	6.26	18.24	19.96
Benzenes	0.17	1.06	1.26	10.37	31.58
Others	5.83	2.68	4.39	13.04	9.17
Gas[a] (wt.%)	30.44	30.87	29.88	51.60	64.27
Compounds (mol%)					
CO	52.11	45.23	51.55	47.79	46.37
CO_2	40.20	39.94	31.69	17.77	17.34
H_2	8.92	9.57	11.44	18.61	18.48
CH_4	0.00	2.31	2.54	8.53	9.99
C_2H_6	0.35	0.54	0.53	0.85	0.94
C_2H_4	1.38	1.54	2.00	4.04	4.25
C_2H_2	0.23	0.17	0.27	0.37	0.26
Char (wt.%)	17.40	12.00	9.97	10.00	7.29

Chapter 5. Unravelling the Formation Characteristics of Cellulose Pyrolysis Products and the Mechanisms of their Transformations

5.1 Introduction

In Chapter 4, a full characterisation of cellulose pyrolysis products was completed and an insight into formation mechanism in cellulose pyrolysis products was provided. At 1023 K the primary products in cellulose pyrolysis were furans, anhydro-sugars, ketones and disaccharides whereas at 823 K and 923 K the detected primary products were furans and anhydro-sugars. The formation of levoglucosenone and 2, 3-andro-mannosan was favored at temperatures of 823 K and 923 K but inhibited at the pyrolysis temperature of 1023 K. It also showed that the liquid compounds from cellulose pyrolysis can be classified into anhydrosugars, furans, ketones, acids, aldehydes, esters, phenols and benzenes. However, the formation mechanism of cellulose pyrolysis products remained unclear. As identified in Chapter 2, residence time is a very important controlling parameter for the pyrolysis process. In pyrolysis reactors of different scales (such as fixed-bed reactor [27], entrained flow reactor [36], fluidised-bed reactor [246, 247]), the residence time could span over several magnitudes, strongly affecting the yields and distribution of pyrolysis products [70]. Against this backdrop, a systematic investigation into the effect of temperature and residence time on the formation of cellulose pyrolysis products is essential to reveal the pyrolysis chemistry.

The objectives of this chapter are to have an improved quantitative understanding of the effect of residence time on the formation of cellulose pyrolysis liquid products, and to provide insights into cellulose pyrolysis mechanisms. The pyrolysis experiments were carried out in a micro fixed-bed reactor to investigate the effect of temperature and residence time on the yields and composition of cellulose

pyrolysis products. Thirteen compounds were identified and quantified in pyrolysis liquids. In order to further assess the reaction mechanism underlying the products' transformations, thermal analysis of important compounds, including cellobiose, levoglucosan, levoglucosenone and DGP was conducted.

5.2 Methodology and experimental details

5.2.1 Cellulose pyrolysis in a micro fixed-bed reactor

Cellulose (powder fibrous form, Sigma-Aldrich) pyrolysis was carried out in a micro fixed-bed reactor as schematically illustrated in Figure 5-1. The experimental rig consisted of a stainless chamber, a platinum filament heating probe (CDS Pyroprobe, model 5200, CDS Analytical Inc. Oxford, PA), a cooling trap and a gas bag for collecting the pyrolysis liquid and pyrolysis gas, respectively. The pyrolysis vapour was purged out of the chamber by nitrogen at four different flow rates (72, 360, 720, 1200 $ml \bullet min^{-1}$). Knowing the volume of the chamber and the gas flow rate, four vapour residence times of the volatiles generated from cellulose could be calculated, namely 30, 50, 100, and 500 ms, respectively. In a typical experiment, when the stainless chamber was heated to 525K, about ca. 10mg cellulose sample was placed into the middle of the quartz tube of the filament heating probe. The probe was inserted into the stainless chamber and then the filament heating probe started to ramp to the desired pyrolysis temperature and held for 60s. The condensable vapour referred to as pyrolysis liquid, was trapped in the cooling trap system. The pyrolysis liquid was obtained by washing the cooling coils using acetone after each experiments and further analysed using GC-MS/FID [103]. The non-condensable gases, known as pyrolysis gas, was collected in a gas bag. Solid products remaining in the quartz tube was regarded as char. The GC-MS/FID has the same operational parameters as the GC-MS/FID used in Chapter 4.

The weights of the char and pyrolysis liquid were taken by the increases in weights of the quartz tube and cooling coil, respectively.

The yields of the char (w_c), pyrolysis liquid (w_l) and pyrolysis gas (w_g) were then calculated from the experimental data using the following equations:

$$w_c = \frac{m_c}{m_0} * 100\% \tag{5.1}$$

$$w_l = \frac{m_l}{m_0} * 100\% \tag{5.2}$$

$$w_g = (1 - w_c - w_l) * 100\% \tag{5.3}$$

where w_c, m_c, m_0, m_l are the yield of char, the weight of char, the initial weight of the cellulose sample used, the weight of pyrolysis liquid, respectively.

Cellulose pyrolysis was carried out at three different temperatures (823 K, 923 K and 1023 K) with four different residence times (30ms, 50ms, 100 ms and 500 ms). Due to the poor thermal conductivity of cellulose, its actual pyrolysis temperature was lower than the set value, reported as 373K lower when the set temperature was 875K. Each experiment was repeated three times and the results shows good repeatability. The results reported in this paper were the average data of the three measurements, with the standard deviations of the data being taken as experimental errors.

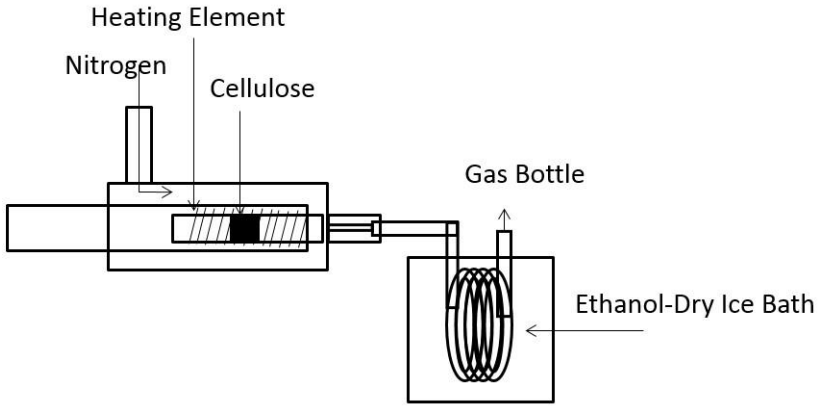

Figure 5-1 A schematic diagram of a micro fixed-bed reactor setup

5.2.2 Product identification and calibration

Table 5-1 Calibration of pure chemicals using GC-FID/MS

Peak No.	Retention time (min)	Calibration range (wt. %)	R^2	Compound
1	2.98	0.0-0.56	0.99	2,3-Butanedione
2	3.12	0.0-2.8	0.99	Acetic Acid
3	3.83	0.0-2.8	0.99	Hydroxyl Acetone
4	6.30	0.0-20.0	0.99	Furfural
5	9.14	0.0-2.0	0.99	Phenol
6	9.67	0.0-4.8	0.99	5-Methyl Furfural
7	11.21	0.0-2.8	0.99	Phenol, 2-methyl
8	12.56	0.0-5.2	0.99	Phenol, 4-methyl
9	15.20	0.0-12.0	0.99	Levoglucosenone
10	18.76	0.0-8.0	0.99	5-HMF
11	24.29	N/A	N/A	DGP
12	27.86	0.0-50.0	0.99	Levoglucosan
13	29.52	N/A	N/A	Levoglucosan-furanose

A Gas Chromatography – Mass Spectrometer (Agilent 7890A GC/ 5975C MS) using a Restek RTX65 column (30m in length and 250μm i.d. and 0.1μm film thickness) was configured to analyse the pyrolysis products. A split ratio of 50:1 was selected for injection. The inlet and the GC-MS interface were kept at 523 K and 573 K, respectively. The initial temperature of the column, 315K was maintained for 2 minutes and was subsequently increased to 573 K at 5 $K \bullet min^{-1}$. The final temperature was maintained for 6 minutes. Helium of ultrahigh purity (99.999%) supplied from BOC Inc. was used a carrier gas and

flowed at 1ml/min. Compounds were ionised at 69.9 eV electron impact conditions and analysed over a mass per charge (m/z) of 50-550.

The compounds were identified by comparing the mass spectra with the standard ones in the NIST library and the reported compounds in the literature. The identified pure compounds were obtained from Sigma-Aldrich, which were used to further confirm the compounds based on mass spectra and retention time. The purchased pure compounds were then used to obtain calibration curves using the same GC setup connected to FID. All standards were dissolved in acetone and injected into GC-FID. Three-point straight line calibration curves (with $R^2 \geq 0.99$) were established. All anhydro-sugars compounds were quantified using the calibration curve of levoglucosan. Table 5-1 shows a list of calibrated compounds with their calibrated concentration range, retention time. Due to the complexities of pyrolysis process, only the most important compounds were identified in the products.

5.3 Results and discussion

5.3.1 Yields of pyrolysis liquid, gas and char

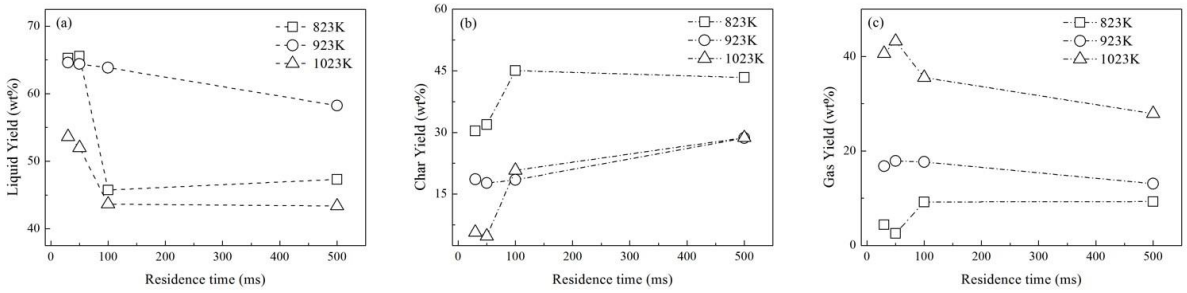

Figure 5-2 Yields of pyrolysis liquid (a), char (b) and gas (c) as a function of temperature and residence time in a micro fixed-bed reactor at 823K, 923K and 1023K

The effects of temperature and residence time on the yields of pyrolysis liquid, gas and char were illustrated in Figure 5-2. As shown in Figure 5-2 (a), the yields of pyrolysis liquid decreased with the increasing residence time at all three temperatures tested and the maximal yields of pyrolysis liquid was reached at 923 K.

Table 5-2 Yields and composition of cellulose pyrolysis products in a micro fixed-bed reactor

Cellulose pyrolysis products	Temperature		
	823 K	923 K	1023 K
Liquid (wt.%)	47.31	58.25	43.37
levoglucosan	18.58	29.01	27.53
levoglucosan-furanose	0.86	1.18	1.40
DGP	2.21	2.18	2.10
levoglucosenone	5.09	2.58	2.32
furfural	4.45	3.48	2.93
5-methyl furfural	0.51	0.37	0.29
5-HMF	2.73	2.61	2.60
acetic acid	2.17	2.25	2.44
hydroxyacetone	1.14	1.17	1.21
2,3-butanedione	0.19	0.24	0.32
phenol	0.27	0.29	0.32
phenol, 2-methyl	0.71	0.77	0.67
phenol, 4-methyl	0.16	0.15	0.09
Char (wt.%)	43.39	28.66	28.73
Gas[a] (wt.%)	9.29	13.09	27.90

[a]All products were acquired with residence time of 500 ms.

Figure 5-2 (b) shows the variations of char yield as a function of temperature and residence time. As can be seen, the formation of char was enhanced with residence time increasing at all three temperatures tested, which suggested that a longer residence time could favor the formation of char such as polymerisation. From Figure 5-2 (c), it can be found that at 823 K and 923 K, the yields of pyrolysis gas first increased with residence time increasing from 30ms to 100 ms but decreased when further increasing residence time from 100 ms to 500 ms. At 1023 K, the yields of pyrolysis gas first increased from 30ms to 50ms but decreased with residence time increasing to 500 ms. Combined with the trend of the yields of pyrolysis liquid and char, it suggested that a longer residence time could favor the formation of pyrolysis gas and char at the expense of pyrolysis liquid through secondary decomposition and repolymerisation [110, 248] while the formation of char was the dominant reactions with longer residence time at 500 ms.

5.3.2 Effect of temperature and residence time on the formation of pyrolysis liquid

Table 5-2 summarises the identified and quantified compounds in cellulose pyrolysis liquid products with residence time of 500 ms and temperature ranging from 823 K to 1023 K. The detected liquid compounds ranged from 80 wt.% to 100 wt.% of the liquid. Weight percentage of GC unknown compounds at 1023 K (normally large molecules such as polyssacharides [249]) was significant lower than the percentage at 823 K and 923 K, indicating a high temperature could favor the fragmentation reactions [69] of large molecules.

Figure 5-3 and Figure 5-4 shows the yields of all detected pyrolysis liquid compounds as a function of temperature and residence time. Figure 5-5 plots the effects of temperature and residence time on the

formation of all detected liquid compounds. It can be seen that the formation characteristics of all detected compounds can be divided into four categories: (1) temperature and residence time promoted, (2) temperature inhibited and residence time promoted, (3) temperature and residence time inhibited and (4) temperature promoted and residence time inhibited. Temperature or residence time promoted refers to the fact that the yields of products varied in the same direction as temperature or residence time, whereas temperature or residence time inhibited refers to the fact that the yields of products move in the opposite direction as temperature or residence time. Especially, the decrease of product yields doesn't necessary indicate that the compound doesn't form but rather decomposes as operating conditions change. Only three anhydrosugar compounds including DGP, levoglucosan and levoglucosan-furanose were residence time inhibited in which levoglucosan and levoglucosan-furanose were temperature promoted and DGP was temperature inhibited. Among all the other ten residence-time-promoted compounds, as temperature increased, the yields of levoglucosenone and furfural, 5-methyl furfural, 5-HMF and phenol, 4-methyl decreased while the yields of acetic acid, hydroxyl acetone, 2, 3-butadione, phenol and phenol, 2-methyl increased.

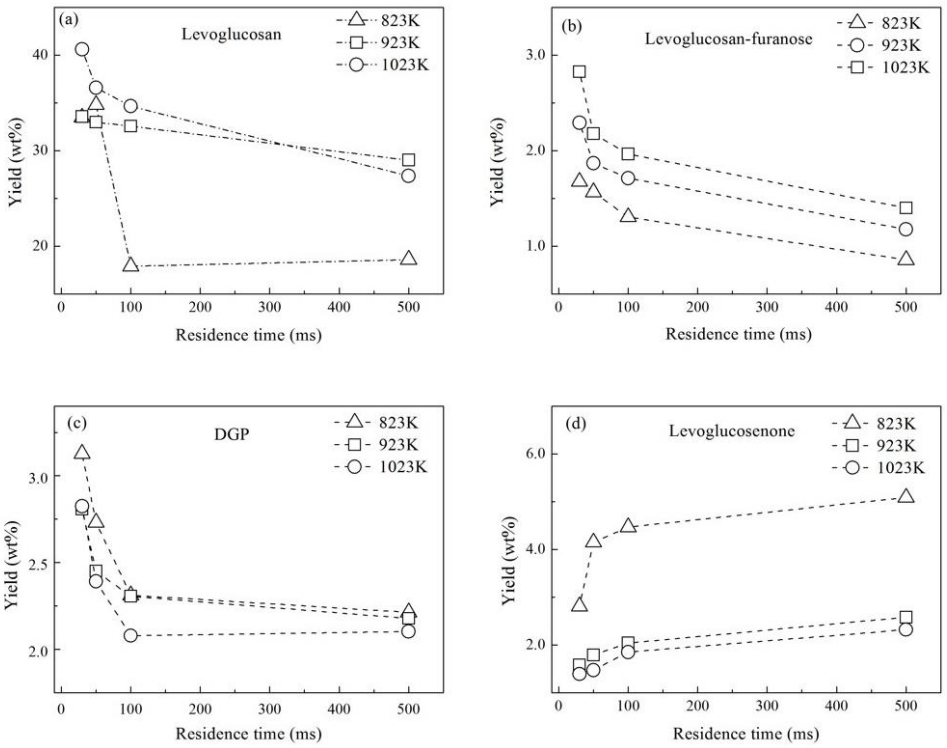

Figure 5-3 Yields of levoglucosan (a), levoglucosan-furanose (b), DGP (c) and levoglucosenone (d) as a function of temperature and residence time in a micro fixed-bed reactor at 823K, 923K and 1023K

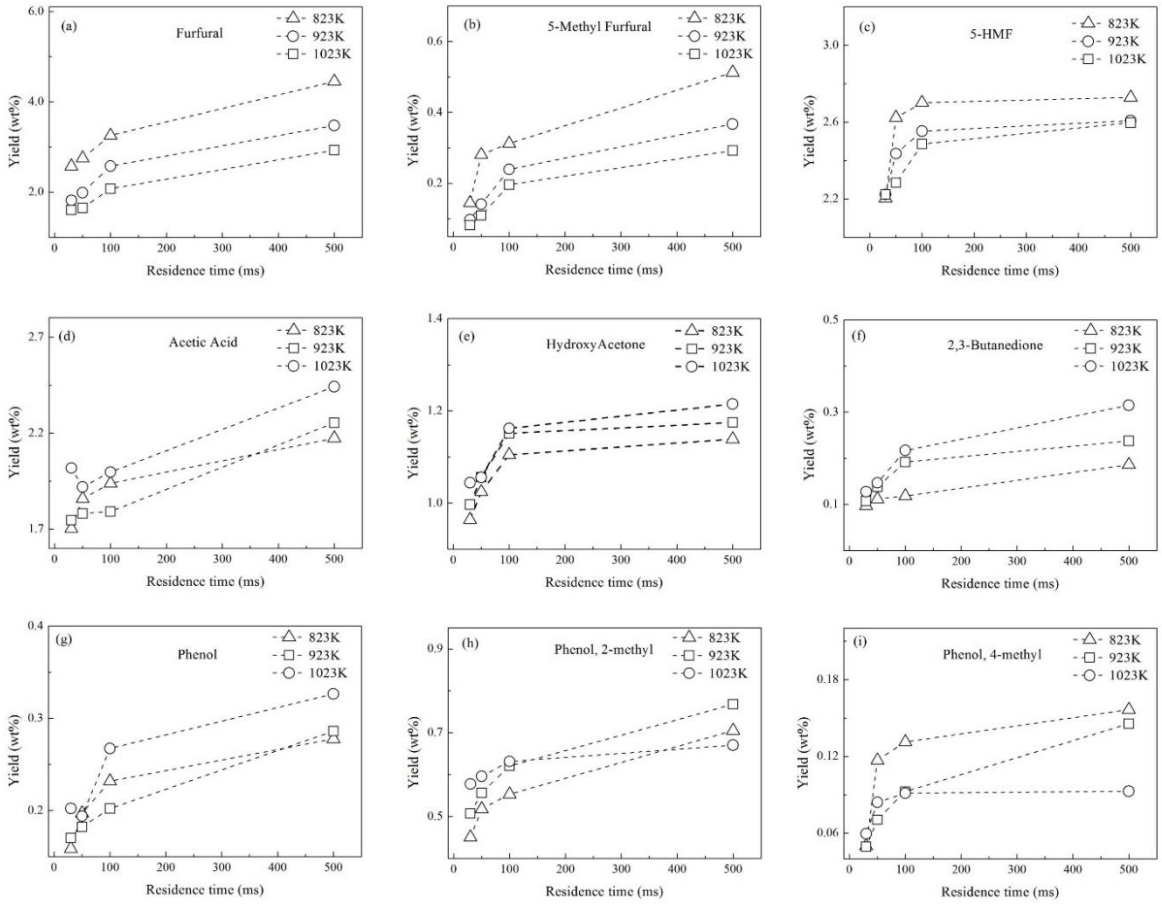

Figure 5-4 Yields of furfural (a), 5-methyl furfural (b), 5-HMF (c), acetic acid (d), hydroxyl acetone (e), 2,3-butanedione (f), phenol (g), phenol, 2-methyl (h), phenol, 4-methyl (i) as a function of temperature and residence time in a micro fixed-bed reactor at 823K, 923K and 1023K

The detected anhydrosugar compounds revealed different formation characteristics. Levoglucosan is the most abundant anhydrosugar compound in pyrolysis liquid (around 30 wt.%) with other anhydrosugar compounds (including levoglucosenone, DGP, levoglucosan-furanose) ranging from 2 to 5 wt.%. The elevated temperature could promote the formation of levoglucosan and levoglucosan-furanose, but inhibit the formation of levoglucosenone and DGP. This indicates that levoglucosenone and DGP were mainly produced in the early stage of the cellulose decomposition while levoglucosan and levoglucosan-furanose were not. For DGP, levoglucosan and levoglucosan-furanose, the characteristics of being

residence time inhibited suggested that these three compounds were not favored to be generated in secondary reactions. For levoglucosenone, the characteristics of being residence time promoted indicates that it was more favored to be generated in secondary reactions. These different dependences on the residence time indicated different formation mechanisms between levoglucosenone and all the other anhydrosugar compounds. In previous studies [99, 108], some researchers argued that levoglucosenone can be transformed from other anhydrosugar compounds such as levoglucosan and DGP.

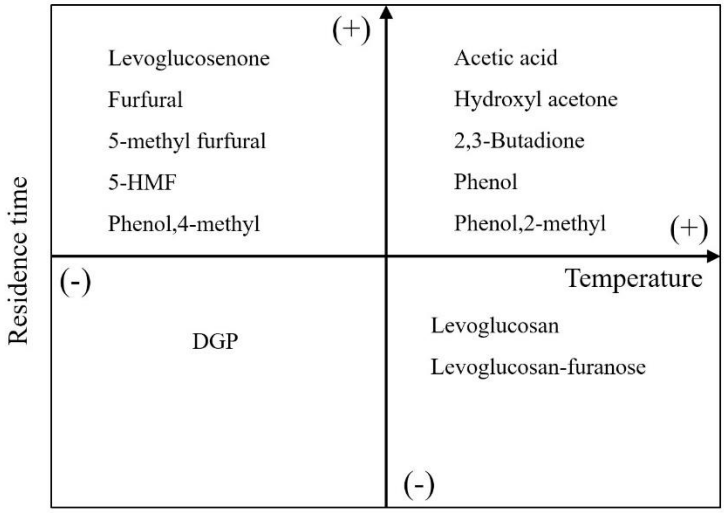

Figure 5-5 Effect of residence time and temperature on the formation of pyrolysis liquid compounds ((+): promoted, (-): inhibited)

Furfural and 5-HMF were the most two abundant furan compounds in pyrolysis liquids, accounting for around 5 wt.% and 2.5 wt.%, respectively. All detected furan compounds (furfural, 5-methyl furfural and 5-HMF) were found to be temperature inhibited and residence time promoted. As residence time increased from 100 ms to 500 ms, the yields of furfural and 5-methyl furfural significantly increased while the yield of 5-HMF remained relatively constant. All detected light oxygenated compounds (including acetic acid, hydroxyl acetone and 2, 3-butadione) were found to be temperature and residence

time promoted. Generally, all light oxygenated compounds were generated from the fragmentation reaction which is enhanced along with the increasing pyrolysis temperature and residence time [250].

5.3.3 Thermal analysis of cellobiose, levoglucosan, levoglucosenone and DGP

Table 5-3 Products yields from pyrolysis of cellobiose, levoglucosenone and DGP

Pyrolysis products	Material		
	Cellobiose	Levoglucosenone	DGP
Liquid (wt.%)	50.23	100	100
Levoglucosan	22.76	N.A	N.A
Levoglucosan-furanose	1.29	N.A	N.A
DGP	1.61	N.A	75.30
Levoglucosenone	3.77	80.02	8.23
Furfural	2.61	1.10	0.92
5-methyl furfural	0.46	0.82	0.51
5-HMF	3.11	2.23	1.52
Acetic acid	0.51	N.A	N.A
Hydroxyacetone	0.26	N.A	N.A
2,3-butanedione	0.03	N.A	N.A
Phenol	0.11	N.A	N.A
Phenol, 2-methyl	0.36	N.A	N.A
Phenol, 4-methyl	0.18	N.A	N.A
Unknown liquid compounds	13.15	15.62	13.52
Char (wt.%)	35.48	N.A	N.A
Gas[a] (wt.%)	14.29	N.A	N.A

[a]All products were acquired with residence time of 500 ms.

Levoglucosan, levoglucosenone and DGP were identified as the main compounds in cellulose pyrolysis products. In order to further understand their different formation dependences on residence time, thermal

analysis on their pyrolytic behaviors was conducted. Pure levoglucosan, levoglucosenone and DGP were subjected to the micro fixed-bed reactor at 923 K with residence time of 500 ms whereas celllobiose as the repeating dimer units of cellulose was also pyrolysed at the same condition.

Shown in Table 5-3 are the quantified products from pyrolysis of cellobiose, levoglucosenone and DGP. In pyrolysis of levoglucosan, no pyrolysis products were produced. This good thermal stability of levoglucosan has also been confirmed in some previous studies [103, 104]. This suggests that in this study all the detected products were formed in parallel with the formation of levoglucosan. Based on the product yields from cellobiose pyrolysis, it showed that less levoglucosan was produced and more fragmented molecules (furans and light oxygenates) produced than with cellulose. This result is attributed to the difference in the presence of the glycosidic linkage, which was found to be crucial for levoglucosan formation [103, 105]. In pyrolysis of levoglucosenone, only a small fraction of furans were detected whereas the majority of levoglucosenone remained intact. It is worth noting that in pyrolysis of DGP, a considerable amount of levoglucosenone (8 wt.%) and a small fraction of other compounds was produced. Combined with the different dependences of levoglucosenone and DGP on the residence time, it can be reasonably inferred that DGP might be an intermediate in the formation of levoglucosenone in pyrolysis process.

5.4 Conclusions

This research studied the effect of temperature and residence time on the yields of cellulose pyrolysis products in a fixed-bed reactor. Pyrolysis of cellobiose, levoglucosan, levoglucosenone and DPG was further conducted to investigate cellulose pyrolysis mechanisms. Thirteen major liquid pyrolysis products were identified and quantified. Among all identified liquid compounds, only DGP,

levoglucosan and levoglucosan-furanose were residence time inhibited in which levoglucosan and levoglucosan-furanose were temperature promoted and DGP was temperature inhibited. Levoglucosenone is the only anhydrosugar compound which was residence time promoted. These results indicate that 1,4:3,6-dianhydro-α-D-glucopyranose (DGP) and levoglucosenone were mainly produced in the early stage of cellulose pyrolysis, while the formation of levoglucosenone was found to be more favored in secondary reactions. All detected furan compounds (furfural, 5-methyl furfural and 5-HMF) were found to be temperature inhibited and residence time promoted. All detected light oxygenated compounds (including acetic acid, hydroxyl acetone and 2, 3-butadione) were found to be temperature and residence time promoted. Further thermal analysis showed levoglucosan was found to be thermally stable and concurrently produced with other pyrolysis products. DGP might be an intermediate for the formation of levoglucosenone. This study provides insights in understanding the fundamentals of the mechanisms of cellulose pyrolysis and the transformations among cellulose pyrolysis products.

Chapter 6. Mechanistic Modelling of Levoglucosenone Formation from Anhydrosugar Intermediates

6.1 Introduction

In Chapter 5, the effect of residence time and temperature on the formation characteristics of cellulose pyrolysis products was studied and the mechanisms underlying their formation and transformation were also discussed. It was found that levoglucosenone is the only anhydrosugar compound which was residence time promoted. These results indicates that 1,4:3,6-dianhydro-α-D-glucopyranose (DGP) and levoglucosenone were mainly produced in the early stage of cellulose pyrolysis, while the formation of levoglucosenone was found to be more favored in secondary reactions. DGP might be an intermediate for the formation of levoglucosenone. Based on these experimental observations, it is necessary to examine any possible reaction pathway for the formation of levoglucosenone from DGP.

In the present work we investigate the reaction mechanism for the uncatalysed formation of levoglucosenone from DGP in more detail using the high-level *ab-initio* G4(MP2) theory [205]. We also consider the water-catalysed reaction and show that a water catalyst can reduce the Gibbs free-activation energy at 298 K ($\Delta G^{\ddagger}_{298}$) for the entire process by as much as 10.5 kcal mol^{-1}. In addition, we show that the water catalyst leads to a change in the RDS for the overall process.

6.2 Methodology and computational details

High-level *ab initio* [251] and density functional theory [252] calculations were carried out using the Gaussian 09 program suite [253]. All geometry optimisations were performed at the B3LYP/6-31G(2df,p) level of theory as prescribed in the G4(MP2) protocol [205]. Zero point vibrational energies, enthalpic,

and entropic corrections have been obtained from such calculations. The equilibrium structures were verified to have all real harmonic frequencies and the transition structures to have only one imaginary frequency. The connectivities of the transition structures were confirmed by performing intrinsic reaction coordinate (IRC) calculations [254, 255].

Gas-phase Gibbs free energies at 298 K (ΔG_{298}) were obtained using the G4(MP2) variant of the Gaussian-4 (G4) composite thermochemical protocol [204, 205]. The G4(MP2) protocol is an efficient composite procedure for approximating the CCSD(T) (coupled cluster energy with singles, doubles, and quasiperturbative triple excitations) energy in conjunction with a large triple-ζ-quality basis set [206, 256]. This protocol is widely used for the calculation of thermochemical and kinetic properties (for a recent review see ref. 169). The G4(MP2) procedure has been found to produce gas-phase thermochemical properties (such as reaction energies, bond dissociation energies, and enthalpies of formation) with a mean absolute deviation (MAD) of 1.04 kcal•mol^{-1} from the 454 experimental energies of G3/05 test set [257]. It has been recently found that G4(MP2) shows a similarly good performance for barrier heights [209, 258-260]. This highly accurate composite method gives thermochemical data at specific temperatures for which the method was parameterized (e.g., enthalpies of formation at 0 K and 298 K, and Gibbs free energies at 298 K). Nevertheless, we expect that the same trends will hold for higher temperatures.

6.3 Results and discussion

6.3.1 Uncatalysed mechanism for the formation of levoglucosenone

Shafizadeh *et al.* proposed a general reaction mechanism for the conversion of DGP to levoglucosenone (Figure 6-2) [108]. This scheme involves three polyol intermediates, however, the steps leading to the

formation of these intermediates were not specified or discussed in detail. We begin by proposing a more detailed seven-step reaction pathway for the formation of levoglucosenone from DGP. Our proposed reaction mechanism is illustrated schematically in Figure 6-1.

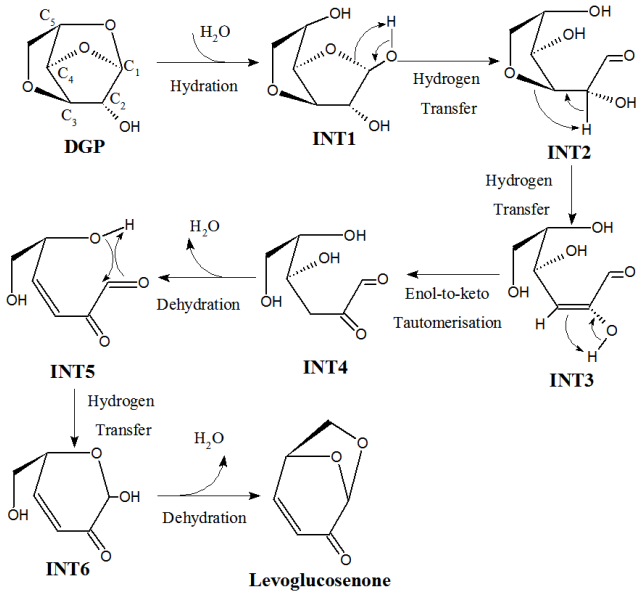

Figure 6-1 Scheme for the conversion of DGP to levoglucosenone proposed

The seven steps in our proposed reaction mechanism are described as follows. (i) In the first step a water molecule is added to the pyranose ring. Specifically, the hydrogen atom is added to the pyranose oxygen and a hydroxyl group is added to the C_1 carbon atom. This ring-opening reaction leads to the formation of the first intermediate (**INT1**, Figure 6-1). (ii) A hydrogen-transfer reaction, in which the hydrogen from the hydroxyl group at the C_1 position is transferred to the cyclic furanose oxygen. In this step the C_1–O bond of the furanose ring breaks, resulting in the formation of **INT2** (Figure 6-1). (iii) A hydrogen-transfer from C_2 to the pyranose oxygen leading to the breaking of the pyranose ring and the formation of an acyclic structure (**INT3**). (iv) An enol-to-keto tautomerisation leading to the formation of **INT4** (Figure 6-1). (v) A dehydration reaction, in which the hydrogen attached to C3 is eliminated with the hydroxyl group attached to C_4, leading to the formation of the C_3=C_4 bond in **INT5**. (vi) A hydrogen-

transfer cyclisation reaction, in which the hydrogen of the hydroxyl group at C_5 shifts to the carbonyl oxygen in the C_1 position, forming a pyranose ring. (vii) A dehydration-cyclisation reaction leading to the formation of the final levoglucosenone product (Figure 6-1).

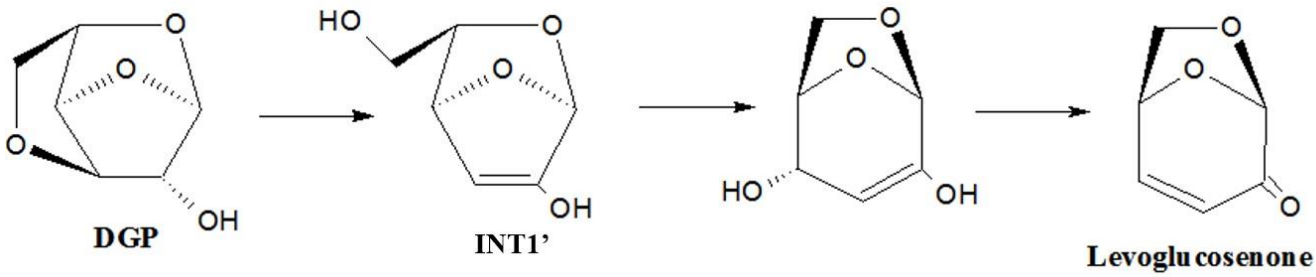

Figure 6-2 Competing reaction mechanism proposed by Shafizadeh *et al.*

Table 6-1 G4(MP2) Gibbs free energies (ΔG_{298}, kcal•mol^{-1}) for the first step in the competing reaction mechanism proposed by Shafizadeh *et al*. (shown in Figure 6-2).

Structure	ΔG_{298}
DGP	0.0
TS1'	73.6
WTS1'	71.1
INT1'	15.6

We note that Shafizadeh *et al.* also proposed an additional reaction mechanism (Scheme 1 in ref. 234). We considered this reaction mechanism and found that the first hydrogen-transfer step has a higher Gibbs free-activation energy than the RDS for the mechanism illustrated in Figure 6-1. For the uncatalysed reaction, the barrier for the first step of this alternative mechanism is $\Delta G^{\ddagger}_{298}$ = 73.6 kcal•mol^{-1}, whilst the barrier for the RDS for the mechanism in Figure 6-1 is 68.6 kcal•mol^{-1} (*vide infra*). Similarly, for the water-catalysed reaction, the barrier for the first step of the alternative mechanism is $\Delta G^{\ddagger}_{298}$ = 71.1 kcal•mol^{-1}, whilst the barrier for the RDS for the mechanism in Figure 6-1 is 58.1 kcal•mol^{-1} (**Section**

6.3.2). Therefore, we will not consider this alternative mechanism here. The specific reaction scheme is shown in Figure 6-2 and the G4(MP2) Gibbs free energies for the first step in the alternative mechanism is shown in Table 6-1.

The G4(MP2) Gibbs free-energy profile (ΔG_{298}) for the uncatalysed reaction pathway is depicted in Figure 6-3 (black line), whilst Figure 6-3 shows the optimised TSs located along the uncatalysed reaction profile. The lowest energy conformation of DGP is chosen as the zero-energy reference point of the reaction profile. The first hydration step has an activation energy of $\Delta G^{\ddagger}_{298}$(TS1) = 58.1 kcal•mol^{-1}. The relatively high activation energy for this step may be attributed to the fact that the bonds that are being broken and formed in TS1 are far from their equilibrium distances. In particular, the bond length of the breaking C_1–O bond of the pyranose ring is 2.603 Å, whilst the bond lengths of the forming O–H and C_1–OH bonds are 1.472 and 2.288 Å, respectively. Interestingly, the product of this hydration reaction (**INT1**) is essentially isoenergetic with the DGP reactant.

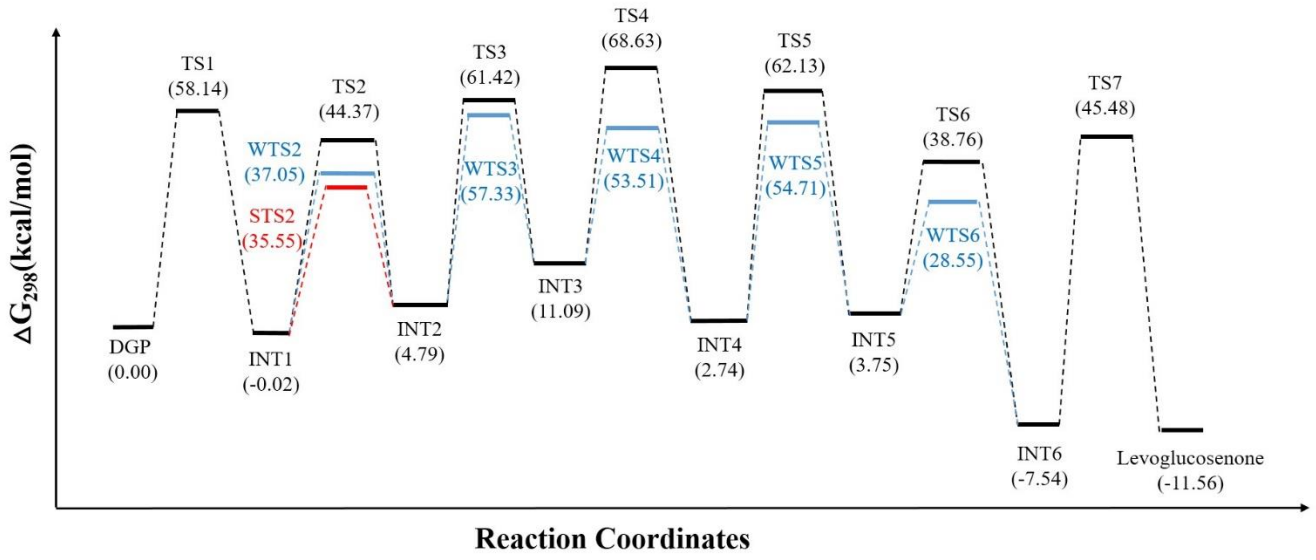

Figure 6-3 Reaction profile (G4(MP2), ΔG_{298}, kcal•mol^{-1}) for the uncatalysed (bslack line), water-

catalysed (blue line), and self-catalysed (red line) conversion of DGP to levoglucosenone.

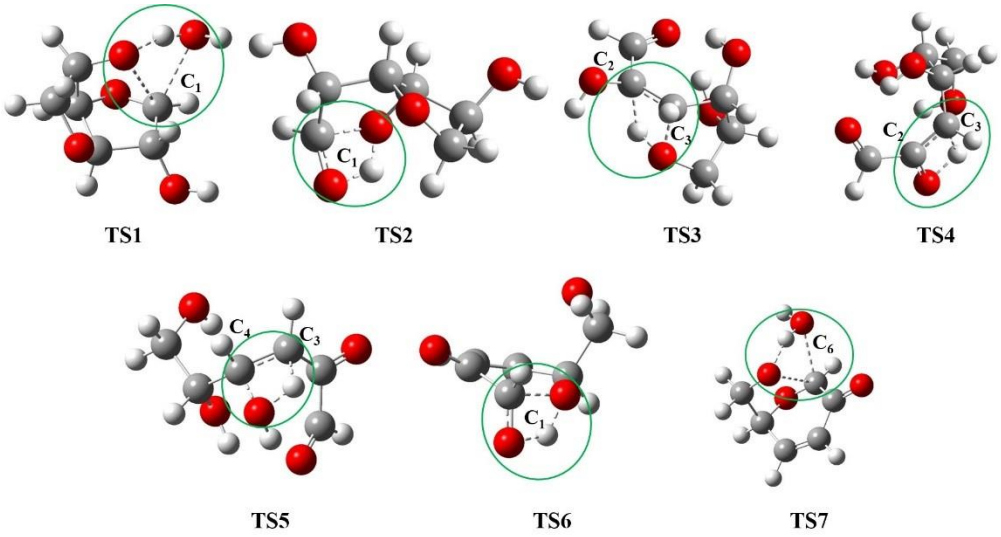

Figure 6-4 B3LYP/6-31G(2df,p) optimised transition structures TS1–TS7 in the reaction profile for the uncatalysed conversion of DGP to levoglucosenone (Figure 6-3). The bonds being broken and formed in the TSs are represented by dashed lines. Atomic color scheme: H, white; C, gray; O, red. The carbon atoms involved in the TSs are labeled in the same way as in Figure 6-1.

The transition structures for the succeeding five steps (**TS2**–**TS6**) share similar structural features – they all involve a strained four-membered ring formed between a migrating hydrogen atom and three heavy C and O atoms (Figure 6-3). The Gibbs free-activation energies for these steps spread over a wide range from 38.8 (**TS6**) to 68.6 (**TS4**) kcal•mol^{-1}. The last dehydration step of the reaction mechanism is associated with a relatively low activation Gibbs free energy of $\Delta G^{\ddagger}_{298}$(TS7) = 45.5 kcal•mol^{-1} (or $\Delta G^{\ddagger}_{298}$(TS7) = 53.0 kcal•mol^{-1}, relative to the stable **INT6** intermediate). The TSs with the highest Gibbs free-activation energies are **TS3**–**TS5**, therefore we will now concentrate on these steps.

The TS for the ring-opening, hydrogen-transfer step (**TS3**, Figure 6-3) involves a hydrogen transfer from

C_2 to the furanose oxygen, breaking of the C_3–O bond, and formation of the C_2=C_3 double bond. This TS has an activation energy of $\Delta G^{\ddagger}_{298}$(TS3) = 61.4 kcal•mol^{-1}. The lengths of the breaking C_3–O and C_2–H bonds are 1.576 Å and 1.554 Å, respectively, whilst the lengths of the forming C_2=C_3 and O–H bonds are 1.500 and 1.175 Å, respectively.

The enol-to-keto tautomerisation (**TS4**, Figure 6-3) is the RDS for the entire process with an activation Gibbs free energy of 68.1 kcal•mol^{-1} relative to the DGP reactant. We note that the reaction barrier relative to the enol tautomer (**INT3**) is 57.5 kcal•mol^{-1}. This reaction barrier is almost identical to the G4(MP2) reaction barrier for the enol-to-keto tautomerisation in vinyl alcohol (56.9 kcal•mol^{-1}) [258]. It has been previously shown that this reaction can be catalysed by a range of catalysts, including water, organic acids, and inorganic acids [261, 262], which alleviate the high strain energy involved in the TS. We also note that the G4(MP2) reaction barrier for the enol-to-keto tautomerisation in vinyl alcohol is in very good agreement with the barrier height calculated at the higher W1-F12 level (56.7 kcal•mol^{-1}) [212, 261]. This close agreement increases our confidence in the G4(MP2) reaction barrier heights.

The transition structure for the first dehydration step (**TS5**, Figure 6-3) involves the elimination of the hydroxyl group at the C_3 position with the hydrogen at the C_4 position (Figure 6-1). Similarly to the TSs for the 1,3-hydrogen transfer steps (**TS2**, **TS3**, **TS4**, and **TS6**), **TS5** involves a strained four-membered ring as shown in Figure 6-3. In **TS5**, the hydroxyl group at the C_4 position has a strong hydrogen bond with the carbonyl oxygen at the C_1 position. This is evident from a relatively short length of the OH•••OC_1 hydrogen bond (namely, 1.686 Å). The Gibbs free-activation energy for this step is 62.1 kcal•mol^{-1}. For comparison, this barrier is significantly lower than the uncatalysed barrier reported by Assary *et al.* [101] for the initial dehydration step in the conversion of levoglucosan to levoglucosenone ($\Delta G^{\ddagger}_{298}$ = 68.7 kcal•mol^{-1}, MP2/6-311++G(3df,3pd)). Another point of reference is the dehydration

reaction in ethanol, the G4(MP2) barrier for this reaction is $\Delta G^{\ddagger}_{298}$ = 66.7 kcal•mol^{-1}. The lower Gibbs free-activation energy for **TS5** may be partially attributed to the abovementioned hydrogen-bonding interaction.

The last two steps of the reaction are highly exergonic. Namely, **INT6** lies 7.5 kcal•mol^{-1} below the reactant and the final levoglucosenone product lies 11.6 kcal•mol^{-1} below the reactant. Both steps are associated with relatively low reaction barrier heights, namely of 38.8 (**TS6**) and 45.5 (**TS7**) kcal•mol^{-1} (or 53.0 kcal•mol^{-1} relative to the stable intermediate **INT6**).

Two important features of the overall reaction profile for the uncatalysed conversion of DGP to levoglucosenone are:

- The enol-to-keto tautomerisation step is clearly the RDS. In particular, **TS4** is higher by amounts ranging from 6.5 (**TS5**) to 29.8 (**TS6**) kcal•mol^{-1} than the other TSs involved in the process.
- The overall process is highly exergonic; the final product lies lower in energy than the reactant by 11.6 kcal•mol^{-1}. This provides a thermodynamic driving force for the entire process [263].

It is well known that the presence of water molecules can significantly enhance the reaction rates of hydrogen transfer reactions in the gas phase relative to the rates of the uncatalysed reactions [258, 261-266]. Thus, **TS2**–**TS6** – which involve a strained four-membered ring formed between a migrating hydrogen and three heavy C and O atoms (Figure 6-3) – could potentially be catalysed by a water catalyst. In the next section we will explore the water-catalysed conversion of DGP to levoglucosenone.

6.3.2 Water-catalysed mechanism for the formation of levoglucosenone

Water is not only a major constituent of raw biomass material [267, 268], but also a significant pyrolytic product along pyrolysis processes such as the hydroperoxide decomposition step [92]. It has been found that water could catalyse certain important reactions in pyrolysis of glucose such as ring-opening [269], tautomerisation [270] and dehydration reactions [270]. In this section we investigate the reaction profile for the conversion of DGP to levoglucosenone catalysed by a water molecule.

We find that an explicit water molecule can act as a hydrogen bridge in the transition structures **TS2–TS6**, thereby lowering the activation energies for these steps by amounts ranging from 4.1 (**TS3**) to 15.1 (**TS4**) kcal•mol^{-1}. As a consequence of this catalytic activity, the enol-to-keto tautomerisation (**TS4**) is no longer the RDS. The RDS for the catalysed process becomes the first dehydration step (**TS1**), which cannot be catalysed by a water molecule.

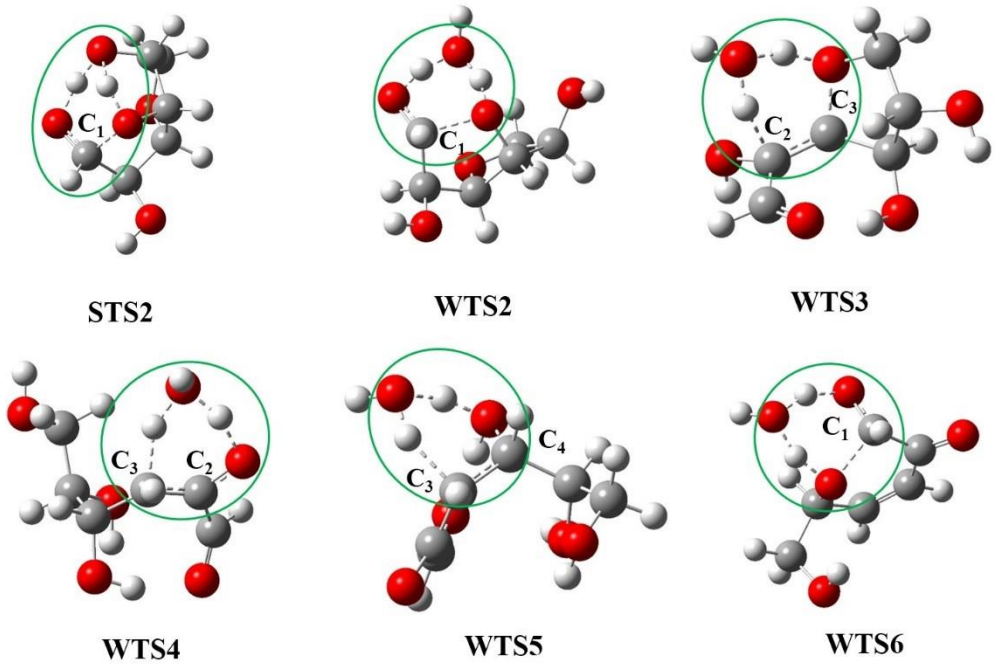

Figure 6-5 B3LYP/6-31G(2df,p) optimised transition structures TS2–TS6 in the reaction profile for the catalysed conversion of DGP to levoglucosenone. The catalysed reaction profile is shown in Figure 6-3.

The bonds being broken and formed in the TSs are represented by dashed lines. Atomic color scheme: H, white; C, gray; O, red. The carbon atoms involved in the TSs are labeled in the same way as in Figure 6-1.

The water-catalysed reaction profile is shown in Figure 6-3 (blue line) and the optimised TSs are depicted in Figure 6-4. In all of these TSs the water molecule assists the hydrogen transfer by converting the four-membered ring TS into a less strained six-membered ring TS (Figures 6-3 and 6-4).

In the second step a water molecule acts as a hydrogen shuttle that transports a hydrogen from the hydroxyl group to the furanose oxygen (**WTS2**, Figure 6-4). The activation energy for the catalysed step is reduced by 7.4 kcal•mol^{-1} relative to the uncatalysed reaction. We also located a self-catalysed TS for this step (**STS2**, Figure 6-4) which is associated with a lower activation energy $\Delta G^{\ddagger}_{298}$(STS2) = 35.5 kcal•mol^{-1} (red line, Figure 6-3). In the self-catalysed TS the hydroxyl group attached to C_5 acts as the hydrogen shuttle.

The activation energy for the enol-to-keto tautomerisation (**WTS4**, Figure 6-4) is reduced by as much as 15.1 kcal•mol^{-1} upon an inclusion of the water catalyst. This step, which is the RDS step of the uncatalysed process, is now associated with an activation energy of $\Delta G^{\ddagger}_{298}$(**WTS4**) = 53.5 kcal•mol^{-1}. Thus, in the catalysed mechanism the reaction barrier for this step is lower by 4.6 kcal•mol^{-1} than the reaction barrier for the hydration step ($\Delta G^{\ddagger}_{298}$(**TS1**) = 58.1 kcal•mol^{-1}). Upon inclusion of the water catalyst, the activation energy for **TS5** is reduced by 8.0 kcal•mol^{-1}, whilst the reaction barrier for **TS6** is reduced by 10.2 kcal•mol^{-1}.

The results above indicate that the involvement of an explicit water molecule in the hydrogen shifts significantly affects the dynamics of the overall reaction. In the uncatalysed mechanism, the RDS is the enol-to-keto tautomerisation ($\Delta G^{\ddagger}_{298}$(**TS4**) = 68.6 kcal•mol^{-1}). In the catalysed mechanism the ring-opening hydration step becomes the RDS ($\Delta G^{\ddagger}_{298}$(**TS1**) = 58.1 kcal•mol^{-1}), and the ring-opening hydrogen-transfer step is associated with a slightly lower activation energy of $\Delta G^{\ddagger}_{298}$(**WTS3**) = 57.3 kcal•mol^{-1}. Overall, the involvement of the water catalyst reduces the Gibbs free-activation energy for the DGP-to-levoglucosenone transformation by 10.5 kcal•mol^{-1}.

6.4 Conclusions

We use the high-level *ab initio* G4(MP2) thermochemical procedures to investigate the uncatalysed and water-catalysed reaction mechanism for the transformation of DGP to levoglucosenone. We draw the following conclusions:

1. The reaction mechanism has seven elementary steps, including ring-opening, ring-closing, enol-to-keto tautomerisation, dehydration, and hydration reactions.
2. In the uncatalysed mechanism, the enol-to-keto tautomerisation is the RDS with an activation Gibbs free energy of $\Delta G^{\ddagger}_{298}$ = 68.6 kcal•mol^{-1} relative to the DGP reactant.
3. In the catalysed mechanism, the enol-to-keto tautomerisation has a reaction barrier of $\Delta G^{\ddagger}_{298}$ = 53.5 kcal•mol^{-1} and is no longer the RDS. In this scenario the ring-opening hydration step becomes the RDS with a barrier of $\Delta G^{\ddagger}_{298}$ = 58.1 kcal•mol^{-1}, this barrier is closely followed by the barrier for the ring-opening hydrogen-transfer step ($\Delta G^{\ddagger}_{298}$ = 57.3 kcal•mol^{-1}).
4. The transformation from DGP to levoglucosenone is thermodynamically favored as the Gibbs free energy of levoglucosenone lies 11.6 kcal•mol^{-1} below DGP.

Our results provide important insights into the molecular mechanisms of biomass pyrolysis. Most notably, that this conversion is water-catalysed and that the ring-opening hydration step is the RDS. We hope that our high-level theoretical results will inspire additional experimental measurements.

Supporting Information

Appendix A1 part contains full computational details. G4(MP2) reaction profile on the enthalpic surface for the uncatalysed and water-catalysed conversion of DGP to levoglucosenone, including zero-point vibrational energy (ZPVE), heat content function ($H_{298}–H_0$), and entropic (ΔS) corrections from G4(MP2) theory (Table S1); absolute energies required to calculate all the data in Table S2; and B3LYP/6-31G(2df,p) optimised geometries for all the local minima and transition structures considered in this work (Table S3).

Chapter 7. Heat of Formation for C_{60} by means of the G4(MP2) Thermochemical Protocol

7.1 Introduction

As shown in Chapter 6, accurate thermochemical and kinetic properties including reaction energies and barrier heights are of great value for the investigation of the feasibility and spontaneity on chemical transformations in biomass pyrolysis. Composite *ab initio* high-level thermochemical approaches are extremely useful where experimental data are lacking. Composite *ab initio* methods can achieve accuracies of at least one order of magnitude better than other contemporary DFT functionals. In pyrolysis, the structure of char remain mainly unclear due to the structural complexity and high molecular weight. C_{60} as high-molecular weight compound is investigated in this Chapter as C_{60} structure could to certain degrees mimic certain structural entities in char product from pyrolysis. High-level thermochemical protocols are also employed.

The fundamental importance of Buckminsterfullerene [271] as a molecular allotrope of carbon and as a key building block in nanotechnology and material science is clearly evident to any chemist [272, 273]. However, its heat of formation has been a matter of controversy with reported experimental values extending over a wide energy range of 199 kJ•mol^{-1}, from 2457 ± 16 [274, 275] to 2656 ± 25 kJ•mol^{-1} [276]. In light of these very large differences, the NIST thermochemical database has adopted a value of $\Delta_f H^{\circ}_{298}[C_{60}(g)]$ = 2560 kJ•mol^{-1} associated with an unusually high error bar of ± 100 kJ•mol^{-1}. The first measurement of heat of formation for C_{60} was carried out by Beckhaus *et al.* in 1992 [277], who reported a standard heat of formation in the gas-phase ($\Delta_f H^{\circ}_{298}[C_{60}(g)]$) of 2464 ± 7 kJ•mol^{-1} [275]. The same year, Steele *et al.* [276] revised this value substantially upwards to 2656 ± 25 kJ•mol^{-1} . The large

discrepancy between these two experimental determinations has stimulated a series of subsequent macro- and micro-combustion calorimetric studies [274, 275, 278-284] (Table S4 of the Supporting information summarises the experimental $\Delta_f H^\circ_{298}[C_{60}(cr)]$ and $\Delta_f H^\circ_{298}[C_{60}(g)]$ values). The reasons for these large discrepancies include the difficulties associated with the production of samples of C_{60} of sufficiently high purity and the limited accuracy of calorimetric measurements on relatively small samples [285, 286]. An additional contributor to the discrepancies between the $\Delta_f H^\circ_{298}[C_{60}(g)]$ values comes about because in some cases the enthalpies of sublimation (used for converting the crystalline heat of formation into the gaseous heat of formation) show a variation of as much as ~50 kJ•mol^{-1} (Table S4, Supporting information). However, even the reported solid-phase heats of formation span a wide energy range of 149 kJ•mol^{-1}. In the light of this state of affairs, the NIST Webbook has adopted a standard heat of formation for C_{60} of 2560 ± 100 kJ•mol^{-1}, which was obtained as the average of six $\Delta_f H^\circ_{298}[C_{60}(g)]$ values (Table S4, Supporting information) [287]. We note that the six $\Delta_f H^\circ_{298}[C_{60}(g)]$ values selected by NIST spread over the abovementioned energy range of 149 kJ•mol^{-1}.

Two recent theoretical studies have obtained the heat of formation for C_{60} through the use of reactions in which C_{60} is broken down into prototypical hydrocarbons [288, 289]. Reference 291 used reactions in which C_{60} is broken down into corannulene:

$$C_{60} + a\ \mathrm{Ar} \rightarrow b\ \text{corannulene} \qquad (7.1)$$

where Ar is benzene or naphthalene. These reactions were chosen because they conserve some of the unique chemical features present in C_{60} (such as curvature in the π system associated with pentagons completely surrounded by hexagons). In order to obtain the heat of formation for C_{60} the reaction

enthalpy was calculated at the DSD-PBEP86-D3/cc-pVQZ level of theory [290], the heat of formation for corannulene was obtained from W1h theory [291, 292], and the heats of formation for Ar were taken from accurate experimental measurements. In this study the best theoretical heat of formation for C_{60} was reported to be $\Delta_f H^\circ_{298}[C_{60}(g)] = 2522 \pm 14$ kJ•mol^{-1}. Shortly thereafter, Dobek *et al.* [289] obtained the heat of formation for C_{60} from CBS-4M and APF-D calculations [293, 294], using a homologous sequence of isodesmic reactions in which C_{60} is broken down into CH_4, C_2H_4, C_2H_6, and C_6H_6. The chosen set of reactions allow for obtaining size-consistent empirical parameters determined from least-squares fitting to W1h enthalpies of formation1 for C_6H_6, $C_{10}H_8$, $C_{14}H_{10}$, and $C_{18}H_{12}$. Using this empirical approach Dobek *et al.* [289] arrived at $\Delta_f H^\circ_{298}[C_{60}(g)] = 2531 \pm 15$ kJ•mol^{-1}, in good agreement with the value reported in ref. 291.

The reactions used by Dobek *et al.* [289] for obtaining the heat of formation for C_{60} do not attempt to balance the strain energy on the two sides of the reaction, whereas reaction 7.1 attempts to do so using corannulene. It is important to note, however, that C_{60} is composed of two fundamental aromatic bowl-shaped fragments (i) a pentagon surrounded by five hexagons (corannulene) and (ii) a hexagon surrounded by three hexagons and three pentagons (sumanene). This is illustrated schematically in Figure 7-1.

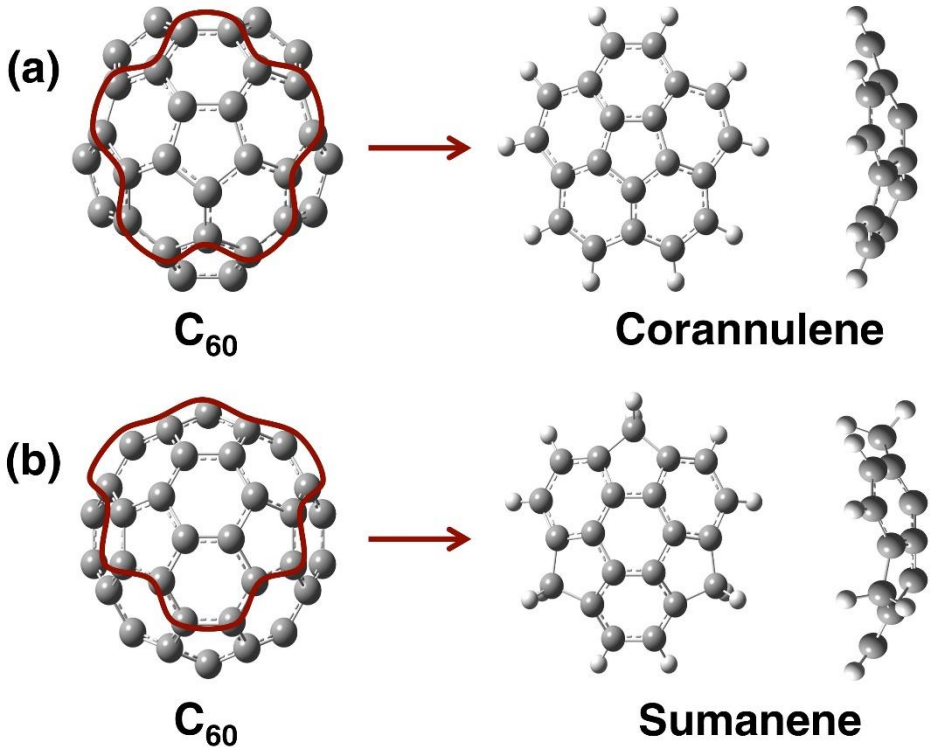

Figure 7-1 B3LYP/6-31G(2df,p) optimised structure of C_{60} and its two basic fragments (a) corannulene ($C_{20}H_{10}$) and (b) sumanene ($C_{21}H_{12}$).

In the present work, we obtain the heat of formation of C_{60} via reactions that conserve some of the unique chemical features present in C_{60} (such as strain energy resulting from curvature in the π system). There are two key differences between the approach taken here and in ref. 291. The first is that here C_{60} is broken down into both corannulene and sumanene, rather than just corannulene. Including sumanene in the thermochemical cycle used for obtaining the heat of formation of C_{60} is important, since corannulene accounts for only one type of strain energy involved in C_{60} (i.e., pentagons completely surrounded by hexagons), whilst sumanene accounts for the strain energy associated with hexagons surrounded by three hexagons and three pentagons (Figure 7-1). A number of studies have previously shown that it is important to conserve such features when calculating the heats of formation of fullerenes and PAHs [295-299]. The second difference is that the reaction energies are obtained at a much higher level of

theory, namely, by means of the G4(MP2) protocol [205], rather than by means of double-hybrid density functional theory (DHDFT). In this context, we note that the CCSD(T)/6-31G(d) calculation for C_{60} stretched our computational resources to the limit. This single-point energy calculation ran for more than two weeks on eight Intel Xeon E5-4650L cores (at 3.1 GHz) with 512 GB of RAM.

7.2 Methodology and computational details

As described in Chapter 6, the geometries and harmonic vibrational frequencies of all structures have been obtained at the B3LYP/6-31G(2*df*,*p*) level of theory. Zero-point vibrational energies (ZPVEs), enthalpic and entropic temperature corrections have been obtained from such calculations. All geometry optimizations and frequency calculations were performed using the Gaussian 09 program suite [253].

The reaction enthalpies of reactions **2** and **3** (below) are obtained by means of the high-level, *ab initio* W1h thermochemical protocol [291, 292] as described in detail in ref. 291 for corannulene. All the high-level ab initio calculations have been carried out with the Molpro 2012.1 program suite [300, 301]. We use these W1h reaction enthalpies to obtain a reliable theoretical heat of formation for sumanene. W1h represents a layered extrapolation to the relativistic, all-electron CCSD(T) (coupled cluster with singles, doubles, and quasiperturbative triple excitations) basis-set-limit energy, and can achieve "sub-chemical accuracy". For example, the large set of 124 accurate atomization energies in the W4-11nonMR database, W1h attains a root-mean-squared deviation (RMSD) of 2.7 kJ•mol^{-1} [212, 302]. However, it should be pointed out that for reaction that conserve large molecular fragments on the two sides of the reaction (such as reactions 7.2 and 7.3), W1h theory should yield even better performance due to a large degree of systematic error cancelation between reactants and products [298, 299, 302-306].

The reaction enthalpies of the reactions involving C_{60} (reactions 7.4–7.9 below) have been obtained by means of the G4(MP2) thermochemical protocol. The G4(MP2) protocol estimates the CCSD(T) energy in conjunction with a triple-ζ quality basis set and has been found to give chemical properties with "near-chemical accuracy". For example, for the set of 124 atomization energies in the W4-11nonMR database G4(MP2) attains an RMSD of 7.5 kJ•mol^{-1} [302]. Whilst for the wide range of 454 experimental thermochemical properties considered in ref. 254 (such as enthalpies of formation, electron affinities, and ionization energies) G4(MP2) attains an RMSD of 6.2 kJ•mol^{-1}. However, as pointed out above, for reaction that conserve large molecular fragments on both sides of the reaction, G4(MP2) theory should yield better performance due to a large degree of systematic error cancelation between reactants and products [298, 299, 302-306]. In this context, we note that reactions 7.4 and 7.6–7.9 conserve both the numbers of each formal bond type and the numbers of carbon atoms in each hybridization state on the two sides of the reaction.

Since both W1h and G4(MP2) approximate the CCSD(T) energy, it is of interest to estimate whether post-CCSD(T) contributions are likely to be significant for the theoretical heats of formation obtained from reactions 7.2–7.9. The percentage of the atomization energy accounted for by parenthetical connected triple excitations, %TAE[(T)], has been shown to be a reliable energy-based diagnostic indicating the importance of post-CCSD(T) contributions [302, 307, 308]. The %TAE[(T)] values for the species involved in reactions 7.2–7.9 (Table S5, Supporting information) range between 0.7 (CH_4) and 3.0 (C_{60}). These values indicate that these systems are dominated by dynamical correlation effects and that post-CCSD(T) excitations are not expected to have a significant contributions to the reaction energies.

7.3 Results and discussion

7.3.1 W1h heat of formation for sumanene

Table 7-1 Experimental ATcT heats of formation at 298 K ($\Delta_f H°_{298}$) for species involved in reactions 7.2–7.4 and 7.6–7.9 (kJ•mol^{-1}) [309-311].

	$\Delta_f H°_{298}$
CH_4	–74.532 ± 0.057
C_2H_4	52.56 ± 0.15
C_2H_6	–83.79 ± 0.17
C_3H_8	–104.41 ± 0.29
C_6H_6	83.18 ± 0.26

We begin by calculating the heat of formation for sumanene by means of the W1h thermochemical protocol. We obtain an accurate theoretical heat of formation for sumanene via reactions that conserve the chemical environments of the reactants and products to various degrees. Specifically, the following reactions are considered:

$$\text{sumanene} + 3\ \text{methane} \rightarrow 4\ \text{benzene} \tag{7.2}$$

$$\text{sumanene} + \frac{3}{5}\,\text{methane} \rightarrow \frac{6}{5}\,\text{triphenylene} \tag{7.3}$$

Sumanene is essentially triphenylene in which the three outer phenyl rings are joined together with three CH_2 groups (Figure 1). Thus, apart from the strain energy involved in sumanene, reaction 7.3 conserves the chemical environments of the reactants and products to a large extent. The reaction enthalpies of

reactions 7.2 and 7.3 are obtained from W1h theory, whilst accurate experimental heats of formation for methane and benzene are taken from the Active Thermochemical Tables (ATcT) network of Ruscic and coworkers (the ATcT values are summarised in Table 1) [309-311]. An experimental heat of formation for triphenylene ($\Delta_f H°_{298}[C_{18}H_{12}(g)]$ = 270.1 ± 4.4 kJ•mol^{-1}) is taken from Roux *et al* [312]. We note that this experimental value is in good agreement with the theoretical W1h value calculated in ref. 291. The component breakdown of the W1h reaction enthalpies and our resultant predicted heats of formation are gathered in Table 7-2. Both reactions 7.2 and 7.3 lead to similar heats of formation for sumanene, namely $\Delta_f H°_{298}[C_{21}H_{12}(g)]$ = 535.3 ± 9 (reaction 7.2) and 530.3 ± 8 (reaction 7.3) kJ•mol^{-1}. Using reaction 7.2 has the advantage that only highly accurate experimental values from ATcT are used, whereas reaction 7.3 has the advantage that larger molecular fragments are being conserved on the two sides of the reaction. Since we believe that our W1h reaction energy should be sufficiently converged for reaction 7.2, we adopt the heat of formation obtained from this reaction since it involves only experimental data associated with well-defined error bars < 0.3 kJ•mol^{-1}. We note that calculating the heat of formation of sumanene via an atomization reaction leads to a very similar value of $\Delta_f H°_{298}[C_{21}H_{12}(g)]$ = 536.7 kJ•mol^{-1}. The atomization energy at 0 K was converted to a heat of formation at 298 K using ATcT atomic heats of formation at 0 K (H 216.034 ± 0.000 and C 711.38 ± 0.06 kJ•mol^{-1}), and the CODATA enthalpy functions, $H_{298}-H_0$, for the elemental reference states (H_2(g) = 8.468 ± 0.001 and C(*cr*,graphite) = 1.050 ± 0.020 kJ•mol^{-1}), while the molecular enthalpy function was obtained within the RRHO approximation from the B3LYP/6-31G(2df,p) calculated geometry and harmonic frequencies.

Table 7-2 Component breakdown of the W1h reaction enthalpies and predicted theoretical enthalpies of formation for sumanene (kJ•mol^{-1}).

Reaction	(7.2)	(7.3)
ΔHF[a]	–244.8	–153.3
ΔCCSD[b]	65.9	142.6
Δ(T)[c]	6.7	27.1
ΔCV[d]	–0.5	0.4
ΔRel[e]	–0.3	–0.6
ΔDBOC[f]	0.0	0.2
ΔZPVE[g]	5.6	18.7
$\Delta(H_{298}–H_0)$[g]	0.9	–9.0
$\Delta_r H°_{298}$[h]	–166.4	26.1
$\Delta_f H°_{298}$[i,j]	535.3 ± 9	530.3 ± 8

[a]Extrapolated from the cc-pVQZ and cc-pV5Z basis sets. [b]Extrapolated from the cc-pVTZ and cc-pVQZ(no *f* on H) basis sets (see ref. 291 for further details). [c]Extrapolated from the cc-pVDZ and cc-pVTZ basis sets. [d]CCSD(T) core–valence correction obtained as: CCSD/cc-pwCVTZ + (T)/cc-pwCVTZ(no *f*) (see ref. 291 for further details). [e]CCSD(T)/cc-pVDZ-DK scalar relativistic correction. [f]HF/cc-pVTZ DBOC correction. [g]Scaled B3LYP/6-31G(2df,p) values. [h]Overall reaction enthalpy at 298 K. [i]Theoretical heats of formation at 298 K for sumanene obtained using the W1h reaction enthalpies and experimental heats of formation (see text). [j]The associated uncertainties are obtained using the reported experimental uncertainties and a conservative uncertainty of ± 7.7 kJ•mol^{-1} for the W1h reaction enthalpies, taken from ref. 305.

7.3.2 Heat of Formation of C_{60}

Having obtained a reliable W1h heat of formation for sumanene paves the way for calculating the heat of formation for C_{60} via reactions in which C_{60} is broken down into sumanene and corannulene. In these thermochemical cycles we will use our best theoretical W1h heats of formation for corannulene ($\Delta_f H^\circ_{298}[C_{20}H_{10}(g)]$ = 485.2 ± 8, from ref. 291) and sumanene ($\Delta_f H^\circ_{298}[C_{21}H_{12}(g)]$ = 535.3 ± 9 kJ•mol^{-1}). In these reactions we will only consider additional species for which accurate experimental heats of formation are available from the ATcT thermochemical network (Table 7-1). In all cases the reaction energies are calculated at the G4(MP2) level.

We begin by stressing that even though we are calculating the reaction energies at the G4(MP2) level, we still need to use reactions that conserve large molecular fragments on the two sides of the reaction. This is clearly demonstrated by considering the following isodesmic reaction, which was used in ref. 147:

$$C_{60} + 30\ C_2H_4 \rightarrow 20\ C_6H_6 \qquad (7.4)$$

Table 7-3 lists the G4(MP2) reaction enthalpy for reaction 7.4 as well as the resulting predicted heat of formation for C_{60} $\Delta_f H^\circ_{298}[C_{60}(g)]$ = 2420.7 kJ•mol^{-1}. This heat of formation is lower than the experimental value adopted by NIST by nearly 140 kJ•mol^{-1} and is also significantly lower than the theoretical values obtained via reactions that conserve larger molecular fragments on the two sides of the reaction (*vide infra*). The experimental uncertainties associated with C_2H_4 and C_6H_6 cannot account for more than about 10 kJ•mol^{-1}. This leaves the G4(MP2) reaction enthalpy as the main source of error, and we conclude that the G4(MP2) level cannot accurately predict the enthalpy of this reaction. We note that using an atomization

reaction calculated at the G4(MP2) level leads to an even lower heat of formation for C_{60}, namely, $\Delta_f H^\circ_{298}[C_{60}(g)]$ = 2402.5 kJ•mol^{-1}. In this context it should be pointed out that the quality of G4(MP2) heats of formation obtained from atomization reactions deteriorates with the size (and complexity) of the molecular system. For example, we obtain the following differences relative to our best W1h or ATcT heats of formation: 1.0 (CH_4), –1.8 (C_2H_4), 1.3 (C_2H_6), 1.4 (C_3H_8), –3.6 (C_6H_6), –31.5 ($C_{20}H_{10}$), and –30.0 ($C_{21}H_{12}$) kJ•mol^{-1} (the differences are G4(MP2) – best expt./theor. value). These differences (in particular, the large underestimations obtained for $C_{20}H_{10}$ and $C_{21}H_{12}$) suggest that the G4(MP2) heat of formation for C_{60} obtained via an atomization reaction will be significantly underestimated.

Table 7-3 G4(MP2) reaction enthalpies for reactions 7.4–7.9 and predicted theoretical enthalpies of formation for C_{60} (kJ•mol^{-1}).

Reaction	$\Delta_r H_{298}$[a]	$\Delta_f H^\circ_{298}[C_{60}(g)]$[b]
7.4	–2333.9	2420.7
7.5	–1619.7	2558.5
7.6	–475.9	2555.3
7.7	18.0	2511.7
7.8	61.9	2515.2
7.9	158.8	2515.0

[a]Reaction enthalpy calculated at the G4(MP2) level. [b]Theoretical heat of formation for C_{60} obtained from the G4(MP2) reaction enthalpies, theoretical W1h heats of formation for sumanene and corannulene, and experimental ATcT heats of formation for methane, ethene, ethane, propane and benzene (see Table 7-1 and text).

Let us now turn to reactions that conserve larger molecular fragments on the two sides of the reaction. We first consider a reaction that involves only sumanene and corannulene:

$$C_{60} + 20 \text{ sumanene} \rightarrow 24 \text{ corannulene} \qquad (7.5)$$

The predicted heat of formation for C_{60} from reaction 7.5 is 2558.5 kJ•mol^{-1}. However, it is important to note that, due to the large stoichiometric coefficients of sumanene and corannulene (20 and 24, respectively), even a small error of ± 1 kJ•mol^{-1} in the W1h heats of formation for these species could translate to an error of 44 kJ•mol^{-1} in the predicted heat of formation for C_{60}. Given that our best W1h theoretical heats of formation for sumanene and corannulene are associated with uncertainties of 8–9 kJ•mol^{-1}, it is desirable to use reactions with much smaller stoichiometric coefficients for these species. In addition, we note that reaction 7.5 does not conserve the numbers of each formal bond type, and the numbers of carbon atoms in each hybridization state on the two sides of the reaction. Two reactions in which these properties are conserved are:

$$C_{60} + 10\ C_6H_6 \rightarrow 6\ \text{corannulene} \tag{7.6}$$

$$C_{60} + 10\ CH_4 \rightarrow \frac{10}{3}\ \text{sumanene} \tag{7.7}$$

Reaction 7.6 was used in ref. 291 for obtaining the heat of formation for C_{60}. Calculating the reaction energy with two DHDFT functionals in conjunction with the cc-pVQZ basis set (and using the ATcT heat of formation for benzene), ref. 291 obtained $\Delta_f H^{\circ}_{298}[C_{60}(g)]$ = 2535.2 (DSD-PBEP86-D3) [292] and 2543.1 (B2GP-PLYP-D3) [313] kJ•mol^{-1}. In the present work we obtain a higher value of $\Delta_f H^{\circ}_{298}[C_{60}(g)]$ = 2555.3 kJ•mol^{-1} using the more accurate G4(MP2) reaction energy. In reaction 7.7 C_{60} is broken down into 3.3 sumanenes. Calculating the reaction energy at the G4(MP2) level (and using the ATcT heat of formation for methane) we obtain a significantly lower heat of formation for C_{60} of $\Delta_f H^{\circ}_{298}[C_{60}(g)]$ = 2511.7 kJ•mol^{-1}. We note however, that since reaction 7.7 involves about three sumanenes, whereas reaction 7.6 involves six corannulenes, reaction 7.7 is less prone to the potential error resulting from the

uncertainty in the W1h heats of formation for corannulene and sumanene. Therefore, we deem the $\Delta_f H^\circ_{298}[C_{60}(g)]$ value obtained from reaction 7.7 more reliable.

What about reactions in which C_{60} is separated into both corannulene and sumanene? The following two reactions conserve the numbers of each formal bond type and the numbers of carbon atoms in each hybridization state on the two sides of the reaction:

$$C_{60} + 7.5\ C_2H_6 + 1.5\ \text{corannulene} \rightarrow 5\ \text{sumanene} \qquad (7.8)$$

$$C_{60} + 6\ C_3H_8 + 2.4\ \text{corannulene} \rightarrow 6\ \text{sumanene} \qquad (7.9)$$

These reactions result in essentially the same predicted heat of formation for C_{60}, namely, $\Delta_f H^\circ_{298}[C_{60}(g)]$ = 2515.2 (reaction 7.8) and 2515.0 (reaction 7.9) kJ•mol^{-1}. These results are in close agreement with the $\Delta_f H^\circ_{298}[C_{60}(g)]$ value obtained via reaction 7.7.

7.4 Conclusions

Corannulene (a pentagon surrounded by five hexagons) and sumanene (a hexagon surrounded by three pentagons and three hexagons) are the two basic building blocks of C_{60}. We obtain the heat of formation of C_{60} via ructions that involve corannulene and sumanene, and hence conserve the chemical environments of the reactants and products to large extents. We calculate the reaction energies by means of the high-level G4(MP2) thermochemical protocol, whilst the heats of formation for the reactants and products are calculated with the W1h thermochemical protocol (for corannulene and sumanene) or taken from the ATcT thermochemical network (for CH_4, C_2H_4, C_2H_6, C_3H_8, and C_6H_6). We show that there is a significant variation in the predicted heat of formation of C_{60} obtained via different reactions. In particular, reactions 7.5

and 7.6 result in $\Delta_f H^\circ_{298}[C_{60}(g)]$ = 2555.3–2558.5, whereas reactions 7.7–7.9 result in $\Delta_f H^\circ_{298}[C_{60}(g)]$ = 2511.7–2515.2 kJ•mol^{-1}. Since the considered reactions conserve the chemical environments of the reactants and products to large extents we assume that our G4(MP2) reaction energies are sufficiently converged. Thus, the main source of error in the predicted heats of formation for C_{60} are the potential errors in the theoretical W1h heats of formation for corannulene and sumanene. We therefore adopt the $\Delta_f H^\circ_{298}[C_{60}(g)]$ value obtained from reaction 7.7 ($\Delta_f H^\circ_{298}[C_{60}(g)]$ = 2511.7 kJ•mol^{-1}) as our best theoretical heat of formation for C_{60} since this reaction is the least prone for this source of error. The revised $\Delta_f H^\circ_{298}[C_{60}(g)]$ value is lower by only 9.9 kJ•mol^{-1} than the best theoretical estimate recommended in ref. 291, but should carry a smaller uncertainty since it is obtained at a considerably higher level of theory. Our best theoretical value is within the limits of the error bars of the experimental value adopted by the NIST thermochemical database (2560 ± 100 kJ•mol^{-1}). However, it suggests that the NIST value should be revised downwards.

Supporting Information

Appendix A2 contains full computational details. Summary of reported experimental heats of formation for C_{60} (Table S4); Diagnostics indicating the importance of post-CCSD(T) correlation effects for the species involved in reactions 7.2–7.9 (Table S5); B3LYP/6-31G(2df,p) optimised geometries for all the species in reactions 7.2–7.9 (Table S6).

Chapter 8. Evaluation and Implications

8.1 Introduction

In the present chapter, the findings from the five preceding chapters are evaluated against the objectives set out in Chapter 2 and their implications are assessed. In evaluating the present work, the results from the present study are compared with the data from the literature and further implications are provided.

8.2 Interactions among cellulose, hemicellulose and lignin during pyrolysis

The study of the interaction among cellulose hemicellulose and lignin in Chapter 3 provides clear evidence that these interactions are important during pyrolysis. As the conversion increased, the activation energy of cellulose remained relatively constant ~ 260.42 kJ•mol^{-1} whereas the activation energy of hemicellulose and lignin increased from 250 kJ•mol^{-1} to 375 kJ•mol^{-1}. As the conversion decreased, the activation energy of the mixture overall decreased even though the activation energy of the individual component increased. Overall, the yield of char increased from 823 K to 923 K and the yield of gas increased from 923 K to 1023 K. The interactions between cellulose, hemicellulose, and lignin promoted the formation of lignin derived compounds while suppressing the formation of compounds derived from cellulose and hemicellulose. Table 8-1 compares the results of the present study with other studies on the interactions among cellulose, hemicellulose and lignin during pyrolysis.

There have been few studies of the kinetics and molecular characterisation of the interactions between cellulose, hemicellulose and lignin. Most research to date has focused on predicting the yields of liquid, char and gas based on the assumption of superposition laws but there is no proof of the superposition law at a molecular level. The findings of the present study may help

explain some of the discrepancies regarding the interactions between cellulose, hemicellulose and lignin.

Table 8-1 Comparison of the results of the present study and previous studies regarding the interactions between cellulose, hemicellulose and lignin during pyrolysis

Study	**Approach**	**Findings**
Yang (2006)	TGA	• Observation of negligible interactions between cellulose, hemicellulose and lignin during pyrolysis.
Worasuwannarak (2007)	TG-MS	• Decreases in tar yield and increases in char yield after cellulose and lignin interaction.
Wang (2008)	TGA	• Cellulose and lignin could not affect each other obviously.
Qu (2011)	Tube furnace	• The superposition law can predict reasonably the trend of product yields of biomass samples from their composition of cellulose, hemicellulose and lignin.
Stefanidis (2013)	TGA and a fixed-bed reactor	• When using superposition law, heat transfer could affect the product distribution which results in accurate calculation
Present Study	TGA and a fixed-bed reactor	• The activation energy of the sample mixture decreased while the activation energy of each individual component increased. • The interactions promoted the formation of lignin derived compounds while suppressing the formation of compounds derived from cellulose and hemicellulose.

There is clearly a need for further research using more sophisticated techniques to provide a comprehensive molecular characterisation of pyrolysis products. The effect of mixing ratio, particle size and residence time also needs to be investigated.

8.3 Identification and characterisation of cellulose pyrolysis products

This study describes the comprehensive identification and characterisation of cellulose pyrolysis products using different product-capture techniques and reactors at different scales. It was found that at 1023 K the main primary products of cellulose pyrolysis were anhydrosugars, furans and ketones while at 823 K and 923 K only furans and anhydro-sugars were detected. Disaccharides were also identified in the primary products.

Table 8-2 Comparison of the results of the present study and previous studies regarding the characterisation of biomass pyrolysis products

Study	Approach	Findings
Bayerbach (2006)	SEC TOF-MS, Py-FIMS	• Average molecular weight of pyrolytic lignin was between 560 and 840Da with a maximal deviation of 20%. • Molecular weight of pyrolytic lignin dimers was between 270 and 400 Da.
D.K. Shen (2010)	Py-GC-MS Py-FTIR	• Seven main compounds in cellulose pyrolysis liquid and six main compounds in hemicellulose pyrolysis liquid were identified and quantified.
Gopakumar (2011)	Py-GC-MS	• Products were identified and classified into six groups and quantified.
Dufour (2013)	Synchrotron mass spectrometer	• Evolution of cellulose (m/z = 162), xylan (m/z = 114) and lignin (m/z = 120, 150, 180) markers.
Present study	Quenching method and GC-MS	• Cellulose pyrolysis products were classified into eight groups. • Cellulose pyrolysis primary products were identified.

Generally speaking, the results of the present study are consistent with the results of previous studies (Table 8-2) and provide important insights into the mechanisms of cellulose pyrolysis.

While most studies have employed capture facilities to condense or detect the products, these facilities were a long distance downstream.

This study reduced this distance so that products generated at the early stage of pyrolysis could be detected. Also, while most studies have focused on the yields of major pyrolysis products (such as levoglucosan), the present research assessed the yield variations in other minor products (such as disaccharides, 2, 3-andro-d-mannosan, D-Allose and pyran compounds). These findings have implications for selective utilization of pyrolysis liquid, especially for cellulose-derived oxygenated compounds.

Because different researchers used different experimental reactors and operated under different conditions, it could be difficult to reach a quantitative agreement among the reported data. Due to the limitation of analytical facilities, the present study failed to further identify unknown high-molecular weight compounds and quantify all identified compounds. Further research using more sophisticated techniques (such as high resolution mass spectrometer) are required to refine these results.

8.4 Formation of cellulose pyrolysis products and their transformations

Based on the experimental findings generated during product characterisation (Chapter 4), a systematic study of the effect of residence time on the formation of cellulose pyrolysis products was conducted. It showed that among the thirteen compounds quantified, DGP, levoglucosan and levoglucosan-furanose were the only compounds identified to be residence time inhibited. Further thermal analysis showed that DGP might be an intermediate for the formation of levoglucosenone. Levoglucosan was found to be thermally stable and produced concurrently with other compounds.

Although residence time is an important parameter in pyrolysis, previous studies have only studied the effect of residence time qualitatively. There has been little effort directed towards understanding the role of residence time quantitatively. The present research quantified the effect of residence time and temperature on the formation of thirteen major cellulose pyrolysis products. The results combined with further thermal analysis of the major anhydrosugars provides a better understanding of the formation of major anhydrosugars (levoglucosan, levoglucosenone and DGP) and the mechanisms underlying their transformations.

These findings may also have implications in reactor and process design. Fixed-bed reactors, fluidised-bed reactors, and other reactors often have residence times spanning over several magnitudes. From the present findings, it can be assumed that residence time may have similar effects of product formation in these reactors, which could be potentially used for process control and product selection. However, the feasibility of various configurations needs further analysis and investigation.

The present study, like most other studies on this topic, failed to provide a real-time analysis of the formation of pyrolysis products. In-situ facilities combined with a real-time analytical approach will be required to unravel the mechanisms underlying pyrolysis.

8.5 Formation of levoglucosenone from anhydrosugar intermediates

In the present study, high-level computational modeling was carried out to elucidate the reaction pathway from DGP to levoglucosenone. A detailed seven-step reaction scheme was proposed and energy profiles were asssessed. The simulated results are in broad agreement with the experimental data shown in Chapter 5 and previous studies described in Table 8-3.

The present study, in combination with experimental data, provide a detailed formation mechanism of LGO from DGP, which was not known before.

Table 8-3 Comparison of the results of the present study and previous studies regarding the formation of levoglucosenone

Study	**Approach**	**Findings**
Shafizadeh. (1979)	GC-MS	• Levoglucosan was proposed the precursor of levoglucosenone.
Assary (2012)	Gn theory	• Water catalysed transformation for the formation of levoglucosenone from levoglucosan with an activation energy of $\Delta H^{\ddagger}_{298}$ = 56.6 kcal•mol^{-1} at the G4 level.
Q Lu (2014)	B3LYP/6-31+G(d,p) level of theory	• Enol-to taurimerisation is the RDS both from *β*-D-glucopyranose and cellobiose with barriers of $\Delta H^{\ddagger}_{298}$ = 69.5 kcal•mol^{-1} and $\Delta H^{\ddagger}_{298}$ = 62.7 kcal•mol^{-1}, respectively.
Present study	G4(MP2) theory	• DGP was proposed to be the precursor of levoglucosenone. • The multistep transformation from DGP to levoglucosenone is thermodynamically favored as the Gibbs free energy of levoglucosenone lies 11.6 kcal•mol^{-1} below DGP.

The results of the present study suggest that water could considerably reduce the reaction energy barrier and shift the RDS from enol-to-keto tautomerisation to a ring-opening reaction. In the industrial pyrolysis process, this catalytic effect may be utilized to reduce power input and enhance product yield.

Future research could be directed towards developing a more detailed reaction scheme with various pyrolysis products using high-level *ab initio* thermochemical protocol. The current molecular simulation in the present study only used two major anhydrosugar compounds which is not sufficient to reveal the complex chemical reactions in cellulose pyrolysis. It was also assumed that all reactions were in the gas phase. However, in reality, pyrolysis is much more complicated and involves reactions in the gas, liquid and solid phases,The interaction and transformations among these three phases is likely to be complex. A more comprehensive modeling approach is required in the future to address these issues.

8.6 Application of high-level thermochemical protocols: heat formation of C_{60}

In order to further apply high-level thermochemical protocol in molecular theoretical calculations, an investigation on the heat formation of C60 using G4(MP2) and Wn theory was conducted. This study used high-level thermochemical protocols with sophisticated thermochemical cycles for obtaining the most accurate theoretical heat of formation of C_{60} to date. The best theoretical value of heat of formation for C_{60} is within the limits of the error bars of the experimental value adopted by the NIST thermochemical database. However, it suggests the NIST value should be revised downwards.

The estimated heat of formation value was validated using different reactions combined with the use of high-level thermochemical protocols. The value is consistent with the value obtained from previous studies (Table S4). High-level thermochemical protocols (such as Gn theory and Wn theory) expects a small level of uncertainty in the theoretical estimate since the considered reactions conserve the chemical environments of the reactants and products to a large extent.

Although the present theoretical calculation provided an accurate estimate of the heat formation of C_{60}, there have been no recent quantitative experimental data to validate the accuracy of this estimate. Therefore, appropriate experimentation should be designed and carried out in the future to validate this result.

8.7 Overall evaluation and implications

The overall aim to study the biomass pyrolysis process including components interactions, product characterisation, parametric effects and reaction pathways has been achieved. The study provides:

- Evidence that the interactions between cellulose, hemicellulose and lignin play an important role during pyrolysis.
- A better understanding of the formation of cellulose pyrolysis products and the mechanism of their transformations based on product characterisation, parametric investigation and molecular simulation.

These findings have various practical implications for pyrolysis process. Understanding the mechanisms of biomass pyrolysis could improve the quality of pyrolysis product and optimise the pyrolysis process. Although the present study provides a better understanding of the fundamentals of biomass pyrolysis through the present studies, our knowledge in this field is far from complete and further improvements are possible and necessary through future research.

Chapter 9. Conclusions and Recommendations

9.1 Introduction

The present research has improved the state of knowledge of the mechanism of biomass pyrolysis. The conclusions and evaluations of the present research have also led some recommendations for future studies in this field.

9.2 Conclusions

9.2.1 Interactions between cellulose, hemicellulose and lignin during pyrolysis

- Kinetic analysis and product characterisation of pyrolysis shows that cellulose, hemicellulose and lignin interact during pyrolysis.

- As the pyrolysis reactions progress, the activation energies of cellulose, hemicellulose and lignin increase. In contrast, the activation energy of sample mixture of cellulose, hemicellulose and lignin decreases. This difference in activation energies suggests that the interaction between cellulose, hemicellulose and lignin has an important impact on pyrolysis.

- During pyrolysis of sample mixture of cellulose, hemicellulose and lignin, the formation of lignin derived compounds increases and the formation of cellulose and hemicellulose derived compounds is suppressed.

9.2.2 Identification and characterisation of cellulose pyrolysis products

- At 1023 K the main primary products of cellulose pyrolysis are anhydrosugars, furans and ketones. At 823 K and 923 K only furans and anhydrosugars are detected. Levoglucosan

and levoglucosenone are the main compounds in these anhydrosugars and furfural is the main furan compound. Disaccharides can be found in the primary products of cellulose pyrolysis.

- In FBR, cellulose pyrolysis liquid products can be classified as anhydrosugars, furans, ketones, acids, aldehydes, esters, phenols and benzenes. Cellulose pyrolysis gas products include CO, CO_2, H_2 and light hydrocarbons (such as CH_4, C_2H_6 and C_2H_4). From 823 K to 923 K, CO and CO_2 are the dominant gas products. From 923 K to 1023 K, the concentrations of H_2, CH_4, C_2H_6, C_2H_4 and C_2H_2 increase. From 823 K to 1023 K, the yields of all oxygenated compounds (including anhydro-sugars, ketones, furans, acids, aldehydes and esters) decrease whereas the yields of phenols and benzenes increase.

9.2.3 Formation of cellulose pyrolysis products and their transformations

- Only the production of DGP, levoglucosan and levoglucosan-furanose are inhibited with increasing residence time. DGP and levoglucosenone are mainly produced in the early stages of cellulose pyrolysis. As pyrolysis temperature increases, the production of levoglucosan and levoglucosan-furanose increases.

- Levoglucosenone is the only anhydrosugar compound identified to be residence time promoted, indicating it is more favored to be generated in secondary reactions.

- The productions of furan compounds (including furfural, 5-methyl furfural and 5-HMF) are inhibited by increasing temperature and promoted by increasing residence time. In contrast, the productions of light fragmented compounds (including acetic acid, hydroxyl

acetone and 2,3-butadione) are promoted as temperature and increasing residence time increase.

- Levoglucosan is thermally stable and produced along with other compounds.

- DGP might be an intermediate for the formation of levoglucosenone.

9.2.4 Formation mechanisms of levoglucosenone

- The reaction mechanism (uncatalysed and catalysed) for the formation of levoglucosenone from DGP proceeds via ring-opening, ring-closing, enol-to-keto tautomerisation, dehydration and hydration reactions.

- In the uncatalysed mechanism, the RDS is the enol-to-keto tautomerisation with the activation of Gibbs free energy of $\Delta G^{\ddagger}_{298}$ = 68.6 kcal•mol^{-1} relative to the DGP reactant.

- In the water-catalysed mechanism, the RDS is the ring–opening reaction with the activation of Gibbs free energy of $\Delta G^{\ddagger}_{298}$ = 58.1 kcal•mol^{-1} relative to the DGP reactant.

- The transformation from DGP to levoglucosenone is thermodynamically favored as the Gibbs free energy of the final product (levoglucosenone) lies 11.6 kcal•mol^{-1} below the starting material (DGP). This provides a thermodynamic driving force for this process.

9.2.5 Heat formation of C_{60} by means of high-level thermochemical protocols

- There is significant variation in the predicted heat of formation of C_{60} obtained via different reactions. The $\Delta_f H°_{298}[C_{60}(g)]$ value obtained from reaction 7.7 ($\Delta_f H°_{298}[C_{60}(g)]$ = 2511.7

kJ•mol^{-1}) was adopted as the best theoretical heat of formation for C_{60} since this reaction is the least prone for this source of error.

- While the best theoretical value is within the limits of the error bars of the experimental value adopted by the NIST thermochemical database (2560 ± 100 kJ•mol^{-1}), the present result suggest that the NIST value should be revised downwards.

9.3 Recommendations

Even though the overall objectives listed in Chapter 2 have been achieved, new knowledge gaps have also been identified, leading to the following recommendations for future research.

- Further parametric analysis of the interactions between cellulose, hemicellulose and lignin (Chapter 3) is recommended to be carried out. This includes the analysis of residence time and particle size, and the impact of different ratios of cellulose, hemicellulose and lignin. The current analysis shows that there are interactions between the three constituents during the pyrolysis. However, it remain unclear whether the interaction occurs prior to the decomposition or the decomposition products react with other constituents.

- In Chapter 4, a method was developed for the characterisation of cellulose pyrolysis products. However, high-molecular-weight compounds are yet to be identified. Although this study provides some valuable data on the formation of high-molecular-weight compounds, the specific structure of these compounds, such as sugar-ring-containing compounds, is still not well understood.

- Chapter 5 provides valuable insights into the transformation among different pyrolysis anhydrosugar compounds under *ex situ* conditions. Further *in situ* analysis of cellulose pyrolysis could provide a better understanding of the mechanism of the transformation.

- Chapter 6 elucidates the formation pathways between DGP and levoglucosenone. However, the main products from cellulose pyrolysis are a complex mixture containing various compounds. Further studies could be directed towards involving more products in investigating the mechanism. A kinetic model could be further constructed based on the PES shown in Chapter 6.

- Chapter 7 employs high-level thermochemical protocols to investigate the heat of formation of C_{60}. High-level thermochemical protocols used this study (Gn theory and Wn theory) is recommended to be further incorporated to better understand the mechanism of biomass pyrolysis with refining accuracy.

References

1. Roy, P. and G. Dias, *Prospects for pyrolysis technologies in the bioenergy sector: A review.* Renewable and Sustainable Energy Reviews, 2017. **77**(Supplement C): p. 59-69.
2. Kumar, G., et al., *A review of thermochemical conversion of microalgal biomass for biofuels: chemistry and processes.* Green Chemistry, 2017. **19**(1): p. 44-67.
3. Parikka, M., *Global biomass fuel resources.* Biomass and Bioenergy, 2004. **27**(6): p. 613-620.
4. Berndes, G., M. Hoogwijk, and R. van den Broek, *The contribution of biomass in the future global energy supply: a review of 17 studies.* Biomass and Bioenergy, 2003. **25**(1): p. 1-28.
5. McKendry, P., *Energy production from biomass (part 2): conversion technologies.* Bioresource Technology, 2002. **83**(1): p. 47-54.
6. Bridgwater, A.V., *Review of fast pyrolysis of biomass and product upgrading.* Biomass and Bioenergy, 2012. **38**: p. 68-94.
7. Zhang, J., M.W. Nolte, and B.H. Shanks, *Investigation of Primary Reactions and Secondary Effects from the Pyrolysis of Different Celluloses.* ACS Sustainable Chemistry & Engineering, 2014. **2**(12): p. 2820-2830.
8. Stiles, H.N. and R. Kandiyoti, *Secondary reactions of flash pyrolysis tars measured in a fluidized bed pyrolysis reactor with some novel design features.* Fuel, 1989. **68**(3): p. 275-282.
9. Patwardhan, P.R., et al., *Distinguishing primary and secondary reactions of cellulose pyrolysis.* Bioresource Technology, 2011. **102**(8): p. 5265-5269.
10. Mohan, D., C.U. Pittman, and P.H. Steele, *Pyrolysis of Wood/Biomass for Bio-oil: A Critical Review.* Energy & Fuels, 2006. **20**(3): p. 848-889.
11. Mettler, M.S., D.G. Vlachos, and P.J. Dauenhauer, *Top ten fundamental challenges of biomass pyrolysis for biofuels.* Energy & Environmental Science, 2012. **5**(7): p. 7797-7809.
12. Kamm, B., et al., *Lignocellulose-based Chemical Products and Product Family Trees*, in *Biorefineries-Industrial Processes and Products*. 2008, Wiley-VCH Verlag GmbH. p. 97-149.
13. Giuntoli, J., *Characterization of 2nd generation biomass under thermal conversion and the fate of nitrogen* 2010, Ingegnere Energetico, Politecnico di Milano geboren te Florence, Itali ë.
14. Contributors, W., *"Cellulose," Wikipedia, The Free Encyclopedia,* .
15. Contributors, W. *"Hemicellulose," Wikipedia, The Free Encyclopedia,* . Available from: http://en.wikipedia.org/wiki/Hemicellulose.
16. Scheller, H.V. and P. Ulvskov, *Hemicelluloses.* Annual Review of Plant Biology, 2010. **61**(1): p. 263-289.
17. Contributors, W., *"Lignin," Wikipedia, The Free Encyclopedia,* .
18. Xu, C. and F. Ferdosian, *Structure and Properties of Lignin*, in *Conversion of Lignin into Bio-Based Chemicals and Materials*. 2017, Springer. p. 1-12.
19. Klein, M.T. and P.S. Virk, *Modeling of Lignin Thermolysis.* Energy & Fuels, 2008. **22**(4): p. 2175-2182.
20. W.G Glasser, H.R.G., *Evaluation of lignin's chemical structure by experimental and computer simulation techniques.* Pap Puu, 1981. **63**(2): p. 71-74.

21. Erickson, M., E. Miksche Gerhard, and I. Somfai, *Charakterisierung der Lignine von Angiospermen durch oxydativen Abbau. II. Monokotylen*, in *Holzforschung - International Journal of the Biology, Chemistry, Physics and Technology of Wood*. 1973. p. 147.
22. Nimz, H., *Das Lignin der Buche — Entwurf eines Konstitutionsschemas.* Angewandte Chemie, 1974. **86**(9): p. 336-344.
23. Pandey, M.P. and C.S. Kim, *Lignin Depolymerization and Conversion: A Review of Thermochemical Methods.* Chemical Engineering & Technology, 2011. **34**(1): p. 29-41.
24. Amen-Chen, C., H. Pakdel, and C. Roy, *Production of monomeric phenols by thermochemical conversion of biomass: a review*. Bioresource Technology, 2001. **79**(3): p. 277-299.
25. Contributors, W. *"Pyrolysis," Wikipedia, The Free Encyclopedia,* . Available from: http://en.wikipedia.org/wiki/Pyrolysis.
26. Patwardhan, P.R., *Understanding the product distribution from biomass fast pyrolysis*, in *Chemical Engineering*. 2010, Iowa State University.
27. A. Pandey, T.B., M. Stocker, R.K. Sukumaran, *Recent Advances In Thermochemical Conversion Of Biomass*, T.B. A. Pandey, M. Stocker, R.K. Sukumaran, Editor. 2015, Elsevier.
28. Contributors, W. *"Stationary or bubbling fluidized bed"*. Available from: http://en.wikipedia.org/wiki/Stationary_or_bubbling_fluidized_bed.
29. Yang, H., et al., *Characteristics of hemicellulose, cellulose and lignin pyrolysis.* Fuel, 2007. **86**(12–13): p. 1781-1788.
30. Contributors, W. *"Rotary Kilns"*. Available from: http://en.wikipedia.org/wiki/Rotary_kiln.
31. Zaman, C.Z., et al., *Pyrolysis: A Sustainable Way to Generate Energy from Waste*, in *Pyrolysis*. 2017, InTech.
32. Lédé, J., et al., *Properties of bio-oils produced by biomass fast pyrolysis in a cyclone reactor.* Fuel, 2007. **86**(12–13): p. 1800-1810.
33. Lédé, J., *The Cyclone: A Multifunctional Reactor for the Fast Pyrolysis of Biomass.* Industrial & Engineering Chemistry Research, 2000. **39**(4): p. 893-903.
34. Bech, N., et al., *Ablative Flash Pyrolysis of Straw and Wood: Bench-scale Results*, in *Proceedings*. 2007.
35. Verma, M., et al., *Biofuels Production from Biomass by Thermochemical Conversion Technologies.* International Journal of Chemical Engineering, 2012. **2012**: p. 18.
36. Brown, A.L., et al., *Design and Characterization of an Entrained Flow Reactor for the Study of Biomass Pyrolysis Chemistry at High Heating Rates.* Energy & Fuels, 2001. **15**(5): p. 1276-1285.
37. Frigge, L., J. Ströhle, and B. Epple, *Release of sulfur and chlorine gas species during coal combustion and pyrolysis in an entrained flow reactor.* Fuel, 2017. **201**: p. 105-110.
38. Van Paasen, S.V.B., et al., *Guideline for sampling and analysis of tar and particles in biomass producer gases.* Final report documenting the Guideline, R& D work and dissemination, 2002: p. 95.
39. Evans, R.J. and T.A. Milne, *Molecular characterization of the pyrolysis of biomass.* Energy & Fuels, 1987. **1**(2): p. 123-137.
40. Harman-Ware, A.E., et al., *Estimation of terpene content in loblolly pine biomass using a hybrid fast-GC and pyrolysis-molecular beam mass spectrometry method.* Journal of Analytical and Applied Pyrolysis, 2017. **124**: p. 343-348.

41. Di Nola, G., W. de Jong, and H. Spliethoff, *The fate of main gaseous and nitrogen species during fast heating rate devolatilization of coal and secondary fuels using a heated wire mesh reactor.* Fuel Processing Technology, 2009. **90**(3): p. 388-395.
42. Brackmann, C., et al., *Optical and Mass Spectrometric Study of the Pyrolysis Gas of Wood Particles.* Applied Spectroscopy, 2003. **57**(2): p. 216-222.
43. Dufour, A., et al., *Evolution of Aromatic Tar Composition in Relation to Methane and Ethylene from Biomass Pyrolysis-Gasification.* Energy & Fuels, 2011. **25**(9): p. 4182-4189.
44. Dufour, A., et al., *Revealing the chemistry of biomass pyrolysis by means of tunable synchrotron photoionisation-mass spectrometry.* RSC Advances, 2013. **3**(14): p. 4786-4792.
45. Wang, W., et al., *Effect of Temperature on the EPR Properties of Oil Shale Pyrolysates.* Energy & Fuels, 2016. **30**(2): p. 830-834.
46. ECN. *'Phyllis Database for Biomass and Waste'*. 2010; Available from: http://www.ecn.nl/phyllis/.
47. Kim, Y., et al., *Composition of corn dry-grind ethanol by-products: DDGS, wet cake, and thin stillage.* Bioresource Technology, 2008. **99**(12): p. 5165-5176.
48. Weng, J., et al., *Pyrolysis study of poplar biomass by tunable synchrotron vacuum ultraviolet photoionization mass spectrometry.* Proceedings of the Combustion Institute, 2013. **34**(2): p. 2347-2354.
49. Weng, J., et al., *On-line product analysis of pine wood pyrolysis using synchrotron vacuum ultraviolet photoionization mass spectrometry.* Analytical and Bioanalytical Chemistry, 2013. **405**(22): p. 7097-7105.
50. Lv, G. and S. Wu, *Analytical pyrolysis studies of corn stalk and its three main components by TG-MS and Py-GC/MS.* Journal of Analytical and Applied Pyrolysis, 2012. **97**(0): p. 11-18.
51. Mullen, C.A., G.D. Strahan, and A.A. Boateng, *Characterization of Various Fast-Pyrolysis Bio-Oils by NMR Spectroscopy†.* Energy & Fuels, 2009. **23**(5): p. 2707-2718.
52. Kim, S.-S., F.A. Agblevor, and J. Lim, *Fast pyrolysis of chicken litter and turkey litter in a fluidized bed reactor.* Journal of Industrial and Engineering Chemistry, 2009. **15**(2): p. 247-252.
53. Hussein, M., et al., *Temperature and gasifying media effects on chicken manure pyrolysis and gasification.* Fuel, 2017. **202**: p. 36-45.
54. Boateng, A.A., et al., *Bench-Scale Fluidized-Bed Pyrolysis of Switchgrass for Bio-Oil Production†.* Industrial & Engineering Chemistry Research, 2007. **46**(7): p. 1891-1897.
55. Tang, M.M. and R. Bacon, *Carbonization of cellulose fibers—I. Low temperature pyrolysis.* Carbon, 1964. **2**(3): p. 211-220.
56. Williams, P.T. and S. Besler, *The influence of temperature and heating rate on the slow pyrolysis of biomass.* Renewable Energy, 1996. **7**(3): p. 233-250.
57. Mok, W.S.L. and M.J. Antal Jr, *Effects of pressure on biomass pyrolysis. I. Cellulose pyrolysis products.* Thermochimica Acta, 1983. **68**(2–3): p. 155-164.
58. Mok, W.S.L. and M.J. Antal Jr, *Effects of pressure on biomass pyrolysis. II. Heats of reaction of cellulose pyrolysis.* Thermochimica Acta, 1983. **68**(2–3): p. 165-186.
59. Pindoria, R.V., et al., *Structural characterization of biomass pyrolysis tars/oils from eucalyptus wood waste: effect of H2 pressure and sample configuration.* Fuel, 1997. **76**(11): p. 1013-1023.
60. Thangalazhy-Gopakumar, S., et al., *Influence of Pyrolysis Operating Conditions on Bio-Oil Components: A Microscale Study in a Pyroprobe.* Energy & Fuels, 2011. **25**(3): p. 1191-1199.

61. Wang, S., et al., *Study of pyrolysis behavior of hydrogen-rich bark coal by TGA and Py-GC/MS.* Journal of Analytical and Applied Pyrolysis, 2017. **128**(Supplement C): p. 136-142.
62. Galano, A., et al., *A combined theoretical-experimental investigation on the mechanism of lignin pyrolysis: Role of heating rates and residence times.* Journal of Analytical and Applied Pyrolysis, 2017. **128**(Supplement C): p. 208-216.
63. Brunner, P.H. and P.V. Roberts, *The significance of heating rate on char yield and char properties in the pyrolysis of cellulose.* Carbon, 1980. **18**(3): p. 217-224.
64. Gong, X., et al., *Formation of Anhydro-sugars in the Primary Volatiles and Solid Residues from Cellulose Fast Pyrolysis in a Wire-Mesh Reactor.* Energy & Fuels, 2014. **28**(8): p. 5204-5211.
65. LeBlanc, J., J. Quanci, and M.J. Castaldi, *Investigating Secondary Pyrolysis Reactions of Coal Tar via Mass Spectrometry Techniques.* Energy & Fuels, 2017. **31**(2): p. 1269-1275.
66. Pecha, M.B., et al., *Effect of a Vacuum on the Fast Pyrolysis of Cellulose: Nature of Secondary Reactions in a Liquid Intermediate.* Industrial & Engineering Chemistry Research, 2017. **56**(15): p. 4288-4301.
67. Waters, C.L., et al., *Staged thermal fractionation for segregation of lignin and cellulose pyrolysis products: An experimental study of residence time and temperature effects.* Journal of Analytical and Applied Pyrolysis, 2017.
68. Sohaib, Q., et al., *Fast pyrolysis of locally available green waste at different residence time and temperatures.* Energy Sources, Part A: Recovery, Utilization, and Environmental Effects, 2017. **39**(15): p. 1639-1646.
69. Lin, Y.-C., et al., *Kinetics and Mechanism of Cellulose Pyrolysis.* The Journal of Physical Chemistry C, 2009. **113**(46): p. 20097-20107.
70. Shen, D.K. and S. Gu, *The mechanism for thermal decomposition of cellulose and its main products.* Bioresource Technology, 2009. **100**(24): p. 6496-6504.
71. Miller, R.S. and J. Bellan, *Analysis of Reaction Products and Conversion Time in the Pyrolysis of Cellulose and Wood Particles.* Combustion Science and Technology, 1996. **119**(1-6): p. 331-373.
72. Şensöz, S., D. Angın, and S. Yorgun, *Influence of particle size on the pyrolysis of rapeseed (Brassica napus L.): fuel properties of bio-oil.* Biomass and Bioenergy, 2000. **19**(4): p. 271-279.
73. Shen, J., et al., *Effects of particle size on the fast pyrolysis of oil mallee woody biomass.* Fuel, 2009. **88**(10): p. 1810-1817.
74. Zhou, X., et al., *Fast pyrolysis of glucose-based carbohydrates with added NaCl part 1: Experiments and development of a mechanistic model.* AIChE Journal, 2016. **62**(3): p. 766-777.
75. Zhou, X., et al., *Fast pyrolysis of glucose-based carbohydrates with added NaCl part 2: Validation and evaluation of the mechanistic model.* AIChE Journal, 2016. **62**(3): p. 778-791.
76. Nowakowski, D.J., et al., *Potassium catalysis in the pyrolysis behaviour of short rotation willow coppice.* Fuel, 2007. **86**(15): p. 2389-2402.
77. Müller-Hagedorn, M., et al., *A comparative kinetic study on the pyrolysis of three different wood species.* Journal of Analytical and Applied Pyrolysis, 2003. **68-69**(Supplement C): p. 231-249.
78. Patwardhan, P.R., et al., *Influence of inorganic salts on the primary pyrolysis products of cellulose.* Bioresource Technology, 2010. **101**(12): p. 4646-4655.

79. Shimada, N., H. Kawamoto, and S. Saka, *Solid-state hydrolysis of cellulose and methyl α- and β-d-glucopyranosides in presence of magnesium chloride.* Carbohydrate Research, 2007. **342**(10): p. 1373-1377.
80. Carvalho, W.S., et al., *Thermal decomposition profile and product selectivity of analytical pyrolysis of sweet sorghum bagasse: Effect of addition of inorganic salts.* Industrial Crops and Products, 2015. **74**(Supplement C): p. 372-380.
81. Di Blasi, C., et al., *Modifications in the Thermicity of the Pyrolysis Reactions of ZnCl2-Loaded Wood.* Industrial & Engineering Chemistry Research, 2015. **54**(51): p. 12741-12749.
82. Dobele, G., et al., *Application of catalysts for obtaining 1,6-anhydrosaccharides from cellulose and wood by fast pyrolysis.* Journal of Analytical and Applied Pyrolysis, 2005. **74**(1): p. 401-405.
83. Mészáros, E., E. Jakab, and G. Várhegyi, *TG/MS, Py-GC/MS and THM-GC/MS study of the composition and thermal behavior of extractive components of Robinia pseudoacacia.* Journal of Analytical and Applied Pyrolysis, 2007. **79**(1): p. 61-70.
84. Guo, X.-j., et al., *Influence of extractives on mechanism of biomass pyrolysis.* Journal of Fuel Chemistry and Technology, 2010. **38**(1): p. 42-46.
85. Wang, T., et al., *Pyrolytic characteristics of sweet potato vine.* Bioresource Technology, 2015. **192**(Supplement C): p. 799-801.
86. Shafizadeh, F. and Y.L. Fu, *Pyrolysis of cellulose.* Carbohydrate Research, 1973. **29**(1): p. 113-122.
87. Bradbury, A.G.W.S., Y.; Shafizadeh, F., *A kinetic model for pyrolysis of cellulose.* Journal of Applied Polymer Science, 1979. **23**(11): p. 3271-3280.
88. Hosoya, T., H. Kawamoto, and S. Saka, *Pyrolysis behaviors of wood and its constituent polymers at gasification temperature.* Journal of Analytical and Applied Pyrolysis, 2007. **78**(2): p. 328-336.
89. Alén, R., E. Kuoppala, and P. Oesch, *Formation of the main degradation compound groups from wood and its components during pyrolysis.* Journal of Analytical and Applied Pyrolysis, 1996. **36**(2): p. 137-148.
90. Ponder, G.R. and G.N. Richards, *Thermal synthesis and pyrolysis of a xylan.* Carbohydrate Research, 1991. **218**(0): p. 143-155.
91. Patwardhan, P.R., R.C. Brown, and B.H. Shanks, *Product Distribution from the Fast Pyrolysis of Hemicellulose.* ChemSusChem, 2011. **4**(5): p. 636-643.
92. Scheirs, J., G. Camino, and W. Tumiatti, *Overview of water evolution during the thermal degradation of cellulose.* European Polymer Journal, 2001. **37**(5): p. 933-942.
93. F.J Kilzer, A.B., Pyrodynamics, 1965. **2**: p. 151.
94. Widyawati, M., et al., *Hydrogen synthesis from biomass pyrolysis with in situ carbon dioxide capture using calcium oxide.* International Journal of Hydrogen Energy, 2011. **36**(8): p. 4800-4813.
95. Worasuwannarak, N., T. Sonobe, and W. Tanthapanichakoon, *Pyrolysis behaviors of rice straw, rice husk, and corncob by TG-MS technique.* Journal of Analytical and Applied Pyrolysis, 2007. **78**(2): p. 265-271.
96. Molton, P.M. and T.F. Demmitt, *Reaction mechanisms in cellulose pyrolysis: a literature review*. 1977. p. Medium: ED; Size: Pages: 90.
97. Golova, O.P., *Chemical Effects of Heat on Cellulose.* Russian Chemical Reviews, 1975. **44**(8): p. 687.
98. Mayes, H.B. and L.J. Broadbelt, *Unraveling the Reactions that Unravel Cellulose.* The Journal of Physical Chemistry A, 2012. **116**(26): p. 7098-7106.
99. Shafizadeh, F., R.H. Furneaux, and T.T. Stevenson, *Some reactions of levoglucosenone.* Carbohydrate Research, 1979. **71**(1): p. 169-191.

100. Halpern, Y., R. Riffer, and A. Broido, *Levoglucosenone (1,6-anhydro-3,4-dideoxy-.DELTA.3-.beta.-D-pyranosen-2-one). Major product of the acid-catalyzed pyrolysis of cellulose and related carbohydrates.* The Journal of Organic Chemistry, 1973. **38**(2): p. 204-209.
101. Assary, R.S. and L.A. Curtiss, *Thermochemistry and Reaction Barriers for the Formation of Levoglucosenone from Cellobiose.* ChemCatChem, 2012. **4**(2): p. 200-205.
102. Lu, Q., et al., *The mechanism for the formation of levoglucosenone during pyrolysis of β-d-glucopyranose and cellobiose: A density functional theory study.* Journal of Analytical and Applied Pyrolysis, 2014. **110**: p. 34-43.
103. Patwardhan, P.R., et al., *Product distribution from fast pyrolysis of glucose-based carbohydrates.* Journal of Analytical and Applied Pyrolysis, 2009. **86**(2): p. 323-330.
104. Lu, Q., et al., *Influence of pyrolysis temperature and time on the cellulose fast pyrolysis products: Analytical Py-GC/MS study.* Journal of Analytical and Applied Pyrolysis, 2011. **92**(2): p. 430-438.
105. Mettler, M.S., et al., *The chain length effect in pyrolysis: bridging the gap between glucose and cellulose.* Green Chemistry, 2012. **14**(5): p. 1284-1288.
106. Degenstein, J.C., et al., *Fast Pyrolysis of 13C-Labeled Cellobioses: Gaining Insights into the Mechanisms of Fast Pyrolysis of Carbohydrates.* The Journal of Organic Chemistry, 2015. **80**(3): p. 1909-1914.
107. Sarotti, A.M., *Theoretical insight into the pyrolytic deformylation of levoglucosenone and isolevoglucosenone.* Carbohydrate Research, 2014. **390**: p. 76-80.
108. Shafizadeh, F., et al., *Acid-catalyzed pyrolytic synthesis and decomposition of 1,4:3,6-dianhydro-α-D-glucopyranose.* Carbohydrate Research, 1978. **60**(2): p. 519-528.
109. Shafizadeh, F. and T.T. Stevenson, *Saccharification of douglas-fir wood by a combination of prehydrolysis and pyrolysis.* Journal of Applied Polymer Science, 1982. **27**(12): p. 4577-4585.
110. Kawamoto, H., M. Murayama, and S. Saka, *Pyrolysis behavior of levoglucosan as an intermediate in cellulose pyrolysis: polymerization into polysaccharide as a key reaction to carbonized product formation.* Journal of Wood Science, 2003. **49**(5): p. 469-473.
111. Shafizadeh, F., G.D. McGinnis, and C.W. Philpot, *Thermal degradation of xylan and related model compounds.* Carbohydrate Research, 1972. **25**(1): p. 23-33.
112. Demirbas, A., *Pyrolysis Mechanisms of Biomass Materials.* Energy Sources, Part A: Recovery, Utilization, and Environmental Effects, 2009. **31**(13): p. 1186-1193.
113. Overend, R.P. and E. Chornet, *Biomass, a Growth Opportunity in Green Energy and Value-added Products : Proceedings of the 4th Biomass Conference of the Americas*. 1999: Elsevier Science.
114. Bayerbach, R. and D. Meier, *Characterization of the water-insoluble fraction from fast pyrolysis liquids (pyrolytic lignin). Part IV: Structure elucidation of oligomeric molecules.* Journal of Analytical and Applied Pyrolysis, 2009. **85**(1–2): p. 98-107.
115. Scholze, B., C. Hanser, and D. Meier, *Characterization of the water-insoluble fraction from fast pyrolysis liquids (pyrolytic lignin): Part II. GPC, carbonyl goups, and 13C-NMR.* Journal of Analytical and Applied Pyrolysis, 2001. **58–59**(0): p. 387-400.
116. Garcia-Perez, M., et al., *Fast Pyrolysis of Oil Mallee Woody Biomass: Effect of Temperature on the Yield and Quality of Pyrolysis Products.* Industrial & Engineering Chemistry Research, 2008. **47**(6): p. 1846-1854.
117. van der Hage, E.R.E., M.M. Mulder, and J.J. Boon, *Structural characterization of lignin polymers by temperature-resolved in-source pyrolysis—mass spectrometry and Curie-*

point pyrolysis—gas chromatography/mass spectrometry. Journal of Analytical and Applied Pyrolysis, 1993. **25**(0): p. 149-183.
118. Hempfling, R. and H.R. Schulten, *Chemical characterization of the organic matter in forest soils by Curie point pyrolysis-GC/MS and pyrolysis-field ionization mass spectrometry.* Organic Geochemistry, 1990. **15**(2): p. 131-145.
119. Patwardhan, P.R., R.C. Brown, and B.H. Shanks, *Understanding the Fast Pyrolysis of Lignin.* ChemSusChem, 2011. **4**(11): p. 1629-1636.
120. Mullen, C.A. and A.A. Boateng, *Characterization of water insoluble solids isolated from various biomass fast pyrolysis oils.* Journal of Analytical and Applied Pyrolysis, 2011. **90**(2): p. 197-203.
121. Evans, R.J., T.A. Milne, and M.N. Soltys, *Direct mass-spectrometric studies of the pyrolysis of carbonaceous fuels: III. Primary pyrolysis of lignin.* Journal of Analytical and Applied Pyrolysis, 1986. **9**(3): p. 207-236.
122. Bai, X., et al., *Formation of phenolic oligomers during fast pyrolysis of lignin.* Fuel, 2014. **128**: p. 170-179.
123. Custodis, V.B.F., et al., *Mechanism of Fast Pyrolysis of Lignin: Studying Model Compounds.* The Journal of Physical Chemistry B, 2014. **118**(29): p. 8524-8531.
124. Zhou, S., *Understanding lignin pyrolysis reactions on the formation of mono-phenols and pyrolytic lignin from lignocellulosic materials*, in *Department of Biological Systems Engineering*. 2013, Washington State University.
125. Ralph, J. and R.D. Hatfield, *Pyrolysis-GC-MS characterization of forage materials.* Journal of Agricultural and Food Chemistry, 1991. **39**(8): p. 1426-1437.
126. Genuit, W., J.J. Boon, and O. Faix, *Characterization of beech milled wood lignin by pyrolysis-gas chromatography-photoionization mass spectrometry.* Analytical Chemistry, 1987. **59**(3): p. 508-513.
127. Klein, M.T., *Model pathways in lignin thermolysis*, in *Department of Chemical Engineering*. 1981, Massachusetts Institute of Technology.
128. Schlosberg, R.H., et al., *Pyrolysis studies of organic oxygenates: 3. High temperature rearrangement of aryl alkyl ethers.* Fuel, 1983. **62**(6): p. 690-694.
129. Asmadi, M., H. Kawamoto, and S. Saka, *Thermal reactions of guaiacol and syringol as lignin model aromatic nuclei.* Journal of Analytical and Applied Pyrolysis, 2011. **92**(1): p. 88-98.
130. Kotake, T., H. Kawamoto, and S. Saka, *Pyrolysis reactions of coniferyl alcohol as a model of the primary structure formed during lignin pyrolysis.* Journal of Analytical and Applied Pyrolysis, 2013. **104**(0): p. 573-584.
131. Gilbert, K.E. and J.J. Gajewski, *Coal liquefaction model studies: free radical chain decomposition of diphenylpropane, dibenzyl ether, and phenethyl phenyl ether via .beta.-scission reactions.* The Journal of Organic Chemistry, 1982. **47**(25): p. 4899-4902.
132. Simmons, M.B. and M.T. Klein, *Free-radical and concerted reaction pathways in dibenzyl ether thermolysis.* Industrial & Engineering Chemistry Fundamentals, 1985. **24**(1): p. 55-60.
133. Brežný, R., V. Mihalov, and V. Kováčik, *Low Temperature Thermolysis of Lignins - I. Reactions of ß—O—4 Model Compounds*, in *Holzforschung - International Journal of the Biology, Chemistry, Physics and Technology of Wood*. 1983. p. 199.
134. Kawamoto, H., M. Ryoritani, and S. Saka, *Different pyrolytic cleavage mechanisms of β-ether bond depending on the side-chain structure of lignin dimers.* Journal of Analytical and Applied Pyrolysis, 2008. **81**(1): p. 88-94.
135. Britt, P.F., et al., *Flash Vacuum Pyrolysis of Methoxy-Substituted Lignin Model Compounds.* The Journal of Organic Chemistry, 2000. **65**(5): p. 1376-1389.

136. Beste, A. and A.C. Buchanan, *Kinetic Analysis of the Phenyl-Shift Reaction in β-O-4 Lignin Model Compounds: A Computational Study.* The Journal of Organic Chemistry, 2011. **76**(7): p. 2195-2203.
137. Beste, A. and A.C. Buchanan Iii, *Substituent effects on the reaction rates of hydrogen abstraction in the pyrolysis of phenethyl phenyl ethers.* Energy & Fuels, 2010. **24**(5): p. 2857-2867.
138. Beste, A. and A.C. Buchanan, *Computational Study of Bond Dissociation Enthalpies for Lignin Model Compounds. Substituent Effects in Phenethyl Phenyl Ethers.* The Journal of Organic Chemistry, 2009. **74**(7): p. 2837-2841.
139. Chu, S., A.V. Subrahmanyam, and G.W. Huber, *The pyrolysis chemistry of a [small beta]-O-4 type oligomeric lignin model compound.* Green Chemistry, 2013. **15**(1): p. 125-136.
140. McKendry, P., *Energy production from biomass (part 1): overview of biomass.* Bioresource Technology, 2002. **83**(1): p. 37-46.
141. Raveendran, K., A. Ganesh, and K.C. Khilar, *Pyrolysis characteristics of biomass and biomass components.* Fuel, 1996. **75**(8): p. 987-998.
142. Orfão, J.J.M., F.J.A. Antunes, and J.L. Figueiredo, *Pyrolysis kinetics of lignocellulosic materials—three independent reactions model.* Fuel, 1999. **78**(3): p. 349-358.
143. Rao, T.R. and A. Sharma, *Pyrolysis rates of biomass materials.* Energy, 1998. **23**(11): p. 973-978.
144. Manyà, J.J., E. Velo, and L. Puigjaner, *Kinetics of Biomass Pyrolysis: a Reformulated Three-Parallel-Reactions Model.* Industrial & Engineering Chemistry Research, 2003. **42**(3): p. 434-441.
145. Yang, H., et al., *In-Depth Investigation of Biomass Pyrolysis Based on Three Major Components: Hemicellulose, Cellulose and Lignin.* Energy & Fuels, 2006. **20**(1): p. 388-393.
146. Wang, G., et al., *TG study on pyrolysis of biomass and its three components under syngas.* Fuel, 2008. **87**(4–5): p. 552-558.
147. Qu, T., et al., *Experimental Study of Biomass Pyrolysis Based on Three Major Components: Hemicellulose, Cellulose, and Lignin.* Industrial & Engineering Chemistry Research, 2011. **50**(18): p. 10424-10433.
148. Hosoya, T., H. Kawamoto, and S. Saka, *Cellulose–hemicellulose and cellulose–lignin interactions in wood pyrolysis at gasification temperature.* Journal of Analytical and Applied Pyrolysis, 2007. **80**(1): p. 118-125.
149. Hosoya, T., H. Kawamoto, and S. Saka, *Solid/liquid- and vapor-phase interactions between cellulose- and lignin-derived pyrolysis products.* Journal of Analytical and Applied Pyrolysis, 2009. **85**(1–2): p. 237-246.
150. Fushimi, C., S. Katayama, and A. Tsutsumi, *Elucidation of interaction among cellulose, lignin and xylan during tar and gas evolution in steam gasification.* Journal of Analytical and Applied Pyrolysis, 2009. **86**(1): p. 82-89.
151. Wang, S., et al., *Influence of the interaction of components on the pyrolysis behavior of biomass.* Journal of Analytical and Applied Pyrolysis, 2011. **91**(1): p. 183-189.
152. Schrödinger, E., *Quantisierung als Eigenwertproblem.* Annalen der Physik, 1926. **385**(13): p. 437-490.
153. Schrödinger, E., *An Undulatory Theory of the Mechanics of Atoms and Molecules.* Physical Review, 1926. **28**(6): p. 1049-1070.
154. Born, M. and R. Oppenheimer, *Zur Quantentheorie der Molekeln.* Annalen der Physik, 1927. **389**(20): p. 457-484.
155. Ostlund, N.S. and A. Szabo, *Modern Quantum Chemistry: Introduction to Advanced Electronic Structure Theory*. 1996: Dover Publications Inc.

156. Pauli, W., *Exclusion Principle and Quantum Mechanics*, in *Writings on Physics and Philosophy*, C.P. Enz and K. von Meyenn, Editors. 1994, Springer Berlin Heidelberg: Berlin, Heidelberg. p. 165-181.
157. Slater, J.C., *The Theory of Complex Spectra.* Physical Review, 1929. **34**(10): p. 1293-1322.
158. Hartree, D.R., *The Wave Mechanics of an Atom with a Non-Coulomb Central Field. Part I. Theory and Methods.* Mathematical Proceedings of the Cambridge Philosophical Society, 1928. **24**(01): p. 89-110.
159. Orlando, R., et al., *Ab initio Hartree-Fock calculations for periodic compounds: application to semiconductors.* Journal of Physics: Condensed Matter, 1990. **2**(38): p. 7769.
160. Fukutome, H., *Unrestricted Hartree–Fock theory and its applications to molecules and chemical reactions.* International Journal of Quantum Chemistry, 1981. **20**(5): p. 955-1065.
161. Sure, R. and S. Grimme, *Corrected small basis set Hartree-Fock method for large systems.* Journal of Computational Chemistry, 2013. **34**(19): p. 1672-1685.
162. Nakata, H., et al., *Derivatives of the approximated electrostatic potentials in unrestricted Hartree–Fock based on the fragment molecular orbital method and an application to polymer radicals.* Theoretical Chemistry Accounts, 2014. **133**(5): p. 1477.
163. Møller, C. and M.S. Plesset, *Note on an Approximation Treatment for Many-Electron Systems.* Physical Review, 1934. **46**(7): p. 618-622.
164. Curtiss, L.A., et al., *Gaussian-3X (G3X) theory: Use of improved geometries, zero-point energies, and Hartree–Fock basis sets.* The Journal of Chemical Physics, 2001. **114**(1): p. 108-117.
165. Leininger, M.L., et al., *Is Mo/ller–Plesset perturbation theory a convergent ab initio method?* The Journal of Chemical Physics, 2000. **112**(21): p. 9213-9222.
166. Cizek, J., *J. chem. Phys., 45, 4256; Ciz ek, J., 1969.* Adv. Chem. Phys, 1966. **14**: p. 35.
167. Bartlett, R.J. and M. Musiał, *Coupled-cluster theory in quantum chemistry.* Reviews of Modern Physics, 2007. **79**(1): p. 291-352.
168. Helgaker, T., P. Jorgensen, and J. Olsen, *Molecular electronic-structure theory*. 2014: John Wiley & Sons.
169. Evangelista, F.A., W.D. Allen, and H.F. Schaefer, *High-order excitations in state-universal and state-specific multireference coupled cluster theories: Model systems.* The Journal of Chemical Physics, 2006. **125**(15): p. 154113.
170. Watts, J.D., J. Gauss, and R.J. Bartlett, *Coupled‐cluster methods with noniterative triple excitations for restricted open‐shell Hartree–Fock and other general single determinant reference functions. Energies and analytical gradients.* The Journal of Chemical Physics, 1993. **98**(11): p. 8718-8733.
171. Boys, S.F., *Electronic Wave Functions. I. A General Method of Calculation for the Stationary States of Any Molecular System.* Proceedings of the Royal Society of London A: Mathematical, Physical and Engineering Sciences, 1950. **200**(1063): p. 542-554.
172. Woon, D.E. and T.H. Dunning, *Gaussian basis sets for use in correlated molecular calculations. V. Core‐valence basis sets for boron through neon.* The Journal of Chemical Physics, 1995. **103**(11): p. 4572-4585.
173. Woon, D.E. and T.H. Dunning, *Benchmark calculations with correlated molecular wave functions. I. Multireference configuration interaction calculations for the second row diatomic hydrides.* The Journal of Chemical Physics, 1993. **99**(3): p. 1914-1929.
174. Dunning, T.H., *A Road Map for the Calculation of Molecular Binding Energies.* The Journal of Physical Chemistry A, 2000. **104**(40): p. 9062-9080.

175. Van, F. and J.V. Duijneveldt, *de Rijdt and JH Van Lenthe.* Chem. Rev, 1994. **94**: p. 1873-1885.
176. Boys, S.F. and F. Bernardi, *The calculation of small molecular interactions by the differences of separate total energies. Some procedures with reduced errors.* Molecular Physics, 1970. **19**(4): p. 553-566.
177. Feller, D., *The use of systematic sequences of wave functions for estimating the complete basis set, full configuration interaction limit in water.* The Journal of Chemical Physics, 1993. **98**(9): p. 7059-7071.
178. Peterson, K.A., D.E. Woon, and T.H. Dunning, *Benchmark calculations with correlated molecular wave functions. IV. The classical barrier height of the H+H2→H2+H reaction.* The Journal of Chemical Physics, 1994. **100**(10): p. 7410-7415.
179. Wilson, A.K. and J. Dunning, Thom H., *Benchmark calculations with correlated molecular wave functions. X. Comparison with "exact" MP2 calculations on Ne, HF, H2O, and N2.* The Journal of Chemical Physics, 1997. **106**(21): p. 8718-8726.
180. Klopper, W., et al., *Multiple basis sets in calculations of triples corrections in coupled-cluster theory.* Theoretical Chemistry Accounts, 1997. **97**(1): p. 164-176.
181. Halkier, A., et al., *Basis-set convergence of the energy in molecular Hartree–Fock calculations.* Chemical Physics Letters, 1999. **302**(5–6): p. 437-446.
182. Hill, R.N., *Rates of convergence and error estimation formulas for the Rayleigh–Ritz variational method.* The Journal of Chemical Physics, 1985. **83**(3): p. 1173-1196.
183. Helgaker, T., et al., *Basis-set convergence of correlated calculations on water.* The Journal of Chemical Physics, 1997. **106**(23): p. 9639-9646.
184. Klopper, W.I.M., *Highly accurate coupled-cluster singlet and triplet pair energies from explicitly correlated calculations in comparison with extrapolation techniques.* Molecular Physics, 2001. **99**(6): p. 481-507.
185. Schwenke, D.W., *The extrapolation of one-electron basis sets in electronic structure calculations: How it should work and how it can be made to work.* The Journal of Chemical Physics, 2005. **122**(1): p. 014107.
186. Martin, J.M.L., *Ab initio total atomization energies of small molecules — towards the basis set limit.* Chemical Physics Letters, 1996. **259**(5–6): p. 669-678.
187. Martin, J.M.L. and G. de Oliveira, *Towards standard methods for benchmark quality ab initio thermochemistry—W1 and W2 theory.* The Journal of Chemical Physics, 1999. **111**(5): p. 1843-1856.
188. Pyykko, P., *Relativistic effects in structural chemistry.* Chemical Reviews, 1988. **88**(3): p. 563-594.
189. Ermler, W.C., R.B. Ross, and P.A. Christiansen, *Spin-Orbit Coupling and.* Advances in quantum chemistry, 1988. **19**: p. 139.
190. Grant, I.P. and H.M. Quiney, *Foundations of the relativistic theory of atomic and molecular structure.* Advances in atomic and molecular physics, 1988. **23**: p. 37.
191. Balasubramanian, K., *Relativity and chemical bonding.* The Journal of Physical Chemistry, 1989. **93**(18): p. 6585-6596.
192. Dirac, P.A. *Quantum mechanics of many-electron systems*. in *Proceedings of the Royal Society of London A: Mathematical, Physical and Engineering Sciences*. 1929. The Royal Society.
193. Nakajima, T. and K. Hirao, *A new relativistic theory: a relativistic scheme by eliminating small components (RESC).* Chemical Physics Letters, 1999. **302**(5–6): p. 383-391.
194. Lenthe, E.v., E.J. Baerends, and J.G. Snijders, *Relativistic regular two‐component Hamiltonians.* The Journal of Chemical Physics, 1993. **99**(6): p. 4597-4610.

195. Csonka, G.I., A. Ruzsinszky, and J.P. Perdew, *Estimation, Computation, and Experimental Correction of Molecular Zero-Point Vibrational Energies.* The Journal of Physical Chemistry A, 2005. **109**(30): p. 6779-6789.
196. Grev, R.S., C.L. Janssen, and H.F. Schaefer, *Concerning zero‐point vibrational energy corrections to electronic energies.* The Journal of Chemical Physics, 1991. **95**(7): p. 5128-5132.
197. Karton, A., D. Gruzman, and J.M.L. Martin, *Benchmark Thermochemistry of the CnH2n+2 Alkane Isomers (n = 2−8) and Performance of DFT and Composite Ab Initio Methods for Dispersion-Driven Isomeric Equilibria.* The Journal of Physical Chemistry A, 2009. **113**(29): p. 8434-8447.
198. Pople, J.A., et al., *Gaussian‐1 theory: A general procedure for prediction of molecular energies.* The Journal of Chemical Physics, 1989. **90**(10): p. 5622-5629.
199. Curtiss, L.A., et al., *Gaussian‐1 theory of molecular energies for second‐row compounds.* The Journal of Chemical Physics, 1990. **93**(4): p. 2537-2545.
200. Curtiss, L.A., et al., *Gaussian‐2 theory for molecular energies of first‐and second‐row compounds.* The Journal of Chemical Physics, 1991. **94**(11): p. 7221-7230.
201. Curtiss, L.A., K. Raghavachari, and J.A. Pople, *Gaussian‐2 theory using reduced Mo/ller–Plesset orders.* The Journal of Chemical Physics, 1993. **98**(2): p. 1293-1298.
202. Curtiss, L.A., et al., *Gaussian-3 (G3) theory for molecules containing first and second-row atoms.* The Journal of Chemical Physics, 1998. **109**(18): p. 7764-7776.
203. Curtiss, L.A., et al., *Gaussian-3 theory using reduced Mo/ller-Plesset order.* The Journal of Chemical Physics, 1999. **110**(10): p. 4703-4709.
204. Curtiss, L.A., P.C. Redfern, and K. Raghavachari, *Gaussian-4 theory.* The Journal of Chemical Physics, 2007. **126**(8): p. 084108.
205. Curtiss, L.A., P.C. Redfern, and K. Raghavachari, *Gaussian-4 theory using reduced order perturbation theory.* The Journal of Chemical Physics, 2007. **127**(12): p. 124105.
206. Curtiss, L.A., P.C. Redfern, and K. Raghavachari, *Gn theory.* Wiley Interdisciplinary Reviews: Computational Molecular Science, 2011. **1**(5): p. 810-825.
207. Boese, A.D., et al., *W3 theory: Robust computational thermochemistry in the kJ/mol accuracy range.* The Journal of Chemical Physics, 2004. **120**(9): p. 4129-4141.
208. Karton, A., et al., *W4 theory for computational thermochemistry: In pursuit of confident sub-kJ/mol predictions.* The Journal of Chemical Physics, 2006. **125**(14): p. 144108.
209. Curtiss, L.A., P.C. Redfern, and K. Raghavachari, *Assessment of Gaussian-4 theory for energy barriers.* Chemical Physics Letters, 2010. **499**(1–3): p. 168-172.
210. Karton, A., *A computational chemist's guide to accurate thermochemistry for organic molecules.* Wiley Interdisciplinary Reviews: Computational Molecular Science, 2016. **6**(3): p. 292-310.
211. Karton, A., P.R. Taylor, and J.M.L. Martin, *Basis set convergence of post-CCSD contributions to molecular atomization energies.* The Journal of Chemical Physics, 2007. **127**(6): p. 064104.
212. Karton, A. and J.M.L. Martin, *Explicitly correlated Wn theory: W1-F12 and W2-F12.* The Journal of Chemical Physics, 2012. **136**(12): p. 124114.
213. Friedman, H.L., *Kinetics of thermal degradation of char-forming plastics from thermogravimetry. Application to a phenolic plastic.* Journal of Polymer Science Part C: Polymer Symposia, 1964. **6**(1): p. 183-195.
214. Wu, W., J. Cai, and R. Liu, *Isoconversional Kinetic Analysis of Distributed Activation Energy Model Processes for Pyrolysis of Solid Fuels.* Industrial & Engineering Chemistry Research, 2013. **52**(40): p. 14376-14383.

215. Liu, P., et al., *Thermogravimetric Studies of Characteristics and Kinetics of Pyrolysis of Buton Oil Sand.* Energy Procedia, 2014. **61**: p. 2741-2744.
216. Liu, P., et al., *Pyrolysis of an Indonesian oil sand in a thermogravimetric analyser and a fixed-bed reactor.* Journal of Analytical and Applied Pyrolysis, 2016. **117**(Supplement C): p. 191-198.
217. Demirbas, A., *Effects of temperature and particle size on bio-char yield from pyrolysis of agricultural residues.* Journal of Analytical and Applied Pyrolysis, 2004. **72**(2): p. 243-248.
218. Garcia-Perez, M., et al., *Effects of Temperature on the Formation of Lignin-Derived Oligomers during the Fast Pyrolysis of Mallee Woody Biomass.* Energy & Fuels, 2008. **22**(3): p. 2022-2032.
219. Rath, J. and G. Staudinger, *Cracking reactions of tar from pyrolysis of spruce wood.* Fuel, 2001. **80**(10): p. 1379-1389.
220. Boroson, M.L., et al., *Product yields and kinetics from the vapor phase cracking of wood pyrolysis tars.* AIChE Journal, 1989. **35**(1): p. 120-128.
221. Solomons, T.W.G. and C.B. Fryhle, *Organic chemistry*. 2008, Hoboken, N.J [etc.]: Wiley.
222. Evans, R.J., T.A. Milne, and M.N. Soltys, *Direct mass-spectrometric studies of the pyrolysis of carbonaceous fuels.* Journal of Analytical and Applied Pyrolysis, 1986. **9**(3): p. 207-236.
223. Bradbury, A.G.W., Y. Sakai, and F. Shafizadeh, *A kinetic model for pyrolysis of cellulose.* Journal of Applied Polymer Science, 1979. **23**(11): p. 3271-3280.
224. Capart, R., L. Khezami, and A.K. Burnham, *Assessment of various kinetic models for the pyrolysis of a microgranular cellulose.* Thermochimica Acta, 2004. **417**(1): p. 79-89.
225. Shen, D.K., S. Gu, and A.V. Bridgwater, *Study on the pyrolytic behaviour of xylan-based hemicellulose using TG–FTIR and Py–GC–FTIR.* Journal of Analytical and Applied Pyrolysis, 2010. **87**(2): p. 199-206.
226. Shen, D.K., S. Gu, and A.V. Bridgwater, *The thermal performance of the polysaccharides extracted from hardwood: Cellulose and hemicellulose.* Carbohydrate Polymers, 2010. **82**(1): p. 39-45.
227. Bridgwater, A.V., D. Meier, and D. Radlein, *An overview of fast pyrolysis of biomass.* Organic Geochemistry, 1999. **30**(12): p. 1479-1493.
228. Bayerbach, R., et al., *Characterization of the water-insoluble fraction from fast pyrolysis liquids (pyrolytic lignin): Part III. Molar mass characteristics by SEC, MALDI-TOF-MS, LDI-TOF-MS, and Py-FIMS.* Journal of Analytical and Applied Pyrolysis, 2006. **77**(2): p. 95-101.
229. Wang, S., et al., *Mechanism research on cellulose pyrolysis by Py-GC/MS and subsequent density functional theory studies.* Bioresource Technology, 2012. **104**(0): p. 722-728.
230. Lowary, T.L. and G.N. Richards, *Mechanisms of pyrolysis of polysaccharides: Cellobiitol as a model for cellulose.* Carbohydrate Research, 1990. **198**(1): p. 79-89.
231. Hurt, M.R., et al., *On-Line Mass Spectrometric Methods for the Determination of the Primary Products of Fast Pyrolysis of Carbohydrates and for Their Gas-Phase Manipulation.* Analytical Chemistry, 2013. **85**(22): p. 10927-10934.
232. Liu, D., Y. Yu, and H. Wu, *Differences in Water-Soluble Intermediates from Slow Pyrolysis of Amorphous and Crystalline Cellulose.* Energy & Fuels, 2013. **27**(3): p. 1371-1380.

233. Scalarone, D., O. Chiantore, and C. Riedo, *Gas chromatographic/mass spectrometric analysis of on-line pyrolysis–silylation products of monosaccharides.* Journal of Analytical and Applied Pyrolysis, 2008. **83**(2): p. 157-164.
234. Fabbri, D., et al., *Gas chromatography/mass spectrometric characterisation of pyrolysis/silylation products of glucose and cellulose.* Rapid Communications in Mass Spectrometry, 2002. **16**(24): p. 2349-2355.
235. Li, K., et al., *Charring shrinkage and cracking of fir during pyrolysis in an inert atmosphere and at different ambient pressures.* Proceedings of the Combustion Institute.
236. Lee, J., et al., *Pyrolysis process of agricultural waste using CO2 for waste management, energy recovery, and biochar fabrication.* Applied Energy, 2017. **185, Part 1**: p. 214-222.
237. Norinaga, K., et al., *Analysis of pyrolysis products from light hydrocarbons and kinetic modeling for growth of polycyclic aromatic hydrocarbons with detailed chemistry.* Journal of Analytical and Applied Pyrolysis, 2009. **86**(1): p. 148-160.
238. Norinaga, K. and O. Deutschmann, *Detailed Kinetic Modeling of Gas-Phase Reactions in the Chemical Vapor Deposition of Carbon from Light Hydrocarbons.* Industrial & Engineering Chemistry Research, 2007. **46**(11): p. 3547-3557.
239. Bai, X., P. Johnston, and R.C. Brown, *An experimental study of the competing processes of evaporation and polymerization of levoglucosan in cellulose pyrolysis.* Journal of Analytical and Applied Pyrolysis, 2013. **99**(0): p. 130-136.
240. Organ, P.P. and J.C. Mackie, *Kinetics of pyrolysis of furan.* Journal of the Chemical Society, Faraday Transactions, 1991. **87**(6): p. 815-823.
241. Simell, P., et al., *Provisional protocol for the sampling and anlaysis of tar and particulates in the gas from large-scale biomass gasifiers. Version 1998.* Biomass and Bioenergy, 2000. **18**(1): p. 19-38.
242. Li, C. and K. Suzuki, *Tar property, analysis, reforming mechanism and model for biomass gasification—An overview.* Renewable and Sustainable Energy Reviews, 2009. **13**(3): p. 594-604.
243. Orita, H. and N. Itoh, *Simulation of phenol formation from benzene with a Pd membrane reactor: ab initio periodic density functional study.* Applied Catalysis A: General, 2004. **258**(1): p. 17-23.
244. Lerf, A., et al., *Structure of graphite oxide revisited‖.* The Journal of Physical Chemistry B, 1998. **102**(23): p. 4477-4482.
245. Dellinger, B., et al., *Formation and stabilization of persistent free radicals.* Proceedings of the Combustion Institute, 2007. **31**(1): p. 521-528.
246. Yu, M.M., et al., *Co-gasification of biosolids with biomass: Thermogravimetric analysis and pilot scale study in a bubbling fluidized bed reactor.* Bioresource Technology, 2015. **175**: p. 51-58.
247. Xue, Y., et al., *Fast pyrolysis of biomass and waste plastic in a fluidized bed reactor.* Fuel, 2015. **156**: p. 40-46.
248. Hosoya, T., H. Kawamoto, and S. Saka, *Different pyrolytic pathways of levoglucosan in vapor- and liquid/solid-phases.* Journal of Analytical and Applied Pyrolysis, 2008. **83**(1): p. 64-70.
249. Boutin, O., M. Ferrer, and J. Lédé, *Radiant flash pyrolysis of cellulose—Evidence for the formation of short life time intermediate liquid species.* Journal of Analytical and Applied Pyrolysis, 1998. **47**(1): p. 13-31.
250. Mettler, M.S., et al., *Revealing pyrolysis chemistry for biofuels production: Conversion of cellulose to furans and small oxygenates.* Energy & Environmental Science, 2012. **5**(1): p. 5414-5424.

251. Hehre, W.J., *Ab initio molecular orbital theory.* Accounts of Chemical Research, 1976. **9**(11): p. 399-406.
252. Koch, W. and M.C. Holthausen, *A Chemist's Guide to Density Functional Theory*. 2001: Wiley-VCH Verlag GmbH.
253. Frisch, M.J., et al., *Gaussian 09*. 2009, Gaussian, Inc.: Wallingford, CT, USA.
254. Gonzalez, C. and H.B. Schlegel, *An improved algorithm for reaction path following.* The Journal of Chemical Physics, 1989. **90**(4): p. 2154-2161.
255. Gonzalez, C. and H.B. Schlegel, *Reaction path following in mass-weighted internal coordinates.* The Journal of Physical Chemistry, 1990. **94**(14): p. 5523-5527.
256. Karton, A., *A computational chemist's guide to accurate thermochemistry for organic molecules.* Wiley Interdisciplinary Reviews: Computational Molecular Science, 2016.
257. Curtiss, L.A., P.C. Redfern, and K. Raghavachari, *Assessment of Gaussian-3 and density-functional theories on the G3/05 test set of experimental energies.* The Journal of Chemical Physics, 2005. **123**(12): p. 124107.
258. Karton, A., R.J. O'Reilly, and L. Radom, *Assessment of Theoretical Procedures for Calculating Barrier Heights for a Diverse Set of Water-Catalyzed Proton-Transfer Reactions.* The Journal of Physical Chemistry A, 2012. **116**(16): p. 4211-4221.
259. Karton, A. and L. Goerigk, *Accurate reaction barrier heights of pericyclic reactions: Surprisingly large deviations for the CBS-QB3 composite method and their consequences in DFT benchmark studies.* Journal of Computational Chemistry, 2015. **36**(9): p. 622-632.
260. Yu, L.-J., et al., *Reaction barrier heights for cycloreversion of heterocyclic rings: An Achilles' heel for DFT and standard ab initio procedures.* Chemical Physics, 2015. **458**: p. 1-8.
261. Karton, A., *Inorganic acid-catalyzed tautomerization of vinyl alcohol to acetaldehyde.* Chemical Physics Letters, 2014. **592**: p. 330-333.
262. da Silva, G., *Carboxylic Acid Catalyzed Keto-Enol Tautomerizations in the Gas Phase.* Angewandte Chemie International Edition, 2010. **49**(41): p. 7523-7525.
263. Assary, R.S., et al., *Mechanistic Insights into the Decomposition of Fructose to Hydroxy Methyl Furfural in Neutral and Acidic Environments Using High-Level Quantum Chemical Methods.* The Journal of Physical Chemistry B, 2011. **115**(15): p. 4341-4349.
264. Karton, A., et al., *Determination of Barrier Heights for Proton Exchange in Small Water, Ammonia, and Hydrogen Fluoride Clusters with G4(MP2)-Type, MPn, and SCS-MPn Procedures—A Caveat.* Journal of Chemical Theory and Computation, 2012. **8**(9): p. 3128-3136.
265. Vereecken, L. and J.S. Francisco, *Theoretical studies of atmospheric reaction mechanisms in the troposphere.* Chemical Society Reviews, 2012. **41**(19): p. 6259-6293.
266. Vöhringer-Martinez, E., et al., *Water Catalysis of a Radical-Molecule Gas-Phase Reaction.* Science, 2007. **315**(5811): p. 497-501.
267. Minkova, V., et al., *Effect of water vapour and biomass nature on the yield and quality of the pyrolysis products from biomass.* Fuel Processing Technology, 2001. **70**(1): p. 53-61.
268. Minkova, V., et al., *Effect of water vapour on the pyrolysis of solid fuels: 1. Effect of water vapour during the pyrolysis of solid fuels on the yield and composition of the liquid products.* Fuel, 1991. **70**(6): p. 713-719.
269. Plazinski, W., A. Plazinska, and M. Drach, *The water-catalyzed mechanism of the ring-opening reaction of glucose.* Physical Chemistry Chemical Physics, 2015. **17**(33): p. 21622-21629.

270. Assary, R.S. and L.A. Curtiss, *Comparison of Sugar Molecule Decomposition through Glucose and Fructose: A High-Level Quantum Chemical Study.* Energy & Fuels, 2012. **26**(2): p. 1344-1352.
271. Kroto, H.W., et al., *C 60: buckminsterfullerene.* Nature, 1985. **318**(6042): p. 162-163.
272. Andreas Hirsch, M.B., *Fullerenes: Chemistry and Reaction*. 2005, New York: Wiley-VCH.
273. Schwerdtfeger, P., L.N. Wirz, and J. Avery, *The topology of fullerenes.* Wiley Interdisciplinary Reviews: Computational Molecular Science, 2015. **5**(1): p. 96-145.
274. Kiyobayashi, T. and M. Sakiyama, *Combustion Calorimetric Studies on C60 and C70.* Fullerene Science and Technology, 1993. **1**(3): p. 269-273.
275. V. Diky, V. and G. J. Kabo, *Thermodynamic properties of C60 and C70 fullerenes.* Russian Chemical Reviews, 2000. **69**(2): p. 95-104.
276. Steele, W., et al., *Standard enthalpy of formation of buckminsterfullerene.* The Journal of Physical Chemistry, 1992. **96**(12): p. 4731-4733.
277. Beckhaus, H.D., et al., *The Stability of Buckminsterfullerene (C60): Experimental determination of the heat of formation.* Angewandte Chemie International Edition in English, 1992. **31**(1): p. 63-64.
278. Diogo, H.P., et al., *Enthalpies of formation of buckminsterfullerene (C60) and of the parent ions C60+, C602+, C603+ and C60.* Journal of the Chemical Society, Faraday Transactions, 1993. **89**(19): p. 3541-3544.
279. Beckhaus, H.D., et al., *C70 is more stable than C60: experimental determination of the heat of formation of C70.* Angewandte Chemie International Edition in English, 1994. **33**(9): p. 996-998.
280. Kolesov, V.P., et al., *Enthalpies of combustion and formation of fullerene C60.* The Journal of Chemical Thermodynamics, 1996. **28**(10): p. 1121-1125.
281. Xu-wu, A., H. Jun, and B. Zheng, *Standard molar enthalpies of combustion and formation of C60.* The Journal of Chemical Thermodynamics, 1996. **28**(10): p. 1115-1119.
282. An, X., B. Chen, and J. He, *Determinations of combustion and formation enthalpies of C60 and C70.* Science in China Series B: Chemistry, 1998. **41**(5): p. 543-548.
283. Rojas-Aguilar, A., *An isoperibol micro-bomb combustion calorimeter for measurement of the enthalpy of combustion. Application to the study of fullerene C60.* The Journal of Chemical Thermodynamics, 2002. **34**(10): p. 1729-1743.
284. Rojas-Aguilar, A. and M. Mart ńez-Herrera, *Enthalpies of combustion and formation of fullerenes by micro-combustion calorimetry in a Calvet calorimeter.* Thermochimica Acta, 2005. **437**(1–2): p. 126-133.
285. Diogo, H. and M. Minas da Piedade, *Enthalpies of Formation of C60 and C70 in the Crystalline State.* Recent Adv. Chem. Phys. Full. Relat. Mater, 1998. **6**: p. 627.
286. Biglova, Y.N., et al., *Review of fullerene organic chemistry.* Oxidation Communications, 2005. **28**(4): p. 753-798.
287. Afeefy, H., J. Liebman, and S. Stein, *Neutral thermochemical data.* NIST chemistry webbook, NIST standard reference database, 2005. **69**.
288. Karton, A., et al., *Evaluation of the Heats of Formation of Corannulene and C60 by Means of High-Level Theoretical Procedures.* The Journal of Physical Chemistry A, 2013. **117**(8): p. 1834-1842.
289. Dobek, F.J., et al., *Evaluation of the Heats of Formation of Corannulene and C60 by Means of Inexpensive Theoretical Procedures.* The Journal of Physical Chemistry A, 2013. **117**(22): p. 4726-4730.

290. Kozuch, S. and J.M.L. Martin, *DSD-PBEP86: in search of the best double-hybrid DFT with spin-component scaled MP2 and dispersion corrections.* Physical Chemistry Chemical Physics, 2011. **13**(45): p. 20104-20107.
291. Martin, J.M.L. and G.d. Oliveira, *Towards standard methods for benchmark quality ab initio thermochemistry—W1 and W2 theory.* The Journal of Chemical Physics, 1999. **111**(5): p. 1843-1856.
292. Martin, J.M.L. and S. Parthiban, *W1 and W2 Theories, and Their Variants: Thermochemistry in the kJ/mol Accuracy Range*, in *Quantum-Mechanical Prediction of Thermochemical Data*, J. Cioslowski, Editor. 2001, Springer Netherlands: Dordrecht. p. 31-65.
293. Jr., J.A.M., et al., *A complete basis set model chemistry. VII. Use of the minimum population localization method.* The Journal of Chemical Physics, 2000. **112**(15): p. 6532-6542.
294. Austin, A., et al., *A density functional with spherical atom dispersion terms.* Journal of chemical theory and computation, 2012. **8**(12): p. 4989-5007.
295. Sun, C.H., et al., *Effects of resonance energy and nonplanar strain energy on the reliability of hyperhomodesmotic reactions for corannulene.* Chemical Physics Letters, 2007. **434**(1–3): p. 160-164.
296. Cioslowski, J., N. Rao, and D. Moncrieff, *Standard enthalpies of formation of fullerenes and their dependence on structural motifs.* Journal of the American Chemical Society, 2000. **122**(34): p. 8265-8270.
297. Yu, J., R. Sumathi, and W.H. Green, *Accurate and Efficient Method for Predicting Thermochemistry of Polycyclic Aromatic Hydrocarbons− Bond-Centered Group Additivity.* Journal of the American Chemical Society, 2004. **126**(39): p. 12685-12700.
298. Ramabhadran, R.O. and K. Raghavachari, *Theoretical Thermochemistry for Organic Molecules: Development of the Generalized Connectivity-Based Hierarchy.* Journal of Chemical Theory and Computation, 2011. **7**(7): p. 2094-2103.
299. Ramabhadran, R.O. and K. Raghavachari, *Connectivity-Based Hierarchy for Theoretical Thermochemistry: Assessment Using Wave Function-Based Methods.* The Journal of Physical Chemistry A, 2012. **116**(28): p. 7531-7537.
300. Werner, H., et al., *MOLPRO, version 2012.1, a package of ab initio programs, 2012, see http://www. molpro. net.* Search PubMed, 2015.
301. Werner, H.J., et al., *Molpro: a general‐purpose quantum chemistry program package.* Wiley Interdisciplinary Reviews: Computational Molecular Science, 2012. **2**(2): p. 242-253.
302. Karton, A., S. Daon, and J.M.L. Martin, *W4-11: A high-confidence benchmark dataset for computational thermochemistry derived from first-principles W4 data.* Chemical Physics Letters, 2011. **510**(4–6): p. 165-178.
303. Wheeler, S.E., et al., *A hierarchy of homodesmotic reactions for thermochemistry.* Journal of the American Chemical Society, 2009. **131**(7): p. 2547-2560.
304. Wodrich, M.D., C.m. Corminboeuf, and S.E. Wheeler, *Accurate thermochemistry of hydrocarbon radicals via an extended generalized bond separation reaction scheme.* The Journal of Physical Chemistry A, 2012. **116**(13): p. 3436-3447.
305. Wheeler, S.E., *Homodesmotic reactions for thermochemistry.* Wiley Interdisciplinary Reviews: Computational Molecular Science, 2012. **2**(2): p. 204-220.
306. Karton, A., D. Gruzman, and J.M. Martin, *Benchmark Thermochemistry of the CnH2n+2 Alkane Isomers (n= 2− 8) and Performance of DFT and Composite Ab Initio Methods for Dispersion-Driven Isomeric Equilibria.* J. Phys. Chem. A, 2009. **113**(29): p. 8434-8447.

307. Karton, A., et al., *W4 theory for computational thermochemistry: In pursuit of confident sub-kJ/mol predictions.* The Journal of chemical physics, 2006. **125**(14): p. 144108.
308. Karton, A. and J.M. Martin, *Performance of W4 theory for spectroscopic constants and electrical properties of small molecules.* The Journal of chemical physics, 2010. **133**(14): p. 144102.
309. Ruscic, B., et al., *Introduction to active thermochemical tables: Several "key" enthalpies of formation revisited.* The Journal of Physical Chemistry A, 2004. **108**(45): p. 9979-9997.
310. Ruscic, B., et al. *Active Thermochemical Tables: thermochemistry for the 21st century*. in *Journal of Physics: Conference Series*. 2005. IOP Publishing.
311. Ruscic, B., *Updated Active Thermochemical Tables (ATcT) Values Based on ver. 1.110 of the Thermochemical Network (2012).* available at ATcT. anl. gov, 2014.
312. Roux, M.V., et al., *Critically evaluated thermochemical properties of polycyclic aromatic hydrocarbons.* Journal of Physical and Chemical Reference Data, 2008. **37**(4): p. 1855-1996.
313. Karton, A., et al., *Highly Accurate First-Principles Benchmark Data Sets for the Parametrization and Validation of Density Functional and Other Approximate Methods. Derivation of a Robust, Generally Applicable, Double-Hybrid Functional for Thermochemistry and Thermochemical Kinetics.* The Journal of Physical Chemistry A, 2008. **112**(50): p. 12868-12886.

Appendix A Supporting Information

A1. Mechanistic insights into water-catalysed formation of levoglucosenone from anhydrosugar intermediates by means of high-level theoretical procedures

Table S1. Reaction profile (G4(MP2), kcal•mol^{-1}) on the electronic (ΔE_e), enthalpic (ΔH_{298}) and Gibbs-free energy (ΔG_{298}) surfaces for the uncatalysed and water-catalysed conversion of DGP to levoglucosenone.

Structure	ΔE_e	ZPVE[a]	$H_{298}-H_0$[b]	T×ΔS[c]	ΔH_{298}	ΔG_{298}
DGP	0.0	0.0	0.0	0.0	0.0	0.0
TS1	48.9	-0.1	-0.8	-10.2	48.0	58.1
INT1	-12.7	3.5	-0.9	-10.2	0.0	0.0
TS2	36.5	-1.1	-0.7	-9.6	34.8	44.4
STS2	26.8	-1.3	-1.5	-11.6	24.0	35.5
WTS2	17.6	1.1	-2.0	-20.3	16.7	37.0
INT2	-5.6	2.1	-0.3	-8.6	4.8	4.8
TS3	54.0	-1.7	-0.5	-9.6	51.8	61.4
WTS3	38.2	0.4	-1.8	-20.6	37.7	57.3
INT3	2.9	0.7	0.5	-6.9	11.1	11.1
TS4	64.6	-3.5	0.4	-7.0	61.6	68.6
WTS4	37.8	-1.3	-0.8	-17.8	35.7	53.5
INT4	-5.8	0.9	0.3	-7.3	2.7	2.7
TS5	57.6	-2.9	0.3	-7.2	54.9	62.1
WTS5	37.8	-0.9	-1.0	-18.2	49.0	54.1
INT5	11.1	-4.1	2.2	5.4	3.8	3.8
TS6	47.6	-6.5	1.4	3.8	42.5	38.8
WTS6	24.5	-3.8	-0.1	-7.9	20.7	28.6
INT6	-3.5	-2.1	1.3	3.2	-4.3	-7.5
TS7	51.3	-4.9	1.0	2.0	47.4	45.5
Levoglucosenone	3.9	-4.9	1.9	12.4	-0.9	-11.6

[a]Zero-point vibrational energy corrections
[b]Heat content function (aka enthalpy function) corrections.
[c]T×ΔS entropic corrections at 298 K.

Table S2. Absolute energies needed for the calculation the G4(MP2) reaction profiles (in Hartree) for all the species considered in the present work.

Structure	Ea	H_0b	H_{298}c	G_{298}d
H2O	-76.376916	-76.355854	-76.352074	-76.373502
DGP	-533.794024	-533.651986	-533.643708	-533.683837
TS1	-610.092944	-609.930042	-609.919337	-609.964690
INT1	-610.191199	-610.022513	-610.011925	-610.057306
TS2	-610.112716	-609.951342	-609.940354	-609.986631
STS2	-610.128268	-609.967254	-609.957555	-610.000694
WTS2	-686.519862	-686.333942	-686.321219	-686.371802
INT2	-610.179850	-610.013420	-610.001906	-610.049710
TS3	-610.084813	-609.924379	-609.913118	-609.959454
WTS3	-686.487047	-686.302215	-686.289270	-686.339479
INT3	-610.166277	-610.002042	-609.989184	-610.039666
TS4	-610.067970	-609.910419	-609.897649	-609.947972
WTS4	-686.487645	-686.305532	-686.290944	-686.345573
INT4	-610.180106	-610.015605	-610.003010	-610.052975
TS5	-610.079149	-609.920745	-609.908242	-609.958335
WTS5	-686.487572	-686.304884	-686.290634	-686.344632
INT5	-533.776285	-533.640858	-533.629084	-533.677853
TS6	-533.718215	-533.586467	-533.575959	-533.622076
WTS6	-610.131843	-609.974785	-609.962845	-610.011844
INT6	-533.799637	-533.661022	-533.650594	-533.695854
TS7	-533.712218	-533.577918	-533.568115	-533.611362
Levoglucosenone	-457.410952	-457.297781	-457.290219	-457.328753

[a]Electronic energy.
[b]Zero-point inclusive energy (or enthalpy at 0 K).
[c]Enthalpy at 298 K.
[d]Gibbs-free energy at 298 K.

Table S3. B3LYP/6-31G(2df,p) optimised geometries for all the local minima and transition structures

Transition structures:

1.1 Uncatalysed reactions:

TS1

O	-0.24297300	-1.46166400	-0.72513300
C	1.44229800	0.13037000	0.45793300
O	0.75684000	-0.27964500	1.46199100
C	-0.65411800	-0.10092700	1.18616400
C	-0.72099900	1.11249600	0.24504800
O	-1.81990400	0.92388400	-0.60610300
C	-2.34508600	-0.40757900	-0.41010700
C	-1.18384400	-1.21788700	0.20103600
C	0.68005300	1.07903600	-0.44697500
O	1.29732200	2.35667900	-0.36024500
H	2.51410700	0.12623400	0.58416600
H	-1.14948400	-0.01811000	2.15194000
H	-0.81355000	2.07467900	0.76121500
H	-3.23422200	-0.35867400	0.23771100
H	-2.62151000	-0.81687800	-1.38344100
H	-1.55381000	-2.09187600	0.77307400
H	0.58553500	0.70358900	-1.46362500
H	1.88166200	2.47244300	-1.11569900
O	2.19073700	-1.80090600	-0.51363200
H	2.46397000	-1.69854700	-1.43235200
H	1.16130200	-1.87269600	-0.56661100

TS2

O	-2.76736600	-0.73542000	-0.61870300
C	1.78056800	0.75288200	-0.21016800
O	0.43112500	0.78262500	-1.27496300
C	-0.48446300	-0.25313900	-0.89197900
C	0.04618700	-0.90209400	0.40751700
O	-0.67943500	-0.33172900	1.48831300
C	-1.56748800	0.67045600	1.00859200
C	-1.83837900	0.32339300	-0.46039900
C	1.55189300	-0.59503300	0.47723500
O	2.19940300	-1.64811100	-0.21593000
H	2.63695500	0.74800700	-0.90841700
H	-0.09087900	-1.98717100	0.42124000
H	-2.47888000	0.64747900	1.61696900
H	-1.11267500	1.66582900	1.10179500
H	1.86475800	-0.51768900	1.52662500
H	3.14829000	-1.48812700	-0.20212100
O	1.42696700	1.87245500	0.35793600
H	-3.56721700	-0.51476300	-0.13165400
H	-0.58759700	-0.95218700	-1.72207100
H	-2.11633700	1.20266500	-1.05724100
H	0.48812800	1.69859900	-0.52313300

TS3

O	1.44211800	0.85966100	-1.24986200
C	-1.74350200	0.90791300	-0.58542300
O	0.52516200	1.47975000	1.52465900
C	0.90903600	0.21215400	1.10367400
C	-0.26005900	-0.75682700	0.76987000
O	0.39996600	-1.71716000	-0.29065500
C	1.81032000	-1.34726400	-0.46992900
C	1.86264500	0.13413900	-0.12389000
C	-1.44972600	-0.38646200	-0.06619900
O	-2.60467100	-1.15435000	0.21637300
H	-2.76710100	0.96803800	-0.99807700
H	1.45758100	-0.23209000	1.94360600
H	-0.54175500	-1.39849100	1.60259000
H	2.39387200	-1.98048400	0.20452200
H	2.07232500	-1.54985700	-1.50766500
H	2.87581500	0.43699700	0.17320800
H	-0.41043300	-1.15484700	-0.92876300
H	-2.59595400	-1.94846100	-0.32443500
O	-1.00106600	1.90470100	-0.66504900
H	0.67415100	1.42239200	-1.03446100
H	-0.02286200	1.87406400	0.81712800

TS4

O	-0.61741300	-0.55909500	-1.42056800
C	2.26855800	0.43449600	-0.51143000
O	0.45136000	-2.13653000	0.77403200
C	-0.42048900	-1.02138100	0.96814600
C	0.27594400	0.28777600	1.23767100
O	-2.03591200	1.46426200	-0.28724300
C	-2.48324000	0.12670100	-0.14467500
C	-1.35980800	-0.91000200	-0.25511800
C	1.16674300	0.94729500	0.34949400
O	0.96674400	2.21683100	0.37967100
H	3.00608700	1.21021500	-0.79241600
H	-1.03767200	-1.27533500	1.83772400
H	0.48071000	0.54327700	2.27797000
H	-2.96251200	0.05247700	0.83681600
H	-3.24314500	-0.10564500	-0.90555600
H	-1.81839600	-1.90232400	-0.38182900
H	-1.51621600	1.48839900	-1.09946500
H	-0.04531400	1.73217100	1.03498600
O	2.38080900	-0.71892100	-0.87090700
H	0.05870700	-1.23348000	-1.55416000
H	1.22680200	-1.83144600	0.28152700

TS5

O	-0.80826200	-0.45788600	-1.46559300
C	1.97225400	-0.05259700	-0.87086800
O	0.44390400	-1.70541600	1.30177900

C	-0.50954900	-0.49760900	1.01188800
C	0.49673700	0.59924000	1.15370600
O	-2.34634600	1.49839900	-0.09962200
C	-2.65486400	0.12370700	-0.13893800
C	-1.40111400	-0.75906000	-0.21339900
C	1.47596800	0.95723500	0.17041000
O	2.12415500	2.00475500	0.13022400
H	2.57208100	0.44602500	-1.65392800
H	-1.15266300	-0.51989300	1.89246300
H	1.04788500	-0.79414400	1.69237600
H	-3.22018000	-0.10125400	0.77111000
H	-3.28557100	-0.13259700	-1.00299000
H	-1.72722600	-1.80996900	-0.17484200
H	-1.77797300	1.68409300	-0.85613000
H	0.23300400	1.40626100	1.82838300
O	1.86447200	-1.27186200	-0.85965300
H	-0.14887700	-1.12376600	-1.68187500
H	0.95954100	-1.82417600	0.45155700

TS6

O	-0.39875500	1.27705900	-0.02703300
C	1.21841400	0.80286300	0.50674400
C	-0.56641000	-0.79644600	-1.31926100
C	0.61479000	-1.27370500	-0.91430100
O	-1.91515600	-0.60629600	1.37748200
C	-2.40989700	-0.00613300	0.20368900
C	-1.26492200	0.40170300	-0.75183600
C	1.41196200	-0.66958200	0.16352300
O	2.28069900	-1.26590800	0.76580700
H	1.17889400	0.99478400	1.59033800
H	-1.12976400	-1.33647500	-2.07733200
H	-3.06154600	-0.73869600	-0.28303800
H	-3.00581700	0.89141000	0.42130100
H	-1.70462600	0.98616200	-1.57214600
H	-1.46251900	0.08068500	1.87842100
H	1.01237000	-2.20102200	-1.31560200
O	1.73769300	1.68746400	-0.29075300
H	0.51354800	1.83240600	-0.57731700

TS7

C	0.54016000	1.26358900	-0.04048800
C	0.68193700	0.15378300	0.96824900
C	-0.86057600	1.62684300	-0.29941800
O	-0.32787900	-0.53128300	1.37685000
O	0.07297900	-0.90414900	-1.29599600
C	-1.84368200	0.77856900	0.03570600
C	-1.48961300	-0.56885300	0.51069200
C	-0.99584300	-1.47183700	-0.75240100
H	1.51871500	0.18257300	1.65380900
H	-2.89123500	0.99660500	-0.14150300

H	-2.25945000	-1.07493900	1.09085300
H	-0.84001700	-2.47804500	-0.30945200
H	-1.88511200	-1.52852900	-1.40977200
O	1.51760700	1.88545800	-0.40079900
H	-1.03487900	2.60806500	-0.72607800
O	2.19064400	-1.21353300	0.00818500
H	1.42949200	-1.23236100	-0.66949700
H	2.14137200	-2.05787700	0.47168900

1.2 Catalysed reactions:

WTS2

O	-2.71096200	0.10167700	-0.85637000
C	1.60239300	0.83542600	-0.35128500
O	0.00110200	0.59210600	-1.05504900
C	-0.36739400	-0.76218600	-0.85780500
C	0.41959200	-1.24579600	0.36196100
O	-0.32064700	-0.75534200	1.47093100
C	-1.71157500	-0.79356200	1.15530200
C	-1.83291900	-0.90061000	-0.38329900
C	1.77719300	-0.55898200	0.30926100
O	2.61312900	-1.39720800	-0.47495200
H	2.15493400	0.88194000	-1.30684600
H	-0.15220300	-1.33355400	-1.76719900
H	0.53923800	-2.33814800	0.39973800
H	-2.18797700	-1.64850500	1.65234600
H	-2.17351800	0.13198600	1.50668100
H	2.16651900	-0.40974600	1.32373800
H	3.47294800	-0.97260400	-0.55627900
O	1.57495200	1.89803400	0.36193700
H	-2.73978200	0.04773000	-1.81744200
H	0.34415000	2.21801200	0.62955200
O	-0.77208700	2.23459500	0.48720100
H	-0.61449300	1.41280100	-0.34843800
H	-1.02205400	3.07180600	0.08007600
H	-2.19539900	-1.89835200	-0.67031700

STS2

O	1.68174900	1.30557300	0.04974500
C	-1.13393100	1.05327900	-0.41864000
O	-0.33437200	1.01181100	1.12012700
C	0.31372200	-0.26789800	1.16889300
C	-0.33137500	-1.19607600	0.11525200
O	0.62023100	-1.39826300	-0.92102800
C	1.92296400	-1.11617300	-0.42820600
C	1.76039300	0.00128400	0.59575800
C	-1.53374500	-0.42860000	-0.43685900
O	-2.62136900	-0.70378300	0.42364000
H	-1.96119200	1.72996000	-0.14906400
H	0.27942100	-0.64886500	2.18887400
H	-0.65529900	-2.15307100	0.54144000

H	2.36222900	-2.00413900	0.05499000
H	2.55264400	-0.82570200	-1.27224500
H	2.53611600	-0.01765700	1.36649000
H	-1.72337100	-0.72861200	-1.47543100
H	-3.37314700	-0.16863900	0.15034100
O	-0.28033000	1.49038900	-1.28578300
H	0.84212700	1.33932500	-0.82435200
H	0.62502900	1.55669600	0.74816300

WTS3

C	1.53942300	-1.42088000	-0.69310600
O	-1.14341900	-1.89877700	0.68071900
C	-1.10627200	-0.51312400	0.80088300
C	0.28226700	0.15239500	0.96084700
O	-0.06765400	1.62526700	0.52086300
C	-1.39003100	1.67841400	-0.08906200
C	-1.75344900	0.23208900	-0.37812600
C	1.49231900	-0.34912700	0.23981400
H	-1.69756100	-0.25975800	1.69108100
H	-2.09276400	2.11095900	0.62917600
H	-1.32742300	2.31900800	-0.97127400
H	0.80494500	1.95677300	-0.27675000
O	0.59841400	-1.97088600	-1.28926100
H	-0.61027500	-2.11270400	-0.12325400
H	0.53852100	0.30941600	2.00924800
O	2.71486600	-0.04009600	0.90816700
O	-3.15063200	0.07152000	-0.42195400
H	-3.31050300	-0.87949500	-0.37390600
H	-1.27840200	-0.11219900	-1.30882700
O	1.66609400	1.88081300	-1.08067500
H	1.71340100	0.80068800	-0.81204300
H	2.58298900	-1.72084900	-0.92463900
H	2.48148500	2.26207100	-0.72738300
H	2.86870100	-0.69525000	1.59818800

WTS4

O	-0.97783400	-1.05985000	-1.05642400
C	1.69375400	-0.94493300	-1.05419100
O	-0.02991500	-1.88243700	1.55331800
C	-0.42594900	-0.54021300	1.26849900
C	0.70949800	0.41640500	0.95547400
C	-2.15417500	0.78030400	-0.10768500
C	-1.51306000	-0.56942700	0.17239900
C	1.57711600	0.28033600	-0.15579000
O	2.36479700	1.20889800	-0.53817600
H	1.85395200	-0.70328300	-2.12092400
H	-0.91083700	-0.17747500	2.18445400
H	-2.28448900	1.32130100	0.84447500
H	-2.30531400	-1.24450200	0.52385800
H	1.77772100	2.28839200	-0.14478900

O	1.78349300	-2.07219600	-0.62586500
H	-0.76777200	-1.99005300	-0.91171400
H	0.75528400	-2.08319200	1.02445200
H	1.21399000	0.81910700	1.83743400
O	0.87800800	2.90421000	0.22330000
H	0.46744900	1.86180300	0.61505100
O	-3.40065300	0.55126200	-0.74306600
H	-3.71931000	1.38893700	-1.09057500
H	-1.48152700	1.37367700	-0.74222600
H	1.13457800	3.41135900	1.00358500

WTS5

O	1.35851600	0.47466700	1.40372900
C	-1.37764700	1.39408800	0.91848200
O	-0.76499700	-1.71493500	0.65738800
C	0.25779900	-1.03173200	-0.24247900
C	-0.40406400	0.04819900	-1.05498300
O	2.67730500	0.56623300	-1.09936500
C	2.75575700	-0.52070200	-0.20560600
C	1.48839300	-0.71440100	0.63481400
C	-0.87674100	1.29070300	-0.52584000
O	-1.05788200	2.34215800	-1.14861200
H	-1.62943900	2.44008000	1.17372800
H	0.55190700	-1.84691700	-0.90886700
H	-1.73752500	-0.85353800	-1.33823500
H	2.94233000	-1.41569700	-0.80858800
H	3.59546300	-0.40806800	0.49730700
H	1.65521000	-1.58251600	1.29079600
H	2.38094900	1.33159400	-0.59319800
H	0.02963500	0.15416100	-2.04621100
O	-1.56697200	0.50236300	1.73604300
H	0.73165200	0.33224900	2.11891000
H	-1.12264000	-0.96634700	1.22388500
O	-2.34411900	-1.74841100	-1.13963400
H	-1.63059800	-1.90103800	-0.09244200
H	-3.24271700	-1.45748700	-0.93979800

WTS6

O	0.40112200	0.58908100	-0.51587500
C	-1.38655400	0.47837500	-0.37684000
C	0.53307300	-1.32373100	0.97039300
C	-0.67086200	-1.78304200	0.61723200
O	2.73528200	-0.91039000	-0.96268400
C	2.57552700	-0.09029600	0.17012600
C	1.10067000	0.01181500	0.58754700
C	-1.62509200	-1.01654200	-0.19706700
O	-2.62114500	-1.50234700	-0.69073900
H	1.18461000	-1.94099800	1.58422600
H	3.16299400	-0.53513900	0.98079600
H	2.95939500	0.92857600	-0.00096000

H	1.03423000	0.67577600	1.46789200
H	2.09669500	-0.59513300	-1.61419100
O	-1.72648000	1.24553800	0.58951900
H	0.35039200	1.79883600	-0.35000000
O	-0.12690400	2.87370300	-0.06722100
H	-1.04805000	2.30396000	0.34486200
H	0.34195900	3.31096300	0.65092200
H	-0.99973600	-2.77845300	0.89950200
H	-1.53806300	0.80745800	-1.41540700

Local minima

H_2O

O	0.00000000	0.00000000	0.11886300
H	0.00000000	0.75665500	-0.47545400
H	0.00000000	-0.75665500	-0.47545400

DGP

O	-0.48014900	-1.24216200	-0.98444300
C	0.83081700	-1.00785000	-0.46660600
O	0.72390400	-1.25402900	0.91919000
C	-0.36114600	-0.36584400	1.14069800
C	0.07405200	0.99601000	0.52894300
O	-1.08293100	1.58737200	-0.03198600
C	-2.02784600	0.55882700	-0.35706400
C	-1.37683800	-0.76009500	0.03637700
C	1.10846400	0.51042200	-0.53018300
O	2.40227400	0.85637900	-0.08113700
H	1.54418400	-1.68397200	-0.93851300
H	-0.69238800	-0.38640000	2.17542700
H	0.53704200	1.69954100	1.22107000
H	-2.95389300	0.72690600	0.20885200
H	-2.26020500	0.58593600	-1.42694200
H	-2.08756300	-1.54825700	0.29394800
H	0.87530500	0.93012900	-1.51580100
H	3.04771800	0.50681200	-0.70402200

INT1

O	-2.06220000	1.17945200	-0.12076400
C	1.20324000	1.05366000	0.12609800
O	0.38274500	0.99373400	-1.04671700
C	-0.31220700	-0.25340000	-1.09537000
C	0.30946200	-1.15012800	0.00197000
O	-0.62551500	-1.14481900	1.07621100
C	-1.91668400	-1.13762900	0.46508800
C	-1.81051700	-0.09967200	-0.65624000
C	1.58479200	-0.41641300	0.40195300
O	2.60059900	-0.88172600	-0.46691600
H	2.06258800	1.68169100	-0.12672900
H	-0.21407400	-0.65606400	-2.10484800
H	0.51829800	-2.17163900	-0.33743900

H	-2.15521500	-2.13481600	0.06341000
H	-2.65440300	-0.85951100	1.21908300
H	1.83094700	-0.56647300	1.45967400
H	3.39514300	-0.36115400	-0.31265100
O	0.56618700	1.67058700	1.20008500
H	-1.35610600	1.75962600	-0.44351100
H	-0.17350000	1.10740000	1.47259000
H	-2.49671300	-0.31539400	-1.48575600

INT2

C	-1.84781800	0.52556000	1.05297000
O	-0.08251900	-1.80641700	-0.12925100
C	0.62319700	-0.67071600	-0.60813500
C	-0.23225600	0.60659500	-0.89585600
O	0.36840800	1.67606000	-0.16029400
C	1.73204200	1.34242600	0.07111600
C	1.72112900	-0.15898600	0.35229800
C	-1.71366500	0.53040700	-0.48231800
H	1.10738900	-0.99855500	-1.53211800
H	2.35696700	1.54655900	-0.81204200
H	2.09109400	1.94795000	0.90531800
O	-1.47830200	-0.38555100	1.76054700
H	-0.48650800	-1.55810600	0.72443400
H	-0.20042000	0.82899100	-1.97176400
O	-2.37398400	-0.56761200	-1.06767500
O	3.00040700	-0.70769400	0.13015000
H	2.95533000	-1.65000700	0.32278100
H	1.38437100	-0.33468100	1.38551600
H	-2.21816500	1.43250000	-0.84478700
H	-2.33890300	1.40912500	1.50656200
H	-1.81900300	-1.34578000	-0.89216900

INT3

C	2.33918300	-0.55752600	-0.66866600
O	-0.13686000	-1.81858500	0.90019200
C	-0.52509800	-0.45957200	0.84742500
C	0.59062800	0.55116000	0.80006500
O	-1.52433800	2.19668700	-0.41237200
C	-2.33267800	1.04162300	-0.23879300
C	-1.54841200	-0.26918900	-0.31406700
C	1.78670900	0.51571200	0.18108000
H	-1.07869000	-0.28724100	1.77959200
H	-2.79366900	1.13350600	0.75016500
H	-3.14670400	0.99745800	-0.97534400
H	-1.17842400	2.18065300	-1.31068900
O	1.80802000	-1.61697700	-0.94344200
H	0.50418600	-1.96714300	0.17832900
H	0.35294900	1.47662200	1.32057700
O	2.69188200	1.54688900	0.23260500
O	-2.48997900	-1.31424600	-0.25946100

H	-1.99213600	-2.08225200	0.05965200
H	-0.98120700	-0.29658600	-1.26451100
H	3.33330700	-0.30344700	-1.08190900
H	2.32859200	2.26504600	0.76169800

INT4

O	0.43943000	-0.44023500	1.52397600
C	-2.19829500	0.74400100	0.42180200
O	-0.68845900	-2.08877700	-0.37285600
C	0.30316900	-1.14751700	-0.76994200
C	-0.30489100	0.17549800	-1.29834700
O	2.30533200	1.14812100	-0.38694200
C	2.47414700	-0.09362600	0.26456500
C	1.22483400	-0.95841000	0.44781900
C	-0.86978200	1.11303300	-0.24921800
O	-0.38868800	2.18394700	0.05457300
H	-2.57155000	1.53306300	1.10315900
H	0.87767100	-1.58840400	-1.59580700
H	-1.11247500	-0.08954500	-1.99232200
H	3.18512900	-0.65654500	-0.35046500
H	2.92611900	0.02891700	1.26037000
H	1.58496800	-1.96327000	0.71873400
H	1.65407200	1.68326300	0.08595400
H	0.46633900	0.72724100	-1.83452800
O	-2.79065000	-0.29101700	0.23272000
H	-0.24404500	-1.10683900	1.67332900
H	-1.55704500	-1.66207500	-0.38026700

INT5

O	-0.59001200	0.65062200	0.99922300
C	1.98357000	0.92683100	0.20263300
C	-0.48654500	-0.74130000	-0.93383600
C	0.75165700	-1.19843200	-0.72837500
O	-3.01288400	-0.72173500	0.55691300
C	-2.63361200	0.37130700	-0.24909400
C	-1.10966000	0.49211400	-0.33289400
C	1.80174000	-0.59433000	0.12186100
O	2.64082400	-1.26063000	0.69314200
H	2.53572800	1.22770700	1.11798700
H	-1.14687500	-1.32254900	-1.57182900
H	-3.05620700	0.20673000	-1.24654500
H	-3.04480200	1.32285600	0.12956500
H	-0.83736900	1.36231500	-0.94778900
H	-2.46934600	-0.66631400	1.35309200
H	1.04503200	-2.15173400	-1.15991600
O	1.69575500	1.69660600	-0.67704900
H	-0.73853400	1.56494700	1.26582900

INT6

O	0.31592400	0.91085400	-0.52356500

C	-1.09252200	0.83650700	-0.43831400
C	0.48909900	-0.96387800	1.01917400
C	-0.69473900	-1.43460900	0.61268600
O	2.65637900	-0.58036200	-0.94780900
C	2.48728100	0.29843600	0.14127400
C	1.02595100	0.37140500	0.59422100
C	-1.57050200	-0.61176000	-0.23305100
O	-2.60622100	-1.00057900	-0.72680500
H	1.12183400	-1.54265300	1.68760800
H	3.10812700	-0.07756900	0.96098800
H	2.82169800	1.31944600	-0.09779100
H	0.95843800	1.06595200	1.44797400
H	2.01134500	-0.31132500	-1.61262500
O	-1.60021800	1.57883800	0.63745600
H	-1.49318100	2.51472000	0.43307100
H	-1.06322800	-2.41526800	0.89501100
H	-1.45935000	1.20008200	-1.40440200

Levoglucosenone

C	1.36622000	-0.04935700	0.00156600
C	0.20815600	-0.97651400	0.42069800
C	0.92121400	1.33693200	-0.27695700
O	-0.65634600	-0.29022600	1.28936300
O	-0.55538500	-1.26998900	-0.75422200
C	-0.36752700	1.65633000	-0.10095000
C	-1.32724900	0.59987900	0.38816300
C	-1.67745600	-0.39010400	-0.75047300
H	-0.75481000	2.64500800	-0.32948400
H	-2.19734100	1.01598000	0.89633400
O	2.50459400	-0.44107800	-0.12106000
H	1.67077600	2.04433100	-0.61551300
H	-2.59192300	-0.94476300	-0.51016600
H	-1.77786100	0.08364300	-1.73066400
H	0.56811100	-1.89685000	0.88455400

A2. Heat of formsation for C_{60} by means of the G4(MP2) thermochemical protocol through reactions in which C_{60} is broken down into corannulene and sumanene

Table S4. Gas-phase experimental heats of formation for C_{60} at 298 K ($\Delta_f H°_{298}[C_{60}(g)]$, in kJ•mol^{-1}).

$\Delta_f H°_{298}[C_{60}(cr)]$ [a]	[a]	$\Delta_f H°_{298}[C_{60}(g)]$ [b]	[c]	Source
2280 ± 5		2464 ± 7	2509 ± 9	Ref.1
2422 ± 14	2656 ± 25	2606 ± 15	2651 ± 16	Ref.2
2273 ± 15		2457 ± 16	2502 ± 17	Ref.3
2278 ± 14	2507 ± 16	2462 ± 15	2507 ± 16	Ref.4
2327 ± 17	2551 ± 15	2511 ± 18	2556 ± 19	Ref.5
2355 ± 15		2539 ± 16	2584 ± 17	Ref.6
2360 ± 10	2588 ± 12	2543 ± 11	2588 ± 12	Ref.7
2336 ± 20	2565 ± 21	2520 ± 21	2565 ± 21	Ref.8
2346 ± 12	2530 ± 13	2530 ± 13	2575 ± 14	Ref.9
2289 ± 30	2470 ± 16	2472 ± 30	2517 ± 30	Ref.10
2278 ± 27		2461 ± 28	2506 ± 28	Ref.11
2293 ± 45		2477 ± 45	2522 ± 45	Ref.11
	2560 ± 100[d]			Ref.12(NIST)

[a]Values reported in the original paper. [b]The reported crystalline heat of formation was converted to a heat of formation in the gas phase using the enthalpy of sublimation from reference 9. ($\Delta_s H°_{298}[C_{60}]$ = 183.7 ± 5.1 kJ•mol^{-1}). [c]The reported crystalline heat of formation was converted to a heat of formation in the gas phase using the enthalpy of sublimation from reference 4. ($\Delta_s H°_{298}[C_{60}]$ = 228.7 ± 7.3 kJ•mol^{-1}). [d]Average of six $\Delta_f H°_{298}[C_{60}(cr)]$ from references 1, 2, 3, 4, 5, 6 converted to $\Delta_f H°_{298}[C_{60}(g)]$ using the enthalpy of sublimation from reference 2 ($\Delta_s H°_{298}[C_{60}]$ = 234.0 kJ•mol^{-1}). Namely, $\Delta_f H°_{298}[C_{60}(g)]$ = (2514 + 2656 + 2507 + 2512 + 2561 + 2589) / 6 = 2556.5 ≈ 2560 kJ•mol^{-1}.

Table S5. %TAE[(T)] diagnostics indicating the importance of post-CCSD(T) contributions for the species considered in the present work (see main text).

	%TAE[(T)][a]
Methane	0.7[b]
Ethylene	1.3[b]
Ethane	0.9[b]
Benzene	2.0[b]
Naphthalene	2.2[b]
Anthracene	2.3[b]
Tetracene	2.4[b]
Triphenylene	2.3[b]
Corannulene	2.6[b]
Sumanene	2.5
C_{60}	3.0

[a]From W1h theory, unless otherwise indicated.
[b]Taken from ref 13
[c]From CCSD(T)/6-31G(d). We note, however, that the %TAE[(T)] diagnostic does not exhibit a strong basis-set dependence, and even a double-ζ basis set should give useful estimates, see discussion in ref 14.

Table S6**.** B3LYP/6-31G(2df,p) Optimised Geometries (Å),

Methane, taken from ref. 13

H	0.630335	0.630335	0.630335
C	0.000000	0.000000	0.000000
H	-0.630335	-0.630335	0.630335
H	-0.630335	0.630335	-0.630335
H	0.630335	-0.630335	-0.630335

Ethylene, taken from ref. 13

C	0.000000	0.000000	0.663667
C	0.000000	0.000000	-0.663667
H	0.000000	0.921459	-1.237793
H	0.000000	-0.921459	-1.237793
H	0.000000	0.921459	1.237793
H	0.000000	-0.921459	1.237793

Ethane, taken from ref. 13

C	0.000000	0.000000	0.764497
C	0.000000	0.000000	-0.764497
H	0.000000	1.019163	1.164773
H	-0.882621	-0.509581	1.164773
H	0.882621	-0.509581	1.164773
H	0.000000	-1.019163	-1.164773
H	-0.882621	0.509581	-1.164773
H	0.882621	0.509581	-1.164773

Propane

C	0.000000	1.276239	-0.259708
H	-0.883333	1.321083	-0.906865
H	0.883333	1.321083	-0.906865
H	0.000000	2.174371	0.366159
C	0.000000	0.000000	0.586363
H	0.876315	0.000000	1.246730
H	-0.876315	0.000000	1.246730
C	0.000000	-1.276239	-0.259708
H	0.883333	-1.321083	-0.906865
H	0.000000	-2.174371	0.366159
H	-0.883333	-1.321083	-0.906865

Benzene, taken from ref. 13

C	0.000000	1.393231	0.000000
C	1.206573	0.696615	0.000000
C	1.206573	-0.696615	0.000000
C	0.000000	-1.393231	0.000000
C	-1.206573	-0.696615	0.000000
C	-1.206573	0.696615	0.000000
H	2.146258	1.239143	0.000000
H	2.146258	-1.239143	0.000000

H	0.000000	-2.478286	0.000000
H	-2.146258	-1.239143	0.000000
H	-2.146258	1.239143	0.000000
H	0.000000	2.478286	0.000000

Triphenylene, taken from ref. 13

C	0.698984	3.695555	0.000000
C	1.380511	2.495679	0.000000
C	0.709343	1.254995	0.000000
C	-0.709343	1.254995	0.000000
C	-1.380511	2.495679	0.000000
C	-0.698984	3.695555	0.000000
C	1.441529	-0.013189	0.000000
C	-1.441529	-0.013189	0.000000
C	-0.732186	-1.241806	0.000000
C	0.732186	-1.241806	0.000000
C	-1.471066	-2.443397	0.000000
H	-0.953963	-3.393647	0.000000
C	-2.850953	-2.453116	0.000000
C	-3.549937	-1.242440	0.000000
C	-2.851577	-0.052282	0.000000
H	1.248457	4.630885	0.000000
H	2.462003	2.522980	0.000000
H	-2.462003	2.522980	0.000000
H	-1.248457	4.630885	0.000000
H	-3.386235	-3.396638	0.000000
H	-4.634692	-1.234246	0.000000
H	-3.415966	0.870667	0.000000
C	1.471066	-2.443397	0.000000
C	2.851577	-0.052282	0.000000
C	2.850953	-2.453116	0.000000
C	3.549937	-1.242440	0.000000
H	0.953963	-3.393647	0.000000
H	3.386235	-3.396638	0.000000
H	4.634692	-1.234246	0.000000
H	3.415966	0.870667	0.000000

Corannulene, taken from ref. 13

C	1.312437	2.985808	-0.248941
C	2.434107	2.170867	-0.248941
C	-1.312437	2.985808	-0.248941
C	0.000000	2.485633	0.092352
C	0.000000	1.203053	0.605999
C	2.363977	0.768103	0.092352
C	-2.434107	2.170867	-0.248941
C	3.245237	-0.325536	-0.248941
C	0.693230	-3.187000	-0.248941
C	-0.693230	-3.187000	-0.248941
C	1.461018	-2.010919	0.092352
C	0.707137	-0.973291	0.605999

C	-0.707137	-0.973291	0.605999
C	-1.461018	-2.010919	0.092352
C	-2.816797	-1.644138	-0.248941
C	-3.245237	-0.325536	-0.248941
C	-2.363977	0.768103	0.092352
C	-1.144172	0.371764	0.605999
C	2.816797	-1.644138	-0.248941
C	1.144172	0.371764	0.605999
H	-4.250055	-0.110280	-0.601407
H	-3.503187	-2.408901	-0.601407
H	-1.208457	-4.076121	-0.601407
H	1.208457	-4.076121	-0.601407
H	3.503187	-2.408901	-0.601407
H	4.250055	-0.110280	-0.601407
H	3.373546	2.587338	-0.601407
H	1.418221	4.007964	-0.601407
H	-1.418221	4.007964	-0.601407
H	-3.373546	2.587338	-0.601407

Sumanene

C	-3.229598	1.039268	0.434182
C	-2.514831	2.277279	0.434182
C	-1.213760	2.362719	-0.065304
C	-2.653055	-0.130213	-0.065304
C	-2.858692	-1.650466	0.182926
C	3.229598	1.039268	0.434182
C	2.653055	-0.130213	-0.065304
C	2.858692	-1.650466	0.182926
C	2.514831	2.277279	0.434182
C	1.213760	2.362719	-0.065304
C	0.715186	1.211349	-0.677567
C	1.406652	0.013695	-0.677567
C	0.691466	-1.225044	-0.677567
C	1.439295	-2.232507	-0.065304
C	0.714766	-3.316548	0.434182
C	-0.714766	-3.316548	0.434182
C	-1.439295	-2.232507	-0.065304
C	-0.691466	-1.225044	-0.677567
C	-1.406652	0.013695	-0.677567
C	-0.715186	1.211349	-0.677567
C	0.000000	3.300933	0.182926
H	2.970875	3.117295	0.950311
H	4.185094	1.014205	0.950311
H	0.000000	3.702528	1.201096
H	-2.970875	3.117295	0.950311
H	-4.185094	1.014205	0.950311
H	-3.606574	-2.082256	-0.495016
H	-1.214220	-4.131501	0.950311
H	1.214220	-4.131501	0.950311
H	3.206483	-1.851264	1.201096

H	-3.206483	-1.851264	1.201096
H	0.000000	4.164513	-0.495016
H	3.606574	-2.082256	-0.495016

C_{60}, taken from ref. 13

C	0.725906	-0.999124	3.322588
C	-0.725906	-0.999124	3.322588
C	-1.422153	-1.957425	2.590511
C	-0.696247	-2.956549	1.827248
C	0.696247	-2.956549	1.827248
C	1.422153	-1.957425	2.590511
C	1.174541	0.381631	3.322588
C	0.000000	1.234985	3.322588
C	-1.174541	0.381631	3.322588
C	-2.301092	0.747670	2.590511
C	-2.596693	-1.575794	1.827248
C	-1.422153	-3.192411	0.592263
C	-0.725906	-3.418635	-0.592263
C	0.725906	-3.418635	-0.592263
C	1.422153	-3.192411	0.592263
C	2.596693	-2.339057	0.592263
C	2.596693	-1.575794	1.827248
C	3.026998	-0.251454	1.827248
C	2.301092	0.747670	2.590511
C	0.000000	2.419511	2.590511
C	1.174541	2.801142	1.827248
C	2.301092	1.982655	1.827248
C	3.026998	1.746794	0.592263
C	3.475632	0.366039	0.592263
C	3.475632	-0.366039	-0.592263
C	3.026998	-1.746794	-0.592263
C	2.301092	-1.982655	-1.827248
C	1.174541	-2.801142	-1.827248
C	-2.596693	-2.339057	0.592263
C	-1.174541	-0.381631	-3.322588
C	-2.301092	-0.747670	-2.590511
C	-3.026998	0.251454	-1.827248
C	-2.596693	1.575794	-1.827248
C	-1.422153	1.957425	-2.590511
C	0.725906	0.999124	-3.322588
C	1.174541	-0.381631	-3.322588
C	0.000000	-1.234985	-3.322588
C	0.000000	-2.419511	-2.590511
C	-1.174541	-2.801142	-1.827248
C	-2.301092	-1.982655	-1.827248
C	-3.475632	-0.366039	-0.592263
C	-3.475632	0.366039	0.592263
C	-3.026998	1.746794	0.592263
C	-2.596693	2.339057	-0.592263
C	-1.422153	3.192411	-0.592263

C	-0.696247	2.956549	-1.827248
C	0.696247	2.956549	-1.827248
C	1.422153	1.957425	-2.590511
C	2.301092	-0.747670	-2.590511
C	3.026998	0.251454	-1.827248
C	2.596693	1.575794	-1.827248
C	2.596693	2.339057	-0.592263
C	1.422153	3.192411	-0.592263
C	0.725906	3.418635	0.592263
C	-0.725906	3.418635	0.592263
C	-1.174541	2.801142	1.827248
C	-2.301092	1.982655	1.827248
C	-3.026998	-1.746794	-0.592263
C	-3.026998	-0.251454	1.827248
C	-0.725906	0.999124	-3.322588

References

1 Beckhaus, H.D., C. Rüchardt, M. Kao, F. Diederich, and C.S. Foote, *The Stability of Buckminsterfullerene (C60): Experimental determination of the heat of formation.* Angewandte Chemie International Edition in English, 1992. **31**(1): p. 63-64.

2 Steele, W., R. Chirico, N. Smith, W. Billups, P. Elmore, and A. Wheeler, *Standard enthalpy of formation of buckminsterfullerene.* The Journal of Physical Chemistry, 1992. **96**(12): p. 4731-4733.

3 Kiyobayashi, T. and M. Sakiyama, *Combustion Calorimetric Studies on C60 and C70.* Fullerene Science and Technology, 1993. **1**(3): p. 269-273.

4 Diogo, H.P., M.E.M. da Piedade, T.J.S. Dennis, J.P. Hare, H.W. Kroto, R. Taylor, and D.R.M. Walton, *Enthalpies of formation of buckminsterfullerene (C60) and of the parent ions C60+, C602+, C603+ and C60.* Journal of the Chemical Society, Faraday Transactions, 1993. **89**(19): p. 3541-3544.

5 Beckhaus, H.D., S. Verevkin, C. Rüchardt, F. Diederich, C. Thilgen, H.U. ter Meer, H. Mohn, and W. Müller, *C70 is more stable than C60: experimental determination of the heat of formation of C70.* Angewandte Chemie International Edition in English, 1994. **33**(9): p. 996-998.

6 Kolesov, V.P., S.M. Pimenova, V.K. Pavlovich, N.B. Tamm, and A.A. Kurskaya, *Enthalpies of combustion and formation of fullerene C60.* The Journal of Chemical Thermodynamics, 1996. **28**(10): p. 1121-1125.

7 Xu-wu, A., H. Jun, and B. Zheng, *Standard molar enthalpies of combustion and formation of C60.* The Journal of Chemical Thermodynamics, 1996. **28**(10): p. 1115-1119.

8 An, X., B. Chen, and J. He, *Determinations of combustion and formation enthalpies of C60 and C70.* Science in China Series B: Chemistry, 1998. **41**(5): p. 543-548.

9 V. Diky, V. and G. J. Kabo, *Thermodynamic properties of C60 and C70 fullerenes.* Russian Chemical Reviews, 2000. **69**(2): p. 95-104.

10 Rojas-Aguilar, A., *An isoperibol micro-bomb combustion calorimeter for measurement of the enthalpy of combustion. Application to the study of fullerene C60.* The Journal of Chemical Thermodynamics, 2002. **34**(10): p. 1729-1743.

11 Rojas-Aguilar, A. and M. Martínez-Herrera, *Enthalpies of combustion and formation of fullerenes by micro-combustion calorimetry in a Calvet calorimeter.* Thermochimica Acta, 2005. **437**(1–2): p. 126-133.

12 Afeefy, H., J. Liebman, and S. Stein, Neutral thermochemical data. NIST chemistry webbook, NIST standard reference database, 2005. 69.
13 Karton, A., B. Chan, K. Raghavachari, and L. Radom, *Evaluation of the Heats of Formation of Corannulene and C60 by Means of High-Level Theoretical Procedures.* The Journal of Physical Chemistry A, 2013. **117**(8): p. 1834-1842.
14 Karton, A., S. Daon, and J.M.L. Martin, *W4-11: A high-confidence benchmark dataset for computational thermochemistry derived from first-principles W4 data.* Chemical Physics Letters, 2011. **510**(4–6): p. 165-178.

Appendix B Publications

Journal publications

1. **Wenchao Wan**, Li-Juan Yu and Amir Karton, *Mechanistic Insights into Water-catalyzed Formation of* levoglucosenone *from Anhydrosugar Intermediates by Means of High-Level Theoretical Procedures*. Australian Journal of Chemistry, 2016. **69**(9): p. 943-949.
2. **Wenchao Wan** and Amir Karton, *Heat of formation of C60 by means of the G4(MP2) thermochemical protocol through reactions in which C60 is broken down into corannulene and sumanene.* Chemical Physics Letters, 2016. **643**: p. 34-38.
3. Li-Juan Yu, **Wenchao Wan** and Amir Karton, *Evaluation of the performance of MP4-based procedures for a wide range of thermochemical and kinetic properties.* Chemical Physics, 2016. **480**: p. 23-35.
4. Farzaneh Sarrami, Li-Juan Yu, **Wenchao Wan** and Amir Karton, *Sulphuric acid catalysed formation of hemiacetal from glyoxal and ethanol.* 2017 Chemical Physics Letter

Publications in conference proceedings

1. **Wenchao Wan**, Mingming Zhu, Zhezi Zhang, Wenxu Zhou, and Dongke Zhang. *Identification and Characterisation of Cellulose Fast Pyrolysis Products using a CDS Pyroprobe in Combination with Liquid Nitrogen Quenching Method.* The 10th Asia-Pacific Conference on Combustion – ASPACC 2015.
2. Zhezi Zhang, Mingming Zhu, Pengfei Liu, **Wenchao Wan**, Wenxu Zhou, Yii Leng Chan, Dongke Zhang, *Effect of Biochar on the Cracking of Tar from the Pyrolysis of a Pine Sawdust in a Fixed-bed Reactor*. The 7th International Conference on Applied Energy – ICAE 2015

3. Pengfei Liu, Mingming Zhu, Zhezi Zhang, **Wenchao Wan**, Setyawati Yani, Dongke Zhang, *Thermogravimetric Studies of Characteristics and Kinetics of Pyrolysis of Buton Oil Sand.* The 7th International Conference on Applied Energy – ICAE 2015